UNIVERSITÀ DI SIENA 1240

Department of Medical Biotechnologies

PhD Course in Medical Biotechnologies
Coordinator: Prof Lorenzo Leoncini
CYCLE XXXV

Phenotypic characterization of novel antivirals for the treatment of multidrug resistant HIV-1 and emerging viruses

SUPERVISOR
PROF. MAURIZIO ZAZZI

CANDIDATE
FEDERICA GIAMMARINO

Academic Year 2021/2022

INDEX

MY PHD ACTIVITIES

During my three years (2019-2022) of the Doctoral School in Medical Biotechnologies, I continuously attended the laboratory of Microbiology and Virology at the Department of Medical Biotechnologies of the University of Siena. The Department has been hosting the Human Immunodeficiency Virus (HIV) Monitoring Laboratory (HML), started as a public health service and involved in a number of HIV related research projects since 1990. The availability of a biosafety laboratory of level 3 has served to carry out different projects involving the use of replication competent viruses in cell cultures.

In the last few years, the HML has extended the research activity on emerging and re-emerging flaviviruses, including Dengue (DENV), West Nile (WNV) and Zika (ZIKV) viruses. Moreover, due to the ongoing Coronavirus Disease 2019 (COVID-19) emergency, part of the research activity has been also directed to the newly discovered Severe Acute Respiratory Syndrome Coronavirus-2 (SARS-CoV-2).

Viruses are causative agents of many human diseases, possibly leading to death. Generally, viral infections can be associated with acute and chronic viral diseases. An acute viral infection is usually characterized by a rapid onset of disease, with mild to severe symptoms, followed by the resolution of the disease in a short time, with severe cases also leading to death rapidly. Conversely, in chronic viral infections, the virus persists in specific cells of the infected host in a variety of forms including true latency, continuous replication or alternating stages of silent and productive infection that can lead to severe long-term consequences for the host (Deigendesch and Stenzel, 2018).

Currently, the main strategy for combating viral infections is a combination of large-scale vaccination and the use of antiviral drugs to shorten the duration of viral infection and reduce related symptoms. However, vaccines are available only for a minority of viral pathogens, thus the demand for new antiviral strategies has significantly increased. Factors contributing to this growing demand include the ever-increasing prevalence of chronic viral infections, the emergence of new and more infectious viruses and the re-emergence of old viruses. Indeed, due to the globalization and climate changes, viruses confined in specific and isolated areas are re-emerging and rapidly spreading to new geographic areas (Pierson and Diamond, 2020). While impressive advances in *de novo* drug design have significantly expedited drug discovery in the last decade, the process leading to the approval of new drugs takes a long time and remains economically challenging. Consequently, drug repurposing has increasingly gained attention as a cost- and time-saving strategy to deliver safe and effective treatment. Anyway, the assessment of antiviral effects *in vitro* is a key approach for the screening of either *de novo* or repurposed candidate

compounds. Among the variety of methods that have been developed, cell-based assays are the most valuable methods to define antiviral activity because they can be developed in a number of different ways to uniquely allow testing drug activity, mechanism of action and resistance in a controlled system mimicking virus-host cell interaction (Boldescu et al., 2017; Gong, 2013).

During my PhD internship I was involved in several projects focused on antiviral drug discovery.

My principal PhD task has been dedicated to the analysis of the *in vitro* susceptibility to antiretroviral drugs of HIV-1 isolates collected from individuals enrolled in the PRESTIGIO registry. PRESTIGIO ("Patients with HIV infection and resistance to reverse transcriptase, integrase and protease inhibitors") is an observational, prospective, multicentre study (ClinicalTrial.gov identifier NCT04098315) including patients affected by HIV-1 presenting documented resistance to the main four classes of antiretroviral drugs: nucleoside reverse transcriptase inhibitors (NRTIs), non-nucleoside reverse transcriptase inhibitors (NNRTIs), protease inhibitors (PIs), and integrase inhibitors (INSTIs).

The PRESTIGIO registry collects data from individuals regarding demographic and clinical characteristics, comorbidities, antiretroviral treatments, laboratory parameters, and HIV genotypic data derived from resistance and viral tropism testing. The registry serves as a basis for studies aiming to evaluate the long-term effectiveness of antiretroviral therapies, the evolution of genotypic and phenotypic susceptibility to antiretroviral drugs, (particularly novel drugs being developed for highly treatment experienced patients often harbouring multidrug resistant virus) the determinants of clinical outcomes including virological/immunological/inflammatory markers, and the incidence of AIDS related conditions and comorbidities. Along with the collection of data, the registry stores samples of plasma and peripheral blood mononuclear cells at enrolment and at the end of each year of follow-up. The collection of clinical information and biological samples is regulated by the approval of local Ethics Committee of each participating centre.

In this context, the HML participated to the study by evaluating the antiviral activity of licensed or investigational HIV-1 inhibitors through cell-based assays.

The phenotypic methods provided by HML for PRESTIGIO were developed in-house and thoroughly assessed in terms of reproducibility and accuracy. In particular, two different phenotypic approaches were set up to estimate the antiviral activity of drugs targeting the early phases of viral replication (from entry to HIV-1 DNA integration) or the post-integration steps, such as assembly, maturation and budding of viral particles. The validation of our phenotypic methods was carried out by comparing the susceptibility levels calculated as fold change values on a panel of clones with different patterns of common resistance mutations previously measured through the PhenoSense assay offered by Monogram Biosciences, which can be considered as the

reference method for HIV-1 phenotypic susceptibility testing. Our protocol is suitable for both laboratory adapted viral strains and replication competent recombinant viruses harboring patient derived viral sequences generated by homologous recombination in eukaryotic cells (Saladini et al., 2018).

Similarly, we developed a cell-based assay for the evaluation of HIV-1 viral tropism which can be applied as well to determine the susceptibility to entry inhibitors. Differently from the above-mentioned phenotypic assays, this protocol includes the generation of virus-like particles expressing patient derived Env protein and competent for only one cycle of replication (Vicenti et al., 2019).

During the last year of my PhD, I have developed a cell-based assay to evaluate the *in vitro* combinatorial activity of ibalizumab together with licensed or investigational antiretrovirals, detecting a few cases of synergistic effects with other drug classes. Ibalizumab is the first monoclonal antibody targeting CD4 receptor recently approved for salvage therapy of heavily treatment-experienced patients with multidrug resistant HIV-1. Upon binding to CD4, ibalizumab prevents the conformational changes of HIV-1 gp120 necessary for the virus to enter the cell while not interfering with normal CD4 immunological functions. Previous studies have shown that no antagonism has been detected between ibalizumab and entry inhibitors (maraviroc and enfuvirtide) or members of the NRTI (abacavir, didanosine, emtricitabine, tenofovir, zidovudine.), NNRTI (efavirenz) and PI (atazanavir) classes *in vitro* (Gombos et al., 2015).

Due to the worldwide circulation of different viruses coupled with the increased frequency and diversity of new outbreaks, the need for antiviral drugs to quickly react against potential pandemic pathogens is a public health priority. In this context, part of my work was focused on the research of compounds actives against different viral targets. Some studies reported that sofosbuvir, an RNA-dependent RNA polymerase (RdRp) inhibitor licensed for the treatment of Hepatitis C Virus (HCV) infection, exerts a measurable antiviral activity against the flaviviruses ZIKV and Yellow Fever Virus (YFV), both *in vitro* and in animal models, as well as against DENV *in vitro*. Since the flavivirus RdRp-coding non-structural protein 5 (NS5) is well conserved among flaviviruses, we investigated whether sofosbuvir may have an activity against WNV. Following exhaustive *in vitro* experiments, we described for the first time sofosbuvir antiviral activity against WNV in the low micromolar range, as well as its genetic barrier through *in vitro* resistance selection experiments. Moreover, two collaborations, one with the Biophysics Institute of the National Research Council (Milano) and another with the Department of Biotechnology, Chemistry and Pharmacy of the University of Siena, allowed us to define the *in vitro* enzymatic activity of sofosbuvir using the purified WNV RdRp and to assess the role of the mutations observed during *in vitro* selection experiments through molecular docking experiments, respectively (Dragoni et al., 2020).

In the area of drug discovery, the HML is currently engaged in a project titled "ORIGINALE CHEMIAE in Antiviral Strategy" which was granted as a PRIN proposal (Progetti di Ricerca di Rilevante Interesse Nazionale). The project is aimed at exploiting Multi-Component Chemistry to synthesize promising broad-spectrum antivirals, which represent an attractive option to treat new emerging viral diseases. The project consists in a network of laboratories working in antiviral drug discovery and development from different Italian Universities (Tuscia, Parma, Roma Tor Vergata, Perugia, Siena and Roma Sapienza). The HML task in this project is to define the antiviral activity of candidate molecules through *in vitro* standardized virus-cell systems, against DENV, WNV, ZIKV, HIV-1 and the newly discovered SARS-CoV-2. Recently, we have published the activity of promising broad-spectrum antivirals which are simultaneously active in the micromolar range against flaviviruses and SARS-CoV-2 (Cesarini et al., 2022).

Finally, we have developed a quantitative live-virus microneutralization assay to determine the evolution of neutralizing response against SARS-CoV-2 in a population of healthcare workers (HCWs) vaccinated with BNT162b2 mRNA COVID-19 vaccine (Pfizer) (Vicenti et al.,2021). The live virus neutralization assay was used also to evaluate the efficacy of licensed Monoclonal Antibodies (mAbs) against different circulating SARS-CoV-2 variants (Fiaschi et al.,2022). Also, the antiviral drugs remdesivir, nirmaltrevir and molnupiravir approved for clinical use for the treatment of COVID-19 were tested against circulating variants using a quantitative cell-based antiviral assay which, similar to the microneutralization assay, uses the VERO E6 cell line and a quantitative read-out. Our results showed that these drugs, contrary to the mAbs, retained activity against all tested variants.
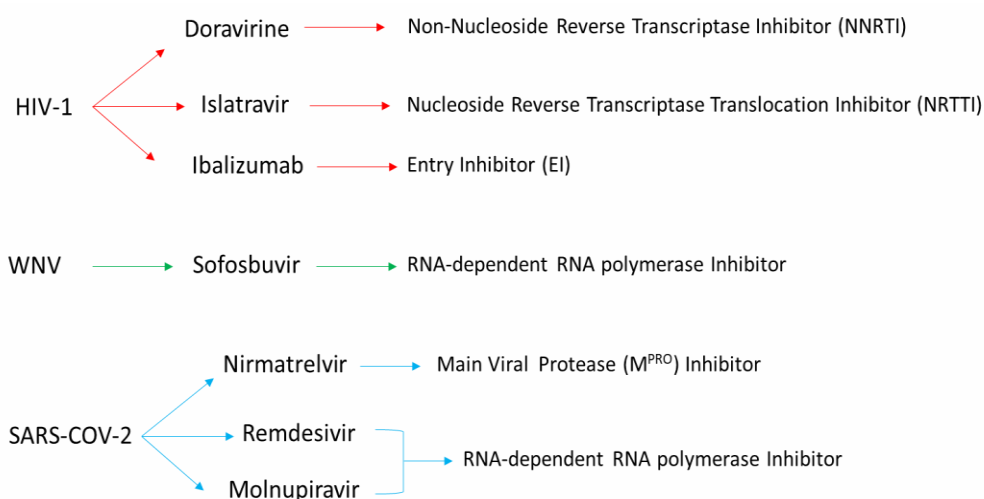

Figure: *Viruses studied during my PhD. Here are listed the drugs used for our experiments and their related target.*

1. DORAVIRINE

Doravirine (DOR, MK-1439) is a novel HIV-1 non-nucleoside reverse transcriptase inhibitor (NNRTI) approved by FDA on 30th August 2018 and by EMA at the beginning of 2019.

Doravirine was approved for the treatment of HIV-1 infection in adult patients without a history of ART, or for the replacement of the current antiretroviral regimen in patients with undetectable plasma viral load on a stable antiretroviral regimen without previous failures to NNRTI-based therapies and no documented doravirine resistance-associated mutations.

Doravirine, like all NNRTIs, binds to an allosteric site about 10A° from the active site of the reverse transcriptase, the so-called NNRTI binding pocket, inhibiting viral DNA synthesis. This binding results in inhibition of the polymerization reaction due to conformational changes inside the reverse transcriptase that shift the active site residues into an inactive conformation.

Doravirine is characterized by a unique resistance profile with potent *in vitro* activity against wild-type HIV-1 and the most common NNRTI-resistant variants. Moreover, doravirine has demonstrated noninferior efficacy in two randomized clinical trials in treatment-naïve patients as compared to ritonavir-boosted darunavir (DRIVE-FORWARD study) and to efavirenz (DRIVE-AHEAD trial) (Colombier and Molina, 2018).

The results of the phase 3 trials in treatment naïve HIV-1 infected patients indicates doravirine as the preferred NNRTI-based regimen for treatment initiation due to its efficacy and safety profile. In fact, ritonavir-boosted darunavir-based and EFV-based regimens have been compared to doravirine regimens for their antiviral activity, resulting in a better profile of doravirine even in patients with higher viral load levels (Colombier and Molina, 2018).

In vitro studies have shown that doravirine preferentially selects the V106A/M mutation in combination with other substitutions including L234I, F227I/C/L and V108I in subtypes A, B and C (Feng *et al.*, 2015). Additionally, it has been found that viruses with these amino acids variants are totally or partially susceptible to the NNRTI efavirenz, rilpivirine and etravirine (Feng *et al.*, 2015; Smith *et al.*, 2016).

The activity of doravirine was also evaluated in a panel of subtypes B clones presenting single or combined mutations (L100I, K101E, K103N, Y181C, Y188L, G190A) selected by NNRTI of clinical use. This study demonstrated that combinations of two or three mutations were associated with varying levels of decreased susceptibility to the drug that were difficult to predict on a genotypic basis. Among single mutants, only Y188L was shown to provide a significant level of resistance (Feng *et al.*, 2016).

The impact of both NRTIs and NNRTIs resistance associated mutations (RAMs) on susceptibility to doravirine was also evaluated in comparison with other NNRTIs through an *in vitro* study conducted with a panel of clones derived from treatment naïve and treatment experienced PLWH. The most common NNRTI RAMs were K103N, V106I and Y181C. Even in the presence of almost all the common NNRTI RAMs, doravirine maintained a higher activity with respect to the other NNRTIs tested. Resistance to doravirine was found in some isolates harbouring only Y188L or Y318F. However, based on the 3-fold biological cut-off, generally at least five NNRTIs RAM were needed to reduce the susceptibility to doravirine. On the contrary, reduction of susceptibility to etravirine, rilpivirine, efavirenz and nevirapine was observed when only two or three NNRTI RAMs were present. Finally, hypersusceptibility to doravirine was associated with common NRTI RAMs like K65R and/or M184I/V, however the clinical significance of this phenomenon remains to be established (Asante-Appiah *et al*., 2021).

During the DRIVE-FORWARD and the DRIVE-AHEAD clinical studies few patients experienced therapeutic failure and only in 8 individuals was observed a phenotypic resistance to doravirine (Martin *et al*., 2020).

During my PhD I further characterized the role of doravirine against viral strains harboring NNRTI mutations in comparison to the already licensed NNRTIs. Firstly, we compared the susceptibility to doravirine and other NNRTIs in a publicly available panel of viruses including the different patterns of major NNRTI mutations isolated from clinical samples (Saladini *et al*., 2021), then we measured the susceptibility of doravirine, etravirine and rilpivirine in isolates collected from heavily treatment experienced individuals enrolled in the Italian PRESTIGIO registry (Saladini *et al*., submitted). Moreover, I focused my attention to the natural reverse transcriptase polymorphism V106I. Since this aminoacid substitution can be found in 2-8% of circulating HIV-1 strains and has been found to emerge during doravirine-based treatments, we investigated the impact of V106I polymorphism in the susceptibility to doravirine in a panel of clinically derived HIV-1 recombinant viruses harbouring V106I and no other NNRTI mutations. In addition, we also evaluated the impact of V106I on the genetic barrier to resistance to doravirine in comparison to the other well established NNRTI resistance associated mutations at the same codon V106A and V106M.

All the information regarding the above-mentioned studies can be found in the manuscript and abstracts presented at international conferences attached at the end of the thesis from page 44 to page 80.

2. ISLATRAVIR

Islatravir (ISL, 4′-ethynyl-2-fluoro-2′-deoxyadenosine, EFdA, or MK-8591) is an investigational drug under a new phase III clinical evaluation. Clinical trials for HIV-1 treatment and prevention have been put on hold by the Food and Drug Administration (FDA) due to reports of reductions in CD4+ T-cells and total lymphocytes counts in some study patients who were receiving islatravir. After extensive analysis of clinical data and additional experiments in animal models (Matthews *et al*., 2022; Correll *et al*., 2022; Vargo *et al*., 2022), clinical trials for HIV-1 treatment have been restarted using the lowest concentration of the drug tested in early clinical trials (0.25 mg), while studies for the HIV-1 prevention have been halted.

Islatravir is a nucleoside reverse transcriptase translocation inhibitor (NRTTI) which, thanks to its unique structure (4'-ethynyl, 3'-hydroxyl, and 2-fluoro groups), can block the RT enzyme of HIV through different mechanisms (Singh *et al*., 2019). The 4'-ethynil group strongly binds to a conserved hydrophobic pocket in HIV-1 reverse transcriptase and prevents the extended primer translocation, causing immediate chain termination. Moreover, reverse transcriptase has a very high binding affinity for the 3'-hydroxyl group, which contributes to the delayed chain termination. Finally, the drug's long intracellular half-life is a result of the 2-fluoro on the adenine base ring, which makes it less susceptible to deamination by adenosine deaminase (Markowitz and Grobler, 2019). In addition, islatravir has a robust resistance profile, suggesting significant potency against viruses harboring drug-resistant mutations (Markowitz and Grobler, 2019). Recent *in vitro* studies on NRTI and/or NNRTI resistant viruses revealed a variable reduced susceptibility to islatravir in the presence of the M184I/V mutation alone or in combinations with other NRTI resistance mutations (Oliveira *et al*., 2017). Hypersusceptibility to islatravir, instead, was conferred by either K65R (Michailidis *et al*., 2013) or L74V or Q151M NRTI mutations (Grobler *et al*., 2018). The reverse transcriptase M184V substitution was also found to be the primary resistance mutation emerging during *in vitro* resistance selection experiments, while the addition of A114S further decreased the susceptibility to islatravir (Cilento *et al*., 2021; Diamond *et al*., 2022).

To further investigate the role of islatravir as a possible salvage therapy after failure of NRTI and NNRTI treatment in HIV multi-resistant patients, during my PhD I led a study aiming to evaluate the *in vitro* antiviral activity of this drug on a panel of HIV-1 infectious clones. These clones expressed patient-derived protease-reverse transcriptase (PR-RT), generated from patients enrolled in the Italian PRESTIGIO cohort, which harbor different combinations of NRTI mutations.

The evaluation of the *in vitro* susceptibility to islatravir was performed in duplicate through a TZM-bl cell-based assay developed by the HIV and Hepatitis monitoring laboratory of the Department of Medical Biotechnology of Siena (Saladini *et al*,

2018). Recombinant viruses were generated by the co-transfection in the 293T cell lines of both the PCR amplicon of the whole reverse transcriptase and RNase H region and the deleted HIV-1 NL4-3 vector.

Then, we infected the reporter cell-line TZM-bl cells with the wild-type NL4-3 strain or NRTI resistant viruses at multiplicity of infection of 0.03 in presence of five-fold dilution of islatravir ranging from 5 µM to 0,000512 nM. After 48 hours, cells were treated with the Glo-Lysis buffer (Promega, Madison, WI, USA) and the Bright-Glo Luciferase Assay (Promega), then relative luminescence units were measured through the GloMax Discover instrument (Promega) and elaborated with GraphPad software to calculate half-maximal inhibitory concentration (IC_{50}) values. Fold-change (FC) values were calculated with respect to the IC_{50} value obtained with the NL4-3 wild-type strain. Patients' demographics were described by median (Q1-Q3) or frequency (%); FC data were described by mean±SD and compared by the Mann-Whitney test.

Sample were collected from patients with a median age of 54 years (48-58), with a time since HIV-1 diagnosis of 27 years (23-31) and with a median time on ART of 24 years (22-26). The majority of them were male (18/20, 90%), 11 (55%) had a previous AIDS diagnosis, median viral load of 4.30 log_{10} copies/mL (3.32-5.16) and median CD4+ cell count of 145 cells/µL (69-280). At the time of sample collection, 13/20 (65%) viruses harbored the M184V mutation.

The mean FC value of islatravir was 6.0±5.1 (table 2.1), while a higher mean FC value was observed in viruses harboring M184V vs. those without M184V (7.9±5.2 vs. 2.6±2.6, p=0.006) (figure 2.1), thus confirming previous findings (Takamatsu Y. et al., 2018). According to the Stanford HIVdb NRTI mutation list, the mean FC values of viruses harboring TAM type 1 only (TAM1, n=2) and TAM1 plus M184V (n=3) was 2.3±0.4 and 13.1±4.6, respectively. The pattern with the addition of L74V to TAM1 only plus M184V (n=2) had a mean FC of 4.0±0.2, showing a reduction to islatravir resistance. In a similar way, viruses with TAM2 only (n=2) and TAM2 only plus M184V (n=3) had FC values of 2.1±1.1 and 10.8±6.0, respectively. The FC values of viruses with both TAM1 and TAM2 mutations plus either M184V (n=3) or the insertion at codon 69 (n=1), or L74V (n=1) was 4.5±1.9, 8.1 and 0.7, respectively (figure 2.2A).

Irrespective of the pattern, the number of TAMs did not significantly affect the susceptibility of islatravir in the absence of M184V and T69ins (figure 2.2B).
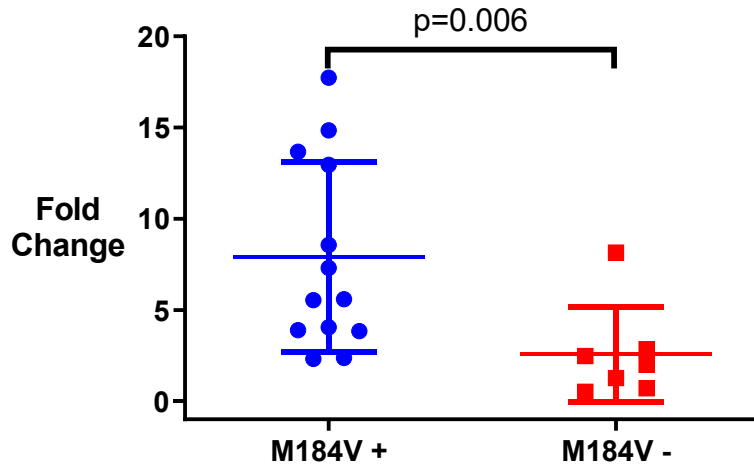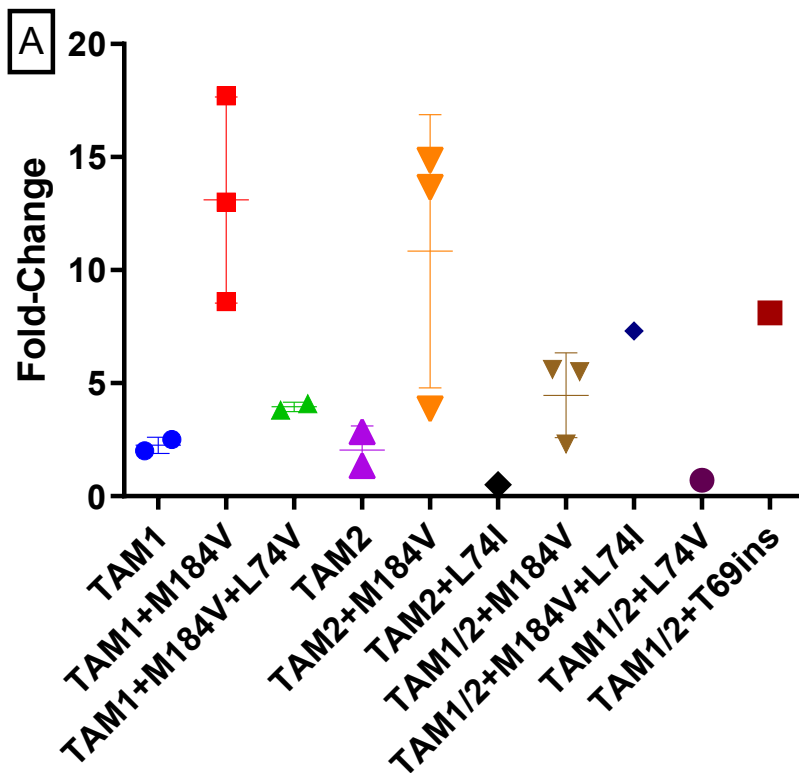
Figure 2.1. *Islatravir fold-change values of the 20 NRTI/NNRTI resistant viruses were calculated with respect to the IC$_{50}$ value of NL4-3 wild-type strain. The fold-change values were distributed according to the presence (M184V+) or absence (M184V-) of the M184V mutation in the NRTI/NNRTI resistant viruses.*
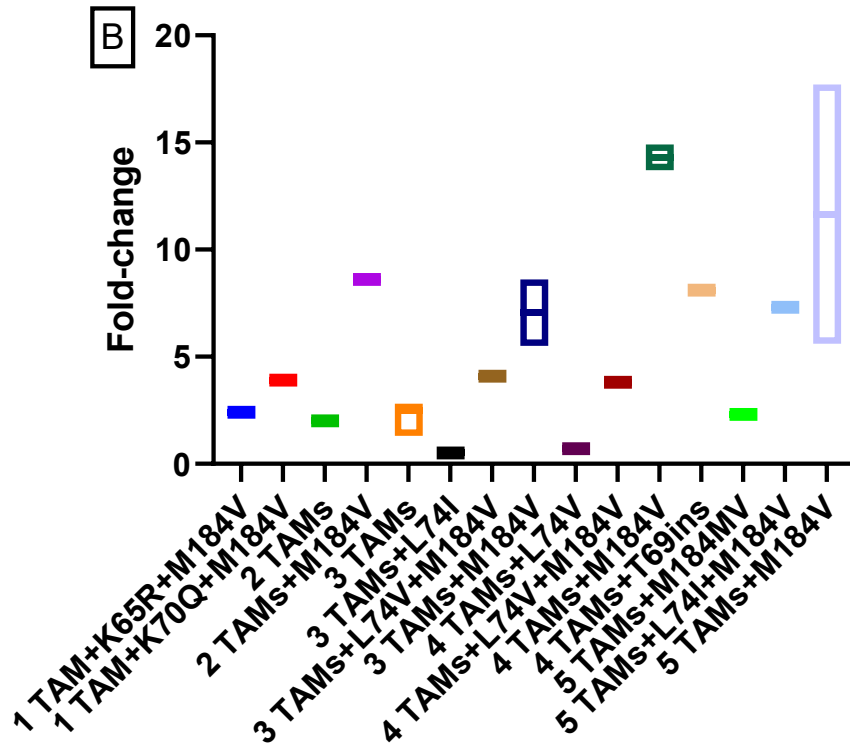
Figure 2.2*. Islatravir fold-change values of the 20 NRTI/NNRTI resistant viruses were calculated with respect to the IC$_{50}$ value of NL4-3 wild-type strain. A) Distribution of fold-change values according to different patterns of NRTI mutations; B) Distribution of fold-change values according to the number of TAMs irrespective of the pattern of mutations*

Table 2.1 *Half-maximal inhibitory concentration (IC$_{50}$) and fold-change values of islatravir calculated with twenty NRTI/NNRTI resistant viruses in a TZM-bl cell based assay.*

Virus ID	NRTI RAMs	NNRTI RAMs	Mean Islatravir IC$_{50}$±SD (nM)	Fold Change (FC)
151970	M41L D67G K70R L74I M184V T215Y K219E	98G 103N 181C 225H	17.5±1.1	7.3
151950	M41L A62V V75I L210W T215CHRY	K103N Y181V	6.0±0.7	2.5
153174	D67N T69D K70R K219Q	K103KNRS Y181C G190S H221HY	6.8±2.4	2.8
153170	K70Q M184V T215F	E138Q V179E Y181C	9.3±3.6	3.9
153230	M41L T69D M184V L210W T215Y	V108I Y181C	20.6±10.8	8.6
153227	M41L M184V T215Y	V106I Y188L K238N	31.1±13.0	13.0
151948	K65R Y115F M184V	Y181C H221Y M230I	5.7±0.4	2.4
153237	D67N K70R M184V T215F K219Q	A98G	32.8±6.4	13.7
153175	M41L E44D L74V M184V L210W T215Y K219N	L100I E138R V179L	9.2±0.1	3.8
153181	M41L E44D D67N T69D M184V L210W T215Y K219KR	K103N Y181I	13.4±8.9	5.6
151984	M41L E44D L74V M184V L210W T215Y	K103N E138A P225H M230L	9.7±5.6	4.1
153225	D67N K70R T215L K219E	K101E Y181C G190A	3.0±0.2	1.3
153223	M41L E44D D67G V75M M184V L210W T215Y K219N	L100V K101H V179F Y181C G190A	42.5±19.7	17.7
153178	M41L A62AV D67N K70G V75I M184MV L210W T215Y K219Q	K101E Y181C G190A	5.6±2.2	2.3
153179	M41L D67N T69S_ES F77L L210W T215Y	K103N	19.6±0.3	8.1
151978	D67N K70R M184V T215F K219E	V108I E138A Y181V	35.6±10.3	14.9
153177	M41L M184V L210W T215C K219E	Y181I	13.3±2.8	5.5
153185	M41L D67N L74V L210W T215C K219N	L100I K103N E138G	1.7±0.3	0.7
153224	D67N T69D K70KR L74I V75S T215L K219Q	A98G L100I K103N E138Q	1.2±1.0	0.5
153233	M41L T215Y	K103N Y181C	4.8±1.1	2.0
153235	L74V	100I 103N 179VI 238N	1.8±0.9	0.8

In conclusion, the results of this study confirmed the negative impact of M184V and aminoacidic insertions at codon 69 together with TAMs in the susceptibility to islatravir. We also demonstrated that the presence of L74V/I may reduce the effect of M184V, thus increasing the susceptibility. Data from *in vivo* activity are needed to better define the clinical role of islatravir in salvage therapy for patients harboring extensive NRTI resistance.

3. IBALIZUMAB

Ibalizumab (TNX-355, Trogarzo) is a humanized IgG4 monoclonal antibody approved by the FDA in March 2018 for the treatment of multi-drug resistant (MDR) HIV-1 infection in adult individuals. Ibalizumab binds to the extracellular domain 2 of the CD4 molecule, causing steric hindrance, which limits the conformational changes in the complex formed between CD4 and the HIV envelope gp120. This subsequently prevents viral fusion and entry into the CD4+ T cell by inhibiting the interaction of gp120 with the CXCR4 or CCR5 co-receptor via the V3 loop and the rearrangement of the gp41 domain.

Thanks to its mechanism of action, ibalizumab does not interfere with major histocompatibility complex class II (MHC-II) mediated immune function, since it binds to a CD4 domain that does not include the MHC-II binding sites (Beccari *et al*., 2019).

The safety and antiviral activity of ibalizumab were demonstrated in a phase I and a phase II clinical trial. Its approval by FDA came following a phase III clinical research that included only 40 patients with MDR HIV-1 infection who had received various treatments. The results of this trial demonstrated that ibalizumab in combination with an optimized background regimen is a valuable option to improve the virological and immunological outcome in this challenging patient population (Emu *et al*., 2018).

The activity of ibalizumab was also evaluated in an *in vitro* study conducted against group A and group B HIV-2 clinical isolates (Le Hingrat *et al*., 2022).

The main mechanism of resistance to ibalizumab appears to be associated with mutations in the gp120 variable region 5 (V5) that disrupt one or more potential N-linked glycosylation sites (PNGS) (Toma *et al*., 2011; Pace *et al*., 2013). In fact, loss of PNGS was the main genetic variation in the phase III study linked to decreased susceptibility to the drug (Beccari *et al*., 2019; Emu *et al*., 2018).

Finally, no antagonism has been detected between ibalizumab and other antiretrovirals, including the entry inhibitors maraviroc and enfuvirtide, or members of the NRTI, NNRTI and PI classes *in vitro*. Moreover, in a recent study it was observed that no intrinsic cross-resistance is present between ibalizumab and the entry inhibitors maraviroc or temsavir (Rose *et al*., 2022). Actually, synergy between ibalizumab and enfuvirtide has been reported in one study (Zhang *et al*., 2006). Notably, no experiments have been reported on ibalizumab plus INSTIs. Thus, knowledge about the possible synergy between ibalizumab and most of the drugs typically used in the context of MDR is lacking.

Considering these data and the importance of the selection of drugs for salvage therapy, during my PhD activities I led a study aiming to the *in vitro* evaluation of the combinatorial activity of ibalizumab together with licensed or investigational antiretrovirals.

The activity of ibalizumab was evaluated in association with tenofovir alafenamide (TAF, NRTI), doravirine (DOR, NNRTI), islatravir (ISL, NRTTI), temsavir (TMV, AI), cabotegravir (CAB, INSTI) or lenacapavir (LEN, CI) against wild-type NL4-3

(X4-tropic). The wild-type strain AD8 (R5-tropic) was used to evaluate the combinatorial activity of ibalizumab together with the entry inhibitors maraviroc, PRO-140 and TMV.

Firstly, the antiviral activity of the single drugs was evaluated in a system based on the infection of MOLT4-CCR5 cells with the NL4-3 and AD8 wild type strains in the presence of serial dilutions of the drugs. After 8 days, the supernatant was used to infect the TZM-bl reporter cells for 48 hours and the luciferase activity was processed with the GraphPad software to determine the IC_{50} values (figure 3.1). The results were in agreement with the expected activity for each drug. All the drugs are active in the nanomolar range except for lenacapavir, which showed IC_{50} values in the low picomolar range (Table 3.1).
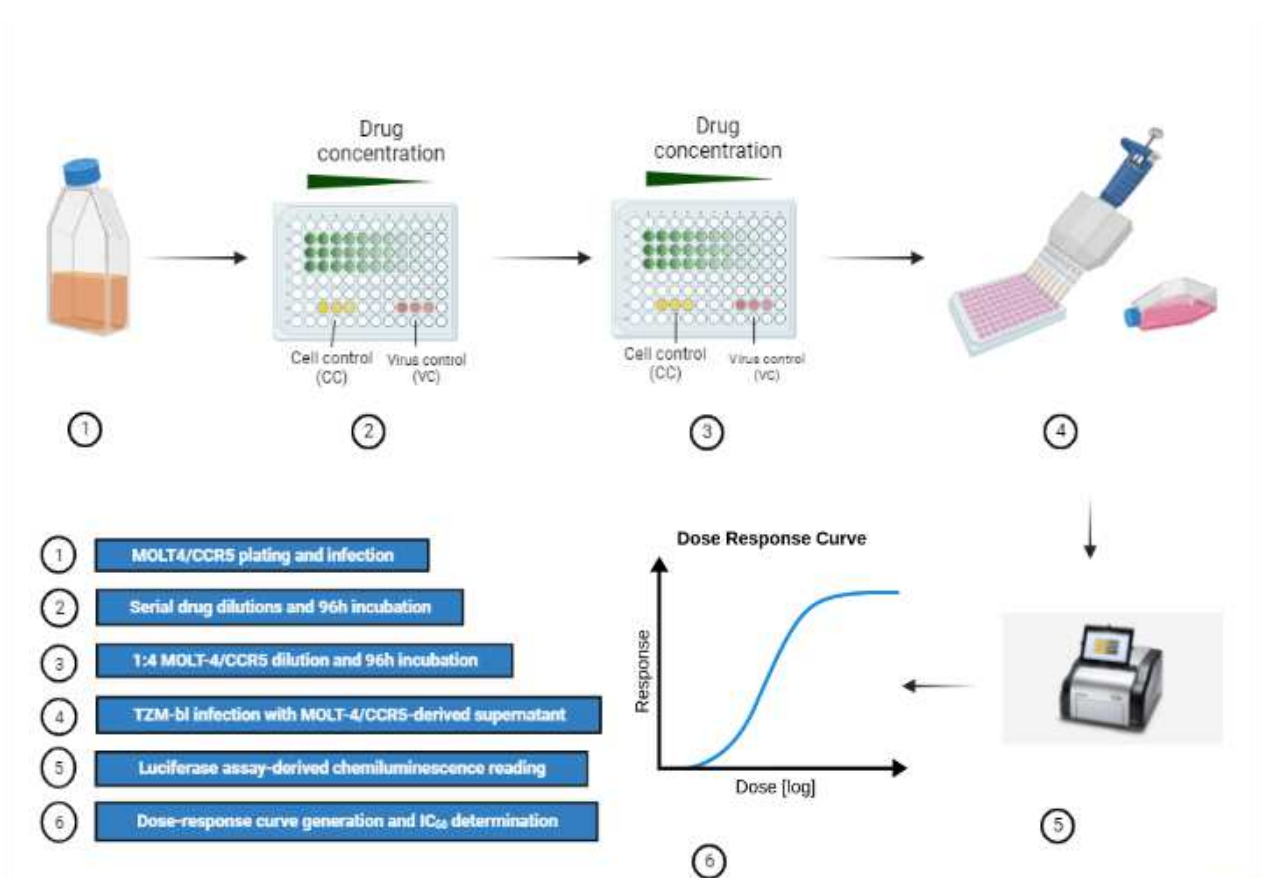

Figure 3.1: *Determination of antiviral activity of the single drugs through a cellular assay based on the infection of the MOLT4-CCR5 cells with the wild-type strains NL4-3 and/or AD8 in the presence of scalar dilutions of the single drugs. After 8 days, the supernatant was used to infect the reporter cell-line TZM-bl and after 48 hours the luciferase activity was evaluated.*

Table 3.1: *Values of IC$_{50}$ ± standard deviation (SD) of each antiviral drug tested against the wild-type strains NL4-3 and/or AD8 calculated as the mean value of at least two measurements.*

Drug	Drug Class	IC$_{50}$ ± SD	Tested vs
Tenofovir alafenamide	NRTI	2.5 ± 0.9 nM	NL4-3
Islatravir (investigational)	NRTTI	0.3 ± 0.2 nM	NL4-3
Doravirine	NNRTI	2.8 ± 1.1 nM	NL4-3
Darunavir	PI	0.2 ± 0.1 nM	NL4-3
Cabotegravir	INSTI	0.5 ± 0.2 nM	NL4-3
Lenacapavir	CI	51.3 ± 0.05 pM	NL4-3
Ibalizumab	EI	2 ± 0.0 ng/ml	NL4-3, AD8
Temsavir		0.2 ± 0.1 nM	NL4-3, AD8
Maraviroc		3.3 ± 0.8 nM	AD8
PRO-140 (investigational)		7.6 ± 2.8 nM	AD8

For the evaluation of the combinatorial activity, MOLT4-CCR5 cells were infected with the NL4-3 and AD8 wild-type strains and exposed to a 6x6 matrix of scalar concentrations of ibalizumab in combination with each of other antiviral drugs. The six concentrations of each drug were selected to determine the inhibition of virus replication from 0 to 100%. As for the measurement of antiviral activity, after 8 days of infection the MOLT4-CCR5 supernatant was used to infect TZM-bl cells and after 48 hours the activity of luciferase was measured (figure 3.2).

The luminescence values were normalized with positive and negative infection controls and elaborated with the SynergyFinder2.0 software. Synergy scores were calculated from the mean of at least two independent replicates and calculated with zero interaction potency (ZIP), Bliss, Loewe and highest single agent (HSA) models.

Each of these models is based on different assumption about the expected effect. ZIP model calculates the possible synergy effect between two drugs assuming that they do not potentiate each other. Bliss model presumed that the drugs don't interact with each other and that their combinatorial activity is the product of the effects of the single drugs alone. HSA model is the simplest one and it stipulates that the expected combinatorial activity corresponds to the higher effect of each drug. Finally, the Loewe model, unlike the HSA and the Bliss independence models, takes in consideration the dose-response curves of the drugs and defined the predicted effect as if a drug was combined with itself (https://synergyfinder.org).

Values lower than -10, from -10 to 10 and higher than 10 were interpreted as associated with antagonism, additive effect, and synergy between drugs, respectively.
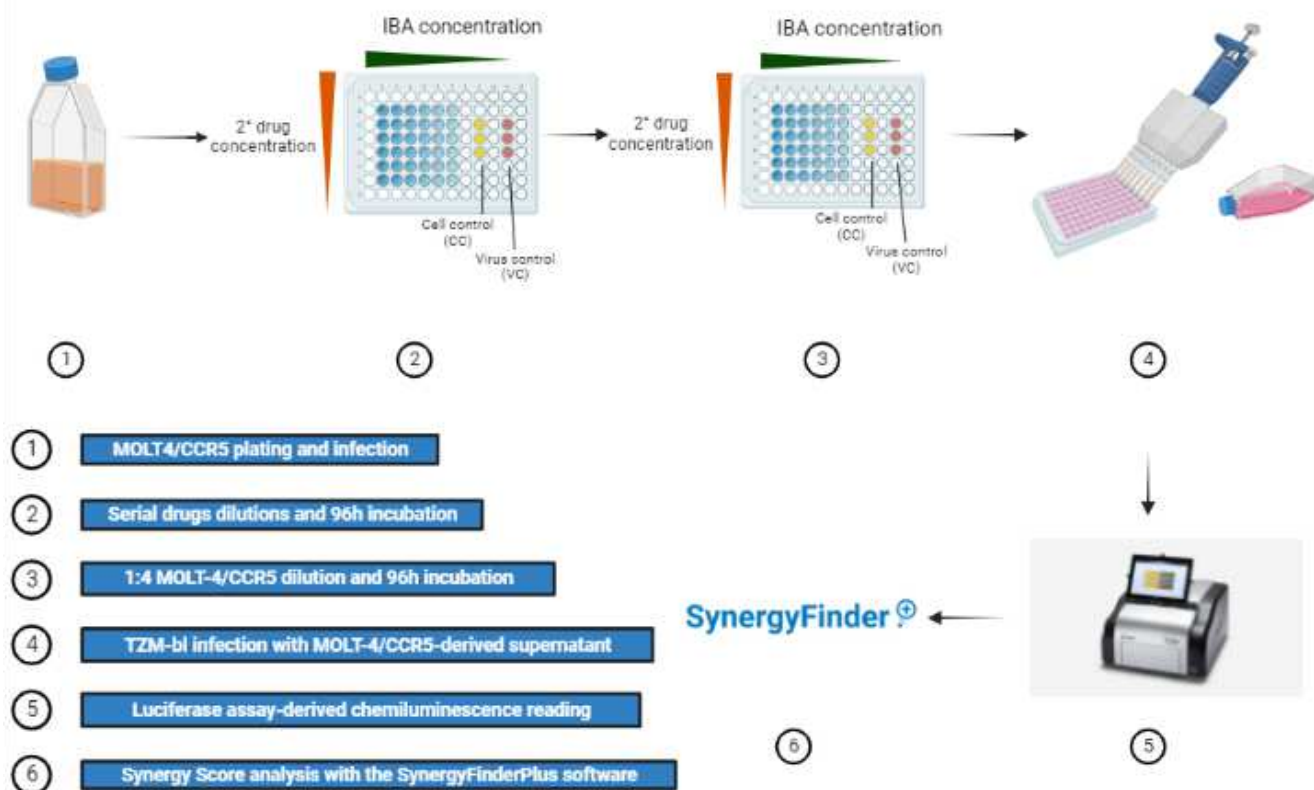
Figure 3.2: *MOLT-4/CCR5 synergy infection assay based on the infection of the cells with the wild-type strains NL4-3 and/or AD8 in a matrix 6x6 of scalar concentrations of ibalizumab in combination with each of the other drugs. After 8 days of infection, the supernatant was used to infect the reporter cell-line TZM-bl and the luciferase activity was evaluated after 48 hours.*

As control for the additive activity and to monitor the reproducibility of the assay, a matrix of ibalizumab plus ibalizumab was used in each run. Sinergy scores obtained from the same drug combination were compared among the different algorithms. In the case of CXCR4-tropic NL4-3 virus, all drug combinations showed an additive effect, except for IBA+LEN showing synergy in the Bliss and ZIP models, and IBA+TMV associated with synergy in the HSA model. Globally, the combinations IBA+LEN, IBA+TMV and IBA+TAF were associated with a stronger additive effect with respect to the other combinations (Table 3.2, Figure 3.3). The same analysis was carried out using combinations of IBA with the entry inhibitors maraviroc (MVC), PRO-140 and temsavir (TMV) against the CCR5-tropic AD8 virus. All the three drug combinations were associated with an additive effect, while IBA+TMV showed synergy with the HSA model (Table 3.3, Figure 3.4).

Table 3.2*: Synergy score (SS) average values ± standard deviation (SD) of IBA in combination with antiviral drugs against the NL4-3 strain.*

Synergy model	IBA+DRV	IBA+LEN	IBA+TMV	IBA+TAF	IBA+ISL	IBA+DOR	IBA+CAB	IBA+IBA
	Average ± SD							
HSA	-0.2 ± 10	9.1 ± 3.9	11.5 ± 3.4	8.2 ± 2.3	-0.1 ± 6.1	2.7 ± 3.9	2.7 ± 3.4	-2.4 ± 2.4
LOEWE	-1.4 ± 10.1	8.2 ± 4.0	7.2 ± 3.1	7.9 ± 1.2	-0.6 ± 6.0	2.3 ± 3.9	2.1 ± 3.7	-1.1 ± 2.6
BLISS	5.6 ± 2.5	12.1 ± 1.0	7.0 ± 1.7	8.8 ± 2.7	-3.7 ± 3.5	-1.8 ± 1.2	-3.4 ± 1.0	-6.3 ± 2.3
ZIP	9.4 ± 6.2	13.8 ±1.7	7.0 ± 2.2	8.8 ± 2.3	-3.8 ± 3.7	-1.2 ± 1.7	0.9 ± 2.7	-5.1 ± 2.3

Table 3.3: *Synergy score (SS) average values ± standard deviation (SD) of IBA in combination with antiviral drugs against the AD8 strain*

Synergy model	IBA+TMV	IBA+MVC	IBA+PRO-140	IBA+IBA
	Average ± SD			
HSA	11 ± 3.8	6.9 ± 13.1	6.4 ± 3.1	-3.6 ± 4.8
LOEWE	8.4 ± 0.6	6.6 ± 13.2	4.3 ± 0.8	-3.9 ± 5.0
BLISS	0.5 ± 4.8	-1.4 ± 8.1	-1.2 ± 5.6	-17.5 ± 5.4
ZIP	0.8 ± 5.3	-1.2 ± 7.7	-0.4 ± 6.2	-15.1 ± 3.3

Figure 3.3: *After the evaluation of the luciferase activity of the combinatorial activity of IBA together with each drug in the 6x6 matrix against the NL4-3 virus, we compared the synergy scores calculated with the different models using the software SynergyFinderPlus. Values lower than -10, from -10 to 10 and higher than 10 were associated with antagonism, additive and synergy effect respectively.*
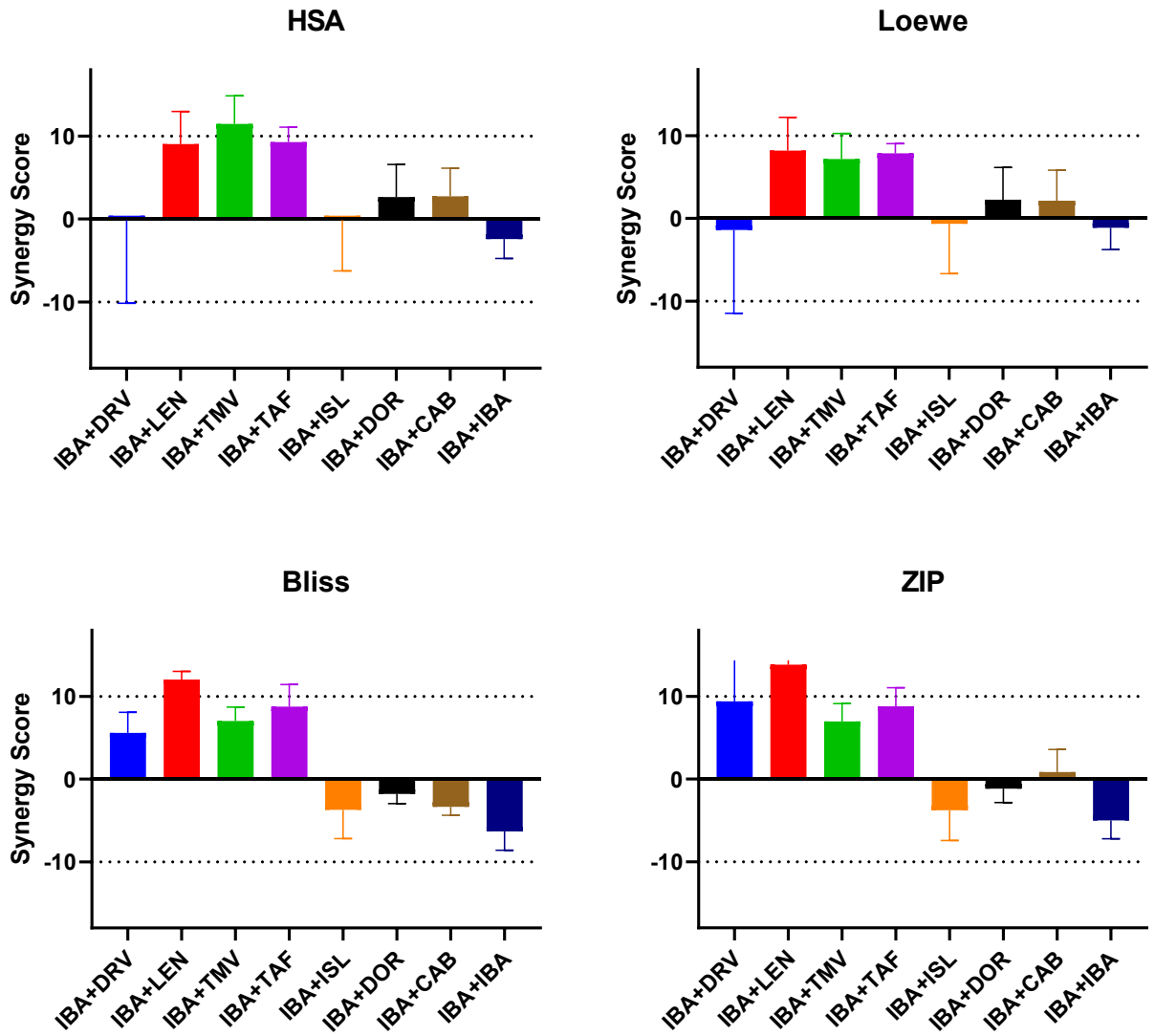
Figure 3.4: *After the evaluation of the luciferase activity of the combinatorial activity of IBA together with each drug in the 6x6 matrix against the AD8 virus, we compared the synergy scores calculated with the different models using the software SynergyFinderPlus. Values lower than -10, from -10 to 10 and higher than 10 were associated with antagonism, additive and* *synergy* *effect, respectively.*
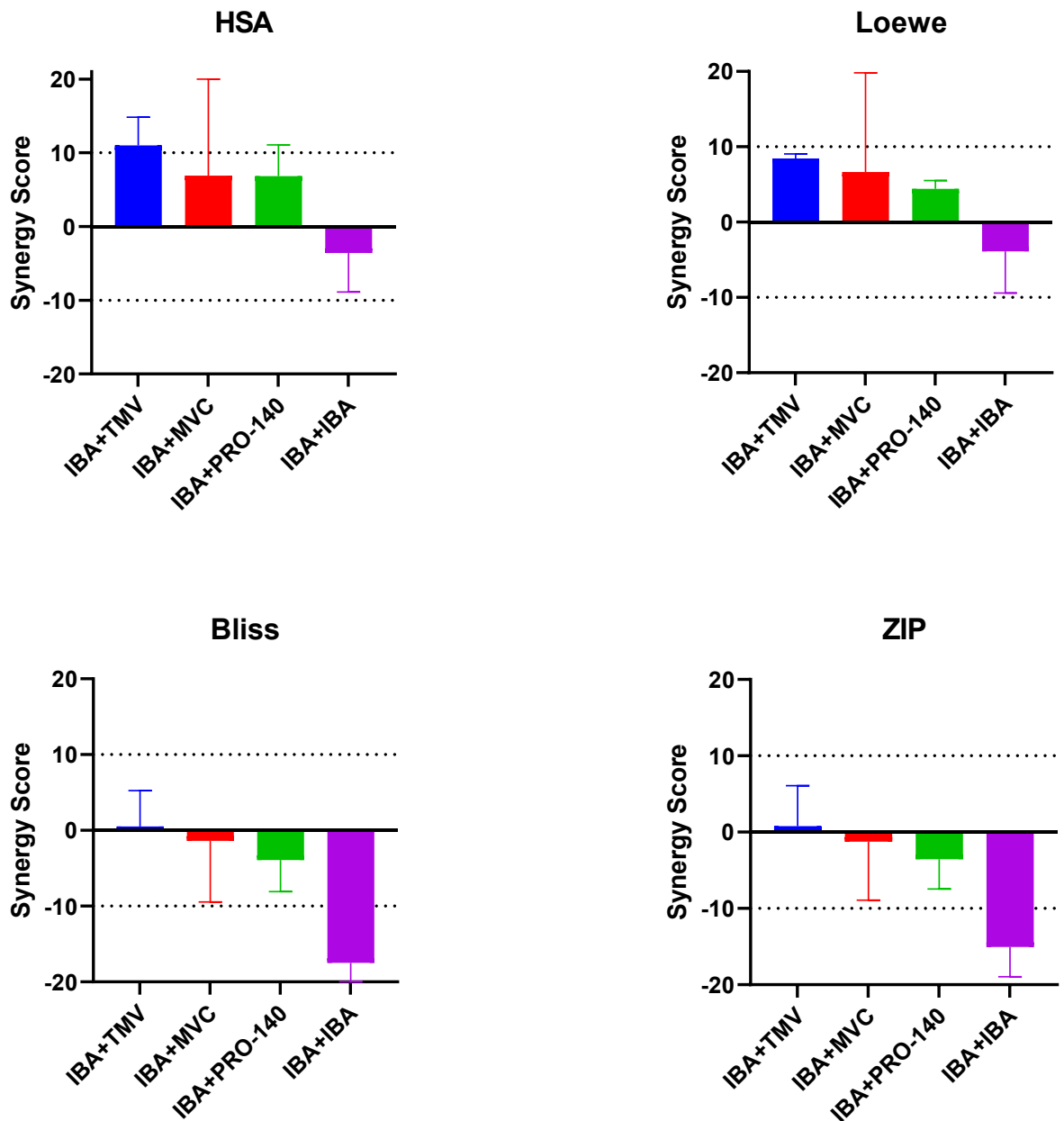
Interestingly, the control combination IBA+IBA was associated with antagonism in the Bliss and ZIP models when using the AD8 virus, while additive effect was observed with the other models and in all cases when using the NL4-3 virus. Considering that the IBA+IBA combination was associated with lower synergy scores with the Bliss and ZIP models when using the NL4-3 virus as well, a possible explanation might rely on the assumptions of the different models. In particular, the

Bliss model assumes that drugs act through independent pathways, thus the combinatorial effect of the same drug might be wrongly considered as antagonistic. In the case of the ZIP model, the variability of the synergy scores between NL4-3 and AD8 viruses might be due to the different dose-response curves, where AD8 has a lower variation among the concentrations used for the dose-response matrix (Figure 3.5).
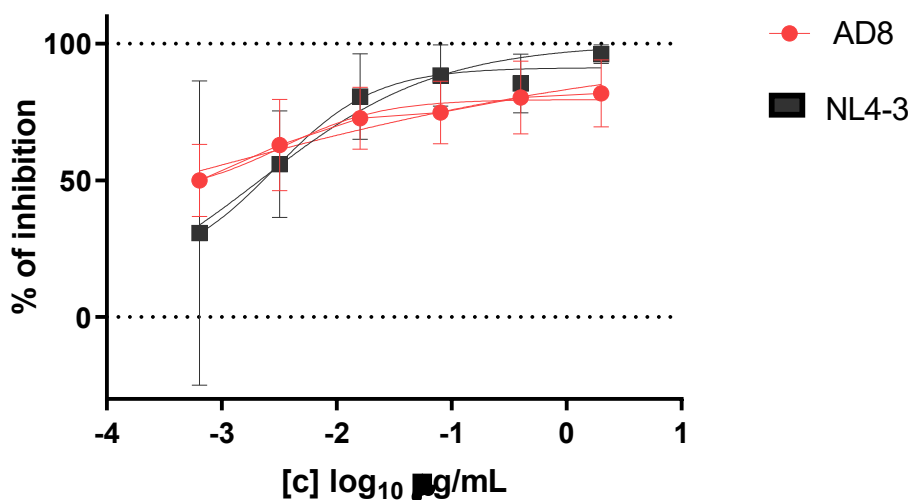

Figure 3.5: *Dose-response curves of ibalizumab calculated with the reference NL4-3 and AD8 strains.*

In conclusion, these preliminary data suggest that ibalizumab positively interacts with other antivirals against both NL4-3 and AD8 strains, with possible synergistic effects in select cases. Further studies are needed to determine the impact of Env variability and viral tropism in combination with other entry inhibitors and to define the clinical potential for such interactions among drug classes in the context of MDR in vivo.

4. Development of a Cell-Based Immunodetection Assay for Simultaneous Screening of Antiviral Compounds Inhibiting Zika and Dengue Virus Replication

The global spread of arboviral infections is challenging to both high- and low/middle-income countries due to the potential effects on public health. Specific antiviral medication for the management of flavivirus infections remains an unmet medical need, despite the urgent need for an effective treatment (Silva *et al.*, 2018).

High-throughput screening of libraries of small molecules is a powerful tool to identify novel flavivirus antivirals. In parallel, repurposing of "old" drugs to identify compounds with novel activity can be a useful strategy to overcome the high cost and the time required for the antiviral drug-discovery pipeline (Balasubramanian *et al.*, 2016; Boldescu *et al.*, 2017).

In the area of drug discovery, the development of methods for the assessment of antiviral effects *in vitro* is a key step for the screening of either *de novo* or repurposed candidate compounds, to be accomplished before the *in vivo* assessment. Among the variety of methods that have been developed (Gong, 2013), cell-based assays are the most predictive methods to define antiviral activity. Candidate anti-flavivirus compounds are usually screened on monkey (VERO E6) or insect (C6/36) cell lines; however *in vitro* screening and analysis of candidate antiviral drugs is best performed by using human cell lines, which are more representative of *in vivo* virus-host interaction during therapy (Julander *et al.*, 2017b; Sacramento *et al.*, 2017). In this context, the development of robust, easy-to-perform, and fast cell-based assays is highly valuable to test candidate inhibitors. Despite Plaque Reduction Assay (PRA) is considered the gold standard method for titration of flavivirus and for the determination of antiviral activity of investigational compounds, this procedure is not amenable for high-throughput screening of candidate antivirals (Boldescu *et al.*, 2017).

In this study we have developed a fast and accurate flavivirus immunodetection assay (IA) which allows the simultaneous quantification of ZIKV and DENV viral antigen in the infected human hepatoma Huh7 cell line, using a specific monoclonal antibody which binds to the fusion loop of domain II of protein E, which is well conserved among flaviviruses. This assay was applied as the read-out of a direct yield reduction assay (YRA), to determine the inhibitory effect of reference compounds. To validate the assay, sofosbuvir and ribavirin half-maximal inhibitory concentrations (IC_{50}) were determined in direct YRA using different viral inputs (100, 50 and 25 50% tissue culture infectious dose, $TCID_{50}$) and compared with values obtained by PRA and with

values previously reported in the literature. In the direct YRA, at 100, 50, and 25 $TCID_{50}$, sofosbuvir IC_{50} values were 5.0 ± 1.5, 2.7 ± 0.5, 2.5 ± 1.1 µM against ZIKV and 16.6 ± 2.8, 4.6 ± 1.4, 2.6 ± 2.2 µM against DENV; ribavirin IC_{50} values were 6.8 ± 4.0, 3.8 ± 0.6, 4.5 ± 1.4 µM against ZIKV and 17.3 ± 4.6, 7.6 ± 1.2, 4.1 ± 2.3 µM against DENV. Based on reproducibility within replicates and correlation with PRA, the viral input corresponding to 50 $TCID_{50}$ was set as the optimal amount to perform the direct YRA.

In addition, viral stocks generated in the direct YRA were transferred to a second cell culture in the absence of drug (secondary YRA), to better characterize antiviral activity exerted at steps occurring later than envelope expression. To evaluate the ability of the system to discriminate between early and late antiviral effects, the IC_{50} of celgosivir, an α-glucosidase inhibitor acting at late steps of DENV infection, was determined by both a direct and secondary YRA, as well as by the reference PRA against both viruses. In agreement with the proposed mechanism of this compound, no antiviral activity was reported for the direct YRA, while celgosivir was able to inhibit DENV replication in the secondary YRA (IC50 11.0 ± 1.0 µM), very close to PRA IC_{50} (10.1 ± 1.1 µM) and to literature results.

In summary, the advantages of the IA with respect to the gold standard PRA include (i) the use of the same protocol for two different viruses, (ii) the ability to distinguish between early and late antiviral effects, (iii) the automated readout directly proportional to virus production and consequently to virus inhibition, (iv) the possibility to perform the entire assay within one week. Thus, the system provides an opportunity to expand the potential for fast cell-based screening of multiple compounds for anti-flavivirus therapy.

All the experimental data are reported in the attached paper at the end of the thesis from page 81 to page 89.

5.Evaluation of sofosbuvir activity and resistance profile against West Nile virus in vitro

Similar to other flaviviruses, West Nile Virus (WNV), which causes serious neurological disease in a small percentage of infected patients, currently has no valid therapeutic options and the treatment of infected patients is based only on supportive care. Therefore, there is an urgent need for the development of new antiviral drugs to decrease WNV related morbidity and mortality (Kok, 2016). A convenient strategy in drug research is drug repurposing, based on the investigation of existing drugs for new therapeutic purposes. The repositioning of "old" drugs to treat both common and rare diseases is increasingly becoming an attractive strategy, because it involves the use of de-risked compounds with potentially lower overall development costs and shorter development timelines.

Sofosbuvir is a nucleotide analog licensed for the treatment of HCV infection, which targets the HCV RNA-dependent RNA polymerase (RdRp) and exerts a potent inhibitory activity against this virus (Götte and Feld, 2016). Given the high degree of structural homology among RdRp enzymes within the Flaviviridae family (Lim *et al*., 2013), the antiviral activity of sofosbuvir has been evaluated as an anti-flavivirus lead candidate, showing inhibitory activity against ZIKV and YFV both *in vitro* and in animal models, as well as against DENV *in vitro* (De Freitas *et al*., 2019; Mesci *et al*., 2018; Sacramento *et al*., 2017); in addition an antiviral activity has been detected also against the alphavirus Chikungunya (CHIKV) both *in vitr*o and in animal models (Ferreira *et al*., 2019).

During my PhD, I was involved in the evaluation of *in vitro* antiviral activity of sofosbuvir against WNV through Plaque Assay (PA) and Immunodetection Assay (IA) in human cell lines and by enzymatic RdRp assay. Moreover, the selection of virus escape mutations in presence of sofosbuvir pressure was investigated *in vitro* by resistance selection experiments consisting in the treatment of Huh7 infected cell lines with two-fold increasing concentrations of sofosbuvir.

All the data are described in detail in the attached published paper at the end of the thesis from page 90 to page 96.

6. ORIGINALE CHEMIAE in Antiviral Strategy - Origin and Modernization of Multi-Component Chemistry as a Source of Innovative Broad Spectrum Antiviral Strategy

Background

General consensus exists on the fact that Multi-Component Chemistry (MCC) gave origin to nucleic acids and heterocyclic secondary metabolites on our planet. This chemistry was characterized by the capability of generating high chemical diversity, setting the molecular pathway for the emergence of the Last Universal Common Ancestor (LUCA) (Shirt-Ediss *et al*., 2017). Even if viruses are simple biological entities, they have evolved from the same prebiotic world leading to the emergence of LUCA. This makes reasonable and attractive the hypothesis that MCC can generate novel antivirals.

Viral pathogens, including old re-emerging viruses and new emerging viruses, still represent a serious threat for global health. Enhanced globalization and climate changes contribute to increase the worldwide spreading of different viruses, which are no longer confined to geographically limited risk areas. Despite different vaccines and antiviral drugs have been developed in the last century, several viruses belonging to different families are still untreatable (De Clercq *et al*., 2016). The availability of broad-spectrum antivirals (BSAs) acting on highly conserved targets (either viral or host) may offer the possibility to immediately initiate prophylactic as well as therapeutic treatments against viral pathogens for which no drugs have been developed so far. In addition, BSAs may offer better treatment options for multi-species co-infections. The original MCC has been recently reproduced in controlled conditions (Rotelli *et al*., 2016) and nowadays the modernization of the MCC associated chemical techniques can speed up the production of complex heterocyclic derivatives (Radi *et al*., 2010). In this context, MCC may represent an innovative approach for the discovery of BSAs. To investigate this hypothesis, a network composed by a panel of experienced laboratories in antiviral drug discovery and development has been formed to fulfill the objectives of the "ORIGINALE CHEMIAE in Antiviral Strategy" project, aimed to explore the modern MCC approaches to generate innovative antiviral molecules.

Among the laboratories involved in the project, our task was to define the antiviral activity of molecules generated by the different research groups in standardized virus-cell systems.

Materials and Methods

Antiviral activity of the candidate antiviral molecules was determined against i) the flaviviruses DENV serotype 2 strain and WNV lineage 1 strain, ii) the lentivirus HIV-1 NL4-3 strain. Following the recent pandemic, the project was also extended to the newly discovered coronavirus SARS-CoV-2, using a strain derived from the first pandemic wave as kindly provided by the University of Milan.

To assess the antiviral activity of candidate molecules against DENV, WNV and HIV-1, cell-based assays were performed as previously published (Dragoni *et al*., 2020; Saladini *et al*., 2018; Vicenti *et al*., 2020a). The immunodetection assay was used as read-out in the infected Huh7 cells to quantify the flaviviruses E protein (Vicenti *et al.,* 2020a), while for HIV-1, the luciferase activity was determined in infected TZM-bl reporter cell line (Saladini *et al*., 2018). For SARS-CoV-2, a new virus-cell line system has been optimized, employing the human colon adenocarcinoma Caco-2 cell line (ATCC HTB-37) and using immunodetection to quantify the SARS-CoV-2 N protein expression (Vicenti *et al*., 2021). Cytotoxicity was evaluated in each cell line as previously described (Vicenti *et al*., 2020a)(Cesarini *et al.*, 2022) using the CellTiter-Glo 2.0 Luminescent Cell Viability Assay to measure cell viability. The luminescent signal generated by cells treated with the test compound was compared with that generated by cells treated with DMSO/water to determine the half-maximal cytotoxic concentration (CC_{50}). The non-toxic compound dose in each cell line was used as starting concentration in the antiviral assays. Half-maximal drug inhibitory concentration (IC_{50}) was determined as previously described (Cesarini *et al*., 2022).

The SARS-CoV-2 antiviral assay was validated using the nucleoside inhibitor remdesivir, which has shown potent anti-SARS-COV-2 activity *in vitro* (Sanders *et al*., 2020)(Wang *et al*., 2020). Sofosbuvir and raltegravir were used as reference compound for flaviviruses and HIV-1 respectively. Indeed sofosbuvir, approved for HCV therapy, inhibits WNV and DENV RNA-dependent RNA polymerase *in vitro* while raltegravir is active against the HIV-1 integrase. Molecules identified by the acronym MR were provided by the research group of Prof. Marco Radi from the University of Parma, molecules which starts with the letter T were provided by the research group of Prof. Serena Massari from the University of Perugia, whereas the remaining compounds were provided by the research group of Prof. Lorenzo Botta from the University of Tuscia.

Results and discussion

Anti-WNV activity: a total of 38 candidate molecules were screened to determine a potential antiviral effect against WNV. Ten compounds showed cytotoxicity in the Huh7 cell line and for this reason were not selected for antiviral activity testing. Of the remaining 28, 2 compounds were active: the T274I with a mean IC_{50} value of 6.7±3.7 µM and the T275I with a mean IC_{50} value of 19.3±1.4 µM (Table 6.1).

Anti-DENV activity: all the candidate molecules were tested against DENV. Eleven compounds showed cytotoxicity in the Huh 7 cell line and were not tested for the antiviral activity. Of the remaining, 5 compounds showed anti-DENV activity in the low micromolar range with IC_{50} value of 2.0±0.8 µM for T183, 9.5±3.5 µM for T274I, 13.0±4.5 µM for T275I; 4.3±1.5 µM for MR477; 14.1±4.1 µM for MR488 (Table 6.1).

Anti-HIV-1 activity: a total of 28 candidate molecules were tested against HIV-1. Of these, 5 were excluded because of cytotoxicity in the H9 cell line. Of the remaining, 3 compounds, MR477, MR472 and MR478 were active with mean IC_{50} value of 40.4±3.4 µM, 21.6±6.2 µM, and 2.0±1.2 µM respectively (Table 6.1).

Anti-SARS-CoV-2 activity: a total of 29 compounds were tested against SARS-CoV-2. Of these, 8 compounds were cytotoxic and consequently were not tested. Of the remaining, 2 compounds were active: MR477 with mean IC_{50} value of 8.5±5.0 µM and T183 with mean IC_{50} value of 17.5±3.3 µM. (Table 6.1).

Among the active candidates, one compound, namely MR477, was able to simultaneously inhibit HIV-1, SARS-CoV-2 and DENV. Moreover, the compound T183 was found to be active against the SARS-CoV-2 and DENV. Notably, the compounds T274I and T275I were able to inhibit both DENV and WNV. Finally, the compound MR488 was found to be active against DENV and the compounds MR472 and MR478 were both able to inhibit HIV-1

Table 6.1. Antiviral activity of candidate compounds against WNV, DENV, HIV-1 and SARS-CoV-2, expressed as the mean of the $IC_{50} \pm$ the standard deviation (SD) and their corresponding selectivity index (SI). Compounds were tested against WNV and DENV in Huh7 cells, against HIV-1 in lymphoblastoid H9 and TZM-bl cells, and against SARS-CoV-2 in Caco-2 cells. Only molecules showing activity at least against one viral strain tested have been reported.
Sofosbuvir, raltegravir and remdesivir were used as positive controls for WNV/DENV, HIV-1 and SARS-CoV-2 inhibitory activities, respectively.

	WNV		DENV		HIV-1		SARS-CoV-2	
CMP ID	IC_{50} (μM) ± SD	SI	IC_{50} (μM) ± SD	SI	IC_{50} (μM) ± SD	SI	IC_{50} (μM) ± SD	SI
MR477	NOT ACTIVE	/	2.0±0.8	3.3	21.6±6.2	4.63	8.5±5.0	28.59
T183	NOT ACTIVE	/	13.0±4.5	30.8	NOT TESTED	/	17.5±3.3	22.9
T274I	6.7±3.7	2.7	4.3±1.5	4.3	NOT TESTED	/	NOT ACTIVE	/
T275I	19.3±1.4	7.3	14.1±4.1	10	NOT TESTED	/	NOT ACTIVE	/
MR472	NOT TESTED	/	NOT ACTIVE	/	40.4±3.4	2.48	NOT ACTIVE	/
MR478	NOT ACTIVE	/	NOT TESTED	/	2.0±1.2	38	NOT ACTIVE	/
MR488	NOT ACTIVE	/	9.5±3.5	2.97	NOT ACTIVE	/	NOT ACTIVE	/
Sofosbuvir	5.3±2.5	75.5	8.1±1.1	49.4	/	/	/	/
Raltegravir	/	/	/	/	2.8±1.7 nM	3571.4	/	/
Remdesivir	/	/	/	/	/	/	0.047±0.02	1702.1

Conclusions

A first panel of candidate antiviral compounds was screened, and antiviral activity was assessed against WNV, DENV, HIV-1 and SARS-CoV-2. A total of 8 of the 47 molecules synthesized had a measurable inhibitory activity against at least one of the viruses tested. However, one of the main objectives of the "ORIGINALE CHEMIAE in Antiviral Strategy" project was aimed at identifying BSAs. Notably, among the active compounds, 3 were able to inhibit simultaneously at least two different viruses, while one showed antiviral activity against 3 different viruses.

7. MONOCLONAL ANTIBODIES AND ANTIVIRALS vs SARS-CoV-2

Thanks to large investments and rapid research progress, the spectrum of medical interventions to prevent and treat COVID-19 has rapidly evolved (Anand et al., 2012). Worldwide vaccination has been the main method to reduce the spread of infection and the severity of disease in healthy individuals. In SARS-CoV-2 infected patients at high risk of disease progression, different therapeutic agents directly targeting the viral replication cycle are currently available (www.covid19treatmentguidelines.nih.gov), including different monoclonal antibodies (mAbs), antiviral drugs coming from repurposing strategies, such as remdesivir (FDA approved) and molnupiravir (authorized under emergency use authorization, EUA), or newly developed, such as nirmatrelvir (EUA). However, development of novel drugs remains a key priority because currently available antivirals are not highly effective, and their use is limited by drug-drug interactions (nirmatrelvir), inconvenient administration (mAbs and remdesivir) or toxicity in the fragile population (molnupiravir).

Among available treatments, neutralizing mAbs have been shown to be safe and reduce disease progression and mortality (Jiang *et al*., 2020). However, the viral spike evolution during the different pandemic waves has progressively led to the loss of efficacy of approved mAbs and the consequent need for renewing the mAb arsenal. During my PhD, we also contributed to document the SARS-CoV-2 variant dependence of licensed mAbs through the determination of their neutralizing activity by an ex vivo assay (Fiaschi *et al*., 2022; Dragoni *et al*., 2022). The live virus microneutralization assay was performed in VERO E6 cells using a quantitative read out based on cell viability, as previously published (Vicenti *et al*., 2021).

Similarly, we evaluated the efficacy of the directly acting antiviral drugs (DAA) nirmatrelvir, remdesivir and molnupiravir against different SARS-CoV-2 variants (Fiaschi *et al*., 2022). Briefly, to determine the IC_{50} of DAAs we infected the VERO E6 cell line using 0.005 MOI and after 72 hours incubation we measured cell viability using the Cell-Titer Glo protocol as previously published (Vicenti *et al*., 2021). Infected and uninfected cells without the drug were used to determine the 100% and the 0% of viral replication, respectively. Different from the mAbs, DAAs retained activity against all tested variants because the viral RNA polymerase inhibited by remdesivir and molnupiravir (Kokic *et al*., 2021; Kabinger *et al*., 2021), and the viral main protease inhibited by nirmatrelvir are less prone to viral evolution.

All the data of the experiments are reported in the paper attached at the end of the thesis from page 108 to page 117.

DISCUSSION

During the last century, emerging and re-emerging viruses have frequently created public health concerns, mostly favoured by climate changes, population density and people's migration and lifestyle, e.g. living in close proximity to wild animals and livestock. As demonstrated by the latest outbreak of SARS-CoV-2, the preparedness to such events must be improved. One critical area is the lack of antiviral drugs to treat severe infections and counteract viral spread. For this reason, the development of broad-spectrum antiviral drugs is a high priority and the setup of accurate, robust and convenient laboratory assays to assess the antiviral activity of candidate molecules is needed.

One of the most troublesome medical crises of our time has been represented by the AIDS (Acquired Immune Deficiency Syndrome) pandemic. Despite continuous efforts to contain viral transmission, there is still a considerable number of new infections (1.5 million in 2021 according to UNAIDS data). Since an important number of new infections is coming from the sub-Saharan Africa, the last 1st December 2022 the WHO (World Health Organization) underlined to global leaders and citizens the marked inequalities between high and low/middle-income countries, which are preventing the achievement of the goals of the 95-95-95 target, i.e. diagnosing 95% of the infections, treating 95% of those diagnosed and achieving treatment success in 95% of those treated.

A positive note is represented by the continuously improving access to antiretroviral therapy. Indeed, 28.7 million people had medications in 2021, compared with only 7.8 million in 2010. Although the vast majority of treated individuals have undetectable viral load thanks to the increased coverage and efficacy of ART, the emergence and accumulation of drug resistance may compromise virological suppression in a small percentage of subjects, particularly in the context of limited treatment options. Therefore, the identification of new antivirals with improved safety, tolerability and efficacy is highly awaited.

Viral disease control may benefit not only from the discovery of new drugs, but also from drug repurposing which has gained more attention in the latest years to fight emerging or re-emerging pathogens. Indeed, this time and cost saving strategy is based on obtaining safe and efficient treatment through the discovery of novel therapeutic targets of pre-existing or already approved drugs (Sahoo *et al.*, 2021).

In these contexts, during my PhD at the HIV Monitoring Laboratory (HML) I could actively participate in the evaluation of newly licensed and investigational drugs tested on laboratory adapted viral isolates, mutant clones and recombinant viruses harbouring clinically derived viral sequences obtained from samples stored in our biobank or received from the PRESTIGIO registry biobank.

Two studies were dedicated to assessing the residual activity of the new NNRTI doravirine against viruses harbouring different patterns of NNRTI resistance

mutations. Globally, these studies confirmed that doravirine has superior antiviral activity with respect to the other NNRTIs, but the activity might be compromised by the presence of multiple NNRTI resistance mutations, even in the absence of specific doravirine mutations. In particular, the presence of three or more NNRTI resistance mutations is likely associated with a partial or complete loss of doravirine activity. In the study analysing the activity of doravirine in viruses collected from individuals harbouring multidrug resistant viruses, we found that only 23% of viruses were still susceptible to doravirine, indicating a relevant degree of cross-resistance among NNRTIs. On the other hand, doravirine may represent a valuable option for salvage therapy in a proportion of subject with limited therapeutic options, thus helping to achieve viral suppression together with the newly licensed drugs approved for the treatment of multidrug resistant viruses such as ibalizumab, fostemsavir and lenacapavir.

Another study was focused on the role of the natural polymorphism of the reverse transcriptase V106I, which was found to emerge together with other mutations in some cases of virological failure during clinical trials. Our study indicated that this aminoacidic variant per se minimally affect the susceptibility to doravirine in clinical isolates and does not impact the genetic barrier to resistance as compared to reference wild-type virus, while viruses including the NNRTI resistant mutation V106A or V106M rapidly showed viral breakthrough under doravirine pressure due to the reduced susceptibility. Our study suggests that the V106I polymorphism does not affect the susceptibility of doravirine in most cases, while sporadic cases of reduced antiviral activity might be due to unknown interactions with the genetic background.

Our data supports the use of doravirine in naïve individuals harbouring the V106I virus and in a proportion of highly treated patients thanks to its improved genetic barrier and partially distinct resistance pathway with respect to other NNRTIs. This role is further supported by doravirine tolerability and low potential for drug-drug interactions.

Continuing my collaboration with the Prestigio Registry, the study focusing on the investigational NRTTI islatravir confirmed the previous findings indicating the prominent role of the M184V mutation in the decrease of susceptibility. Considering the frequent detection of M184V mutation in multidrug resistant viruses due to the long-term exposure to NRTIs, we might figure out that islatravir activity can be partly reduced in this patient population. However, the clinical impact of NRTI mutations in the activity of islatravir has still to be defined and the threshold of fold-change values associated to reduced activity in vivo remains to be established.

In the context of salvage therapy, the humanized IgG4 monoclonal antibody Ibalizumab is a valuable option for the salvage therapy thanks to its safety and efficacy due to the unique mechanism of action. Due to the importance of choice of the best treatment option for the building of an effective salvage therapy, I focused my attention on the evaluation of the combinatorial activity of Ibalizumab together with other antivirals, both approved and investigational. Using a newly developed cell-

based assay consisting in the infection of the MOLT4-R5 cell line and the innovative software SynergyFinderPlus, we found that the combination of ibalizumab and temsavir, the active compound of the attachment inhibitor fostemsavir, showed synergistic activity against both NL4-3 and AD8, suggesting a similar effect on X4- and R5-tropic viruses. The same synergistic activity was not detected with the CCR5 antagonists maraviroc and PRO-140 in this study, while a previous work found that the combination of ibalizumab and the fusion inhibitor enfuvirtide was associated with synergistic activity. All these findings indicate that despite all acting on HIV-1 entry, drugs inhibiting different steps might interact differently with one another, contributing additive or synergistic effects. Since ibalizumab and fostemsavir were licensed for the treatment of individuals with limited therapeutic option, our data support the combined use of these two drugs. However, the impact of the natural variability of the Env protein among individuals might be associated with a different combinatorial activity of ibalizumab and fostemsavir and consequently to a variable synergistic activity. Interestingly, a strong synergy score was identified in the combination of Ibalizumab and Lenacapavir, another drug currently approved for the treatment of patients with multidrug resistant viruses.

Another promising method to counteract viral diseases is the development of broad-spectrum antivirals (BSAs), which may ambitiously allow treatment of multi-species co-infections, as well as treatment against novel viral agents or pathogens for which no drugs have been developed so far. In this scenario, the "ORIGINALE CHEMIAE in Antiviral Strategy" project aims to take advantage of the multi-component chemistry (MCC) strategy to identify promising BSAs. Within this project, we were able to identify 8 molecules which inhibit at least one of the viruses tested (HIV-1, DENV, WNV, SARS-CoV-2). More in detail, 3 were able to inhibit simultaneously at least two different viruses (one DENV and SARS, two WNV and DENV), while one showed antiviral activity against 3 different viruses (DENV, HIV-1, SARS-CoV-2). However, all the active compounds showed relatively low selectivity indexes, indicating that these molecules require further improvement to increase the antiviral activity and/or reduce the cell toxicity in order to identify candidates for preclinical testing in animal models.

In parallel with the evaluation of different BSAs, our laboratory played a role also in drug repurposing, focusing on the possible activity of Sofosbuvir against WNV. After the initial set-up of cell-based and enzymatic assays which were adapted to WNV, we were able to describe for the first time the sofosbuvir antiviral activity against WNV in the low micromolar range. Since sofosbuvir high genetic barrier to resistance is a prominent hallmark of this anti-HCV treatment, we investigated the sofosbuvir genetic barrier against WNV. *In vitro* selection and molecular docking experiments indicated that HCV and WNV share a similar sofosbuvir resistance pattern.

Moreover, we also tested the efficacy of the antiviral drugs remdesivir, molnupiravir and the recent identified nirmatrelvir against dominant variants emerged during the

SARS-CoV-2 pandemic by using a live virus antiviral assay (Fiaschi et al., 2022), resulting in a comparable activity against all the variants tested. These results indicate that despite the spread of different genetic variants, the viral target of these molecules remained well conserved, thus not affecting the activity of the licensed antivirals.

The last few years taught us both the importance of developing new strategies against viruses that can emerge or re-emerge under partly unpredictable circumstances, and the limitations in our preparedness to such pandemic events, despite impressive advancements in many areas of biomedical technology. Notable examples are the inability to clear HIV infection despite more than 35 years of intensive work and the impressive number of deaths caused by COVID-19 despite the rapid development of vaccine that has significantly contributed to generate immunity among humans in a relatively short time. Noteworthy, drug design has also improved dramatically in the ability and speed to develop highly effective and selective antivirals. Since viruses will continue to explore the biosphere, occasionally attacking humans and any kind of living organisms, the importance of virology, and the "One virology one health" paradigm is even more evident. It remains at the core of the multidisciplinary effort required to cope with viral threatens, connecting drug design and vaccine discovery with the final delivery of interventions protecting the human population from severe viral infections.

REFERENCES

- Anand, U.; Jakhmola, S.; Indari, O.; Jha, H.C.; Chen, Z.S.; Tripathi, V.; Pérez de la Lastra, J.M. Potential Therapeutic Targets and Vaccine Development for SARS-CoV-2/COVID-19 Pandemic Management: A Review on the Recent Update. Frontiers in Immunology 2021, 12.
- Asante-Appiah E., Lai J., Wan H., Yang D., Martin E. A., Sklar P., Hazuda D., Petropoulos C.J., Walworth C., Grobler J.A.; Impact of HIV-1 Resistance Associated Mutations on Susceptibility to Doravirine: Analysis of Real-World Clinical Isolates; Antimicrobial Agents and Chemotherapy; 2021.
- Balasubramanian, A., Manzano, M., Teramoto, T., Pilankatta, R., Padmanabhan, R., 2016. High-throughput screening for the identification of small-molecule inhibitors of the flaviviral protease. Antiviral Res. https://doi.org/10.1016/j.antiviral.2016.08.014.
- Beccari, M. V., Mogle, B. T., Sidman, E. F., Mastro, K. A., Asiago-Reddy, E., & Kufel, W. D. (2019). Ibalizumab, a novel monoclonal antibody for the management of multidrug-resistant HIV-1 infection. *Antimicrobial Agents and Chemotherapy*, *63*(6). https://doi.org/10.1128/AAC.00110-19.
- Boldescu, V., Behnam, M.A.M., Vasilakis, N., Klein, C.D., 2017. Broad-spectrum agents for flaviviral infections: Dengue, Zika and beyond. Nat. Rev. Drug Discov. 16, 565–586. https://doi.org/10.1038/nrd.2017.33.
- Cesarini, S., Vicenti I., Poggialini F., Secchi M., Giammarino F., Varasi I., Lodola C., Zazzi M., Dreassi E., Maga G., Botta L. (2022) 'Privileged Scaffold Decoration for the Identification of the First Trisubstituted Triazine with Anti-SARS-CoV-2 Activity', Molecules, pp. 1–11.
- Cilento M.E., Reeve A.B., Michailidis E., Ilina T.V., Nagy E., Mitsuya H., Parniak M.A., Tedbury P.R., Sarafianos S.G. 2021. Development of Human Immunodeficiency Virus Type 1 Resistance to 49-Ethynyl-2-Fluoro-29-Deoxyadenosine Starting with Wild-Type or Nucleoside Reverse Transcriptase InhibitorResistant Strains. Antimicrobial Agentes and Chemotherapy.
- Clercq, E. de, E., D.C., 2016. Approved antiviral drugs over the past 50 years. Clin. Microbiol. Rev. 29, 695–747. https://doi.org/10.1128/CMR.00102-15.Address.
- Colombier, Molina, Doravirine: A review; Current Opinion in HIV and AIDS, 2018.
- Correll T.A., Molina J.M., Klopfer S., Grandhi A., Lahoulou R., Zhou Y.P., Eves K., Squires K. Total Lymphocyte and Lymphocyte Subset Changes in Participants Receiving Islatravir (0.25, 0.75 and 2.25mg QD) and Doravirine (DOR) +/-Lamivudine (3TC): Post-Hoc Analysis from a Phase 2b Dose-Ranging Study (P011). HIV Glasgow 2022.

- De Freitas, C.S., Higa, L.M., Sacramento, C.Q., Ferreira, A.C., Reis, P.A., Delvecchio, R., Monteiro, F.L., Barbosa-Lima, G., James Westgarth, H., Vieira, Y.R., Mattos, M., Rocha, N., Hoelz, L.V.B., Leme, R.P.P., Bastos, M.M., Gisele, G.O., Carla, C.E., Queiroz-Junior, C.M., Lima, C.X., Costa, V. V., Teixeira, M.M., Bozza, F.A., Bozza, P.T., Boechat, N., Tanuri, A., Souza, T.M.L., 2019. Yellow fever virus is susceptible to sofosbuvir both in vitro and in vivo. PLoS Negl. Trop. Dis https://doi.org/10.1371/journal.pntd.0007072.
- Deigendesch, N., Stenzel, W., 2018. Acute and chronic viral infections, 1st ed, Handbook of Clinical Neurology. Elsevier B.V. https://doi.org/10.1016/B978-0-12-802395-2.00017-1.
- Diamond T.L., Ngo W., Xu M., Goh S.L., Rodriguez S., Lai M.T., Asante-Appiah E., Grobler J.A. 2022. Islatravir Has a High Barrier to Resistance and Exhibits a Differentiated Resistance Profile from Approved Nucleoside Reverse Transcriptase Inhibitors (NRTIs). Antimicrobial Agentes and Chemotherapy.
- Dragoni, F., Boccuto, A., Picarazzi, F., Giannini, A., Giammarino, F., Saladini, F., Mori, M., Mastrangelo, E., Zazzi, M., Vicenti, I., 2020. Evaluation of sofosbuvir activity and resistance profile against West Nile virus in vitro. Antiviral Res. 175, 104708. https://doi.org/10.1016/j.antiviral.2020.104708.
- Dragoni, F., Schiaroli, E., Micheli, V., Fiaschi, L., Lai, A., Zehender, G.Rossettti B., Gismondo M.R., Francisci D., Zazzi M., Vicenti, I. (2022). Impact of SARS-CoV-2 omicron BA.1 and delta AY.4.2 variants on the neutralization by sera of patients treated with different authorized monoclonal antibodies. *Elsevier*, (January), 2020–2023.
- Eleftherios Michailidis, Emily M Ryan, Atsuko Hachiya, Karen A Kirby, Bruno Marchand, Maxwell D Leslie, Andrew D Huber, Yee T Ong, Jacob C Jackson, Kamalendra Singh, Eiichi N Kodama, Hiroaki Mitsuya, Michael A Parniak and Stefan G Sarafianos. Hypersusceptibility mechanism of Tenofovir-resistant HIV to EFdA. Retrovirology 2013 Jun 24. DOI: 10.1186/1742-4690-10-65.
- Emu, B., Fessel, J., Schrader, S., Kumar, P., Richmond, G., Win, S., … Lewis, S. (2018). Phase 3 Study of Ibalizumab for Multidrug-Resistant HIV-1. *New England Journal of Medicine*, *379*(7), 645–654. https://doi.org/10.1056/NEJMoa1711460.
- Feng M., Wang D., Grobler J. A., Hazuda D. J., Miller M. D., Lai M. T.; In vitro resistance selection with doravirine (MK-1439), a novel nonnucleoside reverse transcriptase inhibitor with distinct mutation development pathways; Antimicrobial Agents and Chemotherapy, 2015.
- Feng M., Sachs N. A., Xu M., Grobler J., Blair W., Hazuda D. J, Miller M. D., Lai M.T.; Doravirine Suppresses Common Nonnucleoside Reverse Transcriptase Inhibitor-Associated Mutants at Clinically Relevant Concentrations; Antimicrobial Agents and Chemotherapy; 2016.

- Ferreira, A.C., Reis, P.A., de Freitas, C.S., Sacramento, C.Q., Hoelz, L.V.B., Bastos, M.M., Mattos, M., Rocha, N., de Azevedo Quintanilha, I.G., da Silva Gouveia Pedrosa, C., Souza, L.R.Q., Loiola, E.C., Trindade, P., Vieira, Y.R., Barbosa-Lima, G., de Castro Faria Neto, H.C., Boechat, N., Rehen, S.K., Brüning, K., Bozza, F.A., Bozza, P.T., Souza, T.M.L., 2019. Beyond members of the Flaviviridae family, sofosbuvir also inhibits chikungunya virus replication. Antimicrob. Agents Chemother. 63. https://doi.org/10.1128/AAC.01389-18.
- Fiaschi, L., Dragoni, F., Schiaroli, E., Bergna, A., Rossetti, B., Giammarino, F.,Biba C., Gidari A., Lai A., Nencioni C., Francisci D., Zazzi M., Vicenti, I. (2022). Efficacy of Licensed Monoclonal Antibodies and Antiviral Agents against the SARS-CoV-2 Omicron Sublineages BA.1 and BA.2. *Viruses*, *14*(7), 1–9. https://doi.org/10.3390/v14071374.
- Gidari, A.; Sabbatini, S.; Bastianelli, S.; Pierucci S.; Busti C.; Monari, C.; Pasqua, B.L.; Dragoni, F.; Schiaroli, E.; Zazzi M.; Francisci, D. Cross-neutralization of SARS-CoV-2 B.1.1.7 and P.1 variants in vaccinated, convalescent and P.1 infected. The Journal of infection 2021, S0163-4453(21)00362-5.
- Gombos, R. B., Kolodkin-Gal, D., Eslamizar, L., Owuor, J. O., Mazzola, E., Gonzalez, A. M., Korioth-Schmitz, B., Gelman, R. S., Montefiori, D. C., Haynes, B. F., & Schmitz, J. E. (2015). Inhibitory Effect of Individual or Combinations of Broadly Neutralizing Antibodies and Antiviral Reagents against Cell-Free and Cell-to-Cell HIV-1 Transmission. Journal of virology, 89(15), 7813–7828. https://doi.org/10.1128/JVI.00783-15
- Gong, E.Y., 2013. Antiviral Methods and Protocols, Methods in Molecular Biology. Humana Press, Totowa, NJ. https://doi.org/10.1007/978-1-62703-484-5.
- Götte, M., Feld, J.J., 2016. Direct-acting antiviral agents for hepatitis C: Structural and mechanistic insights. Nat. Rev. Gastroenterol. Hepatol. 13, 338–351. https://doi.org/10.1038/nrgastro.2016.60
- Grobler JA, Huang Q, Hazuda D, Lai M-T. Efficacy of MK-8591 against diverse HIV-1 subtypes and NRTI-resistant clinical isolates. Glasgow HIV; 28–31 2018 October.
- Jiang, S.; Hillyer, C.; Du, L. Neutralizing Antibodies against SARS-CoV-2 and Other Human Coronaviruses. *Trends in Immunology* 2020, *41*, 355–359.
- Julander, J.G., Siddharthan, V., Evans, J., Taylor, R., Tolbert, K., Apuli, C., Stewart, J., Collins, P., Gebre, M., Neilson, S., Van Wettere, A., Lee, Y.M., Sheridan, W.P., Morrey, J.D., Babu, Y.S., 2017b. Efficacy of the broad-spectrum antiviral compound BCX4430 against Zika virus in cell culture and in a mouse model. Antiviral Res. https://doi.org/10.1016/j.antiviral.2016.11.003
- Kabinger, F., Stiller, C., Schmitzová, J., Dienemann, C., Kokic, G., Hillen, H. S., Hobartner C., Cramer, P. (2021). Mechanism of molnupiravir-induced

SARS-CoV-2 mutagenesis. *Nature Structural and Molecular Biology*, *28*(9), 740–746. https://doi.org/10.1038/s41594-021-00651-0

- Kok, W.M., 2016. New developments in flavivirus drug discovery. Expert Opin. Drug Discov. 11, 433–445. https://doi.org/10.1517/17460441.2016.1160887.
- Kokic, G., Hillen, H. S., Tegunov, D., Dienemann, C., Seitz, F., Schmitzova, J., Farnung L., Siewert A., Hobartner C., Cramer, P. (2021). Mechanism of SARS-CoV-2 polymerase stalling by remdesivir. *Nature Communications*, *12*(1), 1–7. https://doi.org/10.1038/s41467-020-20542-0
- Le Hingrat Q., Collin G., Bachelard A., Ghosn J., Chalal S., Pacanowski J., Peytavin G., Weinheimer S., Marsolais C., Damond F., Matheron S., Charpentier C., Descamps D., and the ANRS CO5 HIV-2 cohort; (2022). Ibalizumab shows in-vitro activity against group A and group B HIV-2 clinical isolates; AIDS Volume 36 - Issue 8 - p 1055-1060
- Lim, S.P., Koh, J.H.K., Seh, C.C., Liew, C.W., Davidson, A.D., Chua, L.S., Chandrasekaran, R., Cornvik, T.C., Shi, P.Y., Lescar, J., 2013. A crystal structure of the dengue virus non-structural protein 5 (NS5) polymerase delineates interdomain amino acid residues that enhance its thermostability and de novo initiation activities. J. Biol. Chem. 288, 31105–31114. https://doi.org/10.1074/jbc.M113.508606
- Martin Markowitz and Jay A. Grobler. Islatravir for the treatment and prevention of infection with the human immunodeficiency virus type 1. Curr Opin HIV AIDS. 2020 Jan;15(1):27-32. doi: 10.1097/COH.0000000000000599.
- Martin E.A., Lai M.T., Ngo W., Feng M., Graham D., Hazuda D.J., Kumar S., Hwang C., Sklar P., Asante-Appiah E.; Review of Doravirine Resistance Patterns Identified in Participants During Clinical Development; Journal of Acquired Immune Deficiency Syndrome 2020.
- Matthews R.P., Fillgrove K.L., Patel M., Liu W., Matthews C.Z., Liu Y., Mirkin I., Stoch S.A., Iwamoto M. Characterization of the Absorption, Metabolism, and Excretion of Islatravir, an HIV Nucleoside Reverse Transcriptase Translocation Inhibitor, in Humans. IAS 2022.
- Maureen Oliveira, Bluma G. Brenner, Hongtao Xu, Ruxandra-Ilnca Ibanescu, Thibault Mesplède, Mark A. Wainberg. M184I/V substitutions and E138K/M184I/V double substitutions in HIV reverse transcriptase do not significantly affect the antiviral activity of EFdA. 2017, Nov. PMID: 28961903. PMCID: PMC5890679. DOI: 10.1093/jac/dkx280
- Matthews R.P., Handy W., Ankrom W., Patel M., Matthews C., Xu Z., Gravesande K., Stoch S.A., Iwamoto M. No Pharmacokinetic Interaction Between Islatravir and Methadone. IAS 2022
- Mesci, P., Macia, A., Moore, S.M., Shiryaev, S.A., Pinto, A., Huang, C.T., Tejwani, L., Fernandes, I.R., Suarez, N.A., Kolar, M.J., Montefusco, S., Rosenberg, S.C., Herai, R.H., Cugola, F.R., Russo, F.B., Sheets, N.,

Saghatelian, A., Shresta, S., Momper, J.D., Siqueira-Neto, J.L., Corbett, K.D., Beltrão-Braga, P.C.B., Terskikh, A. V., Muotri, A.R., 2018. Blocking Zika virus vertical transmission. Sci. Rep. 8, 1–13. https://doi.org/10.1038/s41598-018-19526-4

- Michailidis, E.; Huber, A.D.; Ryan, E.M.; Ong, Y.T.; Leslie, M.D.; Matzek, K.B.; Singh, K.; Marchand, B.; Hagedorn, A.N.; Kirby, K.A.; et al. 4'-ethynyl-2-fluoro-2'-deoxyadenosine (efda) inhibits HIV-1 reverse transcriptase with multiple mechanisms. J. Biol. Chem. 2014, 289, 24533–24548.

- Pace, C. S., Fordyce, M. W., Franco, D., Kao, C. Y., Seaman, M. S., & Ho, D. D. (2013). Anti-CD4 monoclonal antibody ibalizumab exhibits breadth and potency against HIV-1, with natural resistance mediated by the loss of a V5 glycan in envelope. *Journal of Acquired Immune Deficiency Syndromes*, *62*(1), 1–9. https://doi.org/10.1097/QAI.0b013e3182732746.

- Pierson, T.C., Diamond, M.S., 2020. The continued threat of emerging flaviviruses. Nat. Microbiol. https://doi.org/10.1038/s41564-020-0714-0

- Radi, M., Botta, L., Casaluce, G., Bernardini, M., Botta, M., 2010. Practical one-pot two-step protocol for the microwave-assisted synthesis of highly functionalized rhodanine derivatives. J. Comb. Chem. https://doi.org/10.1021/cc9001789.

- Rose, R., Gartland, M., Li, Z., Zhou, N., Cockett, M., Beloor, J., … Krystal, M. (2022). Clinical evidence for a lack of cross-resistance between temsavir and ibalizumab or maraviroc. *Aids*, *36*(1), 11–18. https://doi.org/10.1097/QAD.0000000000003097.

- Rotelli, L., Trigo-Rodríguez, J.M., Moyano-Cambero, C.E., Carota, E., Botta, L., Di Mauro, E., Saladino, R., 2016. The key role of meteorites in the formation of relevant prebiotic molecules in a formamide/water environment. Sci. Rep. https://doi.org/10.1038/srep38888.

- Sacramento, C.Q., Melo, G.R. De, Rocha, N., Villas, L., Hoelz, B., Mesquita, M., Freitas, C.S. De, Fintelman-rodrigues, N., Marttorelli, A., Ferreira, A.C., Barbosa-lima, G., Bastos, M.M., Volotao, E.D.M., Tschoeke, D.A., Leomil, L., Bozza, F.A., Bozza, P.T., Boechat, N., Thompson, F.L., Filippis, A.M.B. De, Bruning, K., 2017. Next ○ The clinically approved antiviral drug sofosbuvir impairs Brazilian zika virus replication Neurochecklists Cérebro Reverso Ibrahim Imam. Nat. Publ. Gr. 7, 2016–2018. https://doi.org/10.1038/srep40920.

- Saladini F, Giannini A, Boccuto A, Vicenti I, Zazzi M. Agreement between an in-house replication competent and a reference replication defective recombinant virus assay for measuring phenotypic resistance to HIV-1 protease, reverse transcriptase, and integrase inhibitors. (2018) Journal of Clinical Laboratory Analysis, 32 (1), art. no. e22206.

- Salie, Z.L.; Kirby, K.A.; Michailidis, E.; Marchand, B.; Singh, K.; Rohan, L.C.; Kodama, E.N.; Mitsuya, H.; Parniak, M.A.; Sarafianos, S.G. Structural

basis of HIV inhibition by translocation-defective rt inhibitor 4'-ethynyl-2-fluoro-2'-deoxyadenosine (efda). Proc. Natl. Acad. Sci. USA 2016, 113, 9274–9279.

- Sanders, J.M., Monogue, M.L., Jodlowski, T.Z., Cutrell, J.B., 2020. Pharmacologic Treatments for Coronavirus Disease 2019 (COVID-19): A Review. JAMA - J. Am. Med. Assoc. https://doi.org/10.1001/jama.2020.6019

- Shirt-Ediss, B., Murillo-Sànchez, S., Ruiz-Mirazo, K., 2017. Framing major prebiotic transitions as stages of protocell development: Three challenges for origins-of-life research. Beilstein J. Org. Chem. https://doi.org/10.3762/bjoc.13.135.

- Silva, J.V.J., Lopes, T.R.R., Oliveira-Filho, E.F. d., Oliveira, R.A.S., Durães-Carvalho, R., Gil, L.H.V.G., 2018. Current status, challenges and perspectives in the development of vaccines against yellow fever, dengue, Zika and chikungunya viruses. Acta Trop. https://doi.org/10.1016/j.actatropica.2018.03.009.

- Singh Kamal, Sarafianos Stefan G., Sönnerborg, Anders. Long-Acting Anti-HIV Drugs Targeting HIV-1 Reverse Transcriptase and Integrase. Pharmaceuticals. 2019, April. PMID: 31010004. PMCID: PMC6631967. DOI: 10.3390/ph12020062.

- Smith S.J., Pauly G.T., Akrmam A., Melody K., Amborse Z., Schneider J.P., Hughes S.H.; Rilpivirine and Doravirine have complementary efficacies against NNRTI-Resistant HIV-1 mutants; J Acquir Immune Defic Syndr.; 2016.

- Takamatsu Y, Das D, Kohgo S, Hayashi H, Delino NS, Sarafianos SG, Mitsuya H, Maeda K. The High Genetic Barrier of EFdA/MK-8591 Stems from Strong Interactions with the Active Site of Drug-Resistant HIV-1 Reverse Transcriptase. Cell Chem Biol. 2018 Oct 18;25(10):1268-1278.e3. doi: 10.1016/j.chembiol.2018.07.014. Epub 2018 Aug 30. PubMed PMID: 30174310; PubMed Central PMCID: PMC6261781.

- Toma, J., Weinheimer, S. P., Stawiski, E., Whitcomb, J. M., Lewis, S. T., Petropoulos, C. J., & Huang, W. (2011). Loss of Asparagine-Linked Glycosylation Sites in Variable Region 5 of Human Immunodeficiency Virus Type 1 Envelope Is Associated with Resistance to CD4 Antibody Ibalizumab. *Journal of Virology*, 85(8), 3872–3880. https://doi.org/10.1128/jvi.02237-10

- Vargo R., Robey S., Zang X., Du L., Kandala B., Roberts J., Klopfer S., Correll T., Squires K. Modeling and Simulation to Optimize Islatravir Once Daily (QD) Doses in HIV Treatment Naïve and Virologically Suppressed Populations. HIV Glasgow 2022.

- Vicenti I, Meini G, Saladini F, Giannini A, Boccuto A, Schiaroli E, Zazzi M. Development of an internally controlled quantitative PCR to measure total cell-associated HIV-1 DNA in blood. (2018) Clinical Chemistry and Laboratory Medicine, 56 (3), pp. e75-e77.

- Vicenti, I., Dragoni, F., Giannini, A., Giammarino, F., Spinicci, M., Saladini,

F., Boccuto, A., Zazzi, M., 2020a. Development of a Cell-Based Immunodetection Assay for Simultaneous Screening of Antiviral Compounds Inhibiting Zika and Dengue Virus Replication. SLAS Discov. 25, 506–514. https://doi.org/10.1177/2472555220911456.

- Vicenti, I.; Gatti, F.; Scaggiante, R.; Boccuto, A.; Moldolo, E.; Zago, D.; Basso, M.; Dragoni, F.; Bartolini, N.; Zazzi, M.; et al. Time Course of Neutralizing Antibody in Healthcare Workers with Mild or Asymptomatic COVID-19 Infection. *Open Forum Infectious Diseases* **2021**, doi:10.1093/ofid/ofab312.

- Vicenti, I.; Gatti, F.; Scaggiante, R.; Boccuto, A.; Zago, D.; Basso, M.; Dragoni, F.; Zazzi, M.; Parisi, S.G. Single-Dose BNT162b2 MRNA COVID-19 Vaccine Significantly Boosts Neutralizing Antibody Response in Health Care Workers Recovering from Asymptomatic or Mild Natural SARS-CoV-2 Infection. *International Journal of Infectious Diseases* **2021**, *108*, doi:10.1016/j.ijid.2021.05.033.

- Vicenti I., Martina M.G., Boccuto A., De Angelis M., Giavarini G., Dragoni F., Marchi S., Trombetta C.M., Crespan E., Maga G., Eydoux C., Decroly E., Montomoli E., Nencioni L., Zazzi M., Radi M. (2021) "System-oriented optimization of multi-target 2,6-diaminopurine derivatives: Easily accessible broad-spectrum antivirals active against flaviviruses, influenza virus and SARS-CoV-2", Elsevier, (July).

- Wainberg MA, Zaharatos GJ, Brenner BG. Development of antiretroviral drug resistance. NEnglJMed2011; 365: 637–46.

- Wang, Chunyan, Li, W., Drabek, D., Okba, N.M.A., van Haperen, R., Osterhaus, A.D.M.E., van Kuppeveld, F.J.M., Haagmans, B.L., Grosveld, F., Bosch, B.J., 2020. A human monoclonal antibody blocking SARS-CoV-2 infection. Nat. Commun. https://doi.org/10.1038/s41467-020-16256-y.

PUBLISHED PAPERS INCLUDED

- In vitro cross-resistance to doravirine in a panel of HIV-1 clones harbouring multiple NNRTI resistance mutations. F. Saladini, F. Giammarino, B. A. Hosseini, A. Giannini, A. Boccuto, F. Dragoni, I. Vicenti, R. W. Shafer and Maurizio Zazzi. J Antimicrob Chemother. 2020.

- Residual phenotypic susceptibility to doravirine in multidrug resistant HIV-1 from subjects enrolled in the PRESTIGIO Registry. F. Saladini‡, F. Giammarino‡, F. Maggiolo, M. Ferrara, G. Cenderello, B. M. Celesia, F. Martellotta, V. Spagnuolo, G. M. Corbelli, N. Gianotti, M. M. Santoro, S. Rusconi, M. Zazzi, A. Castagna for the PRESTIGIO STUDY GROUP. IN PRESS. International Journal of Antimicrobial Agents. 2023.

- Development of a Cell-Based Immunodetection Assay for Simultaneous Screening of Antiviral Compounds Inhibiting Zika and Dengue Virus Replication. I. Vicenti, F. Dragoni, A. Giannini, F. Giammarino, M. Spinicci, F. Saladini, A. Boccuto, and M. Zazzi. SLAS Discovery. 2020.

- Evaluation of sofosbuvir activity and resistance profile against West Nile virus in vitro. F. Dragoni, A. Boccuto, F. Picarazzi, A. Giannini, F. Giammarino, F. Saladini, M. Mori, E. Mastrangelo, M. Zazzi, I. Vicenti. Antiviral Research. 2020.

- Privileged Scaffold Decoration for the Identification of the First Trisubstituted Triazine with Anti-SARS-CoV-2 Activity. S. Cesarini, I. Vicenti, F. Poggialini, M. Secchi, F. Giammarino, I. Varasi, C. Lodola, M. Zazzi, E. Dreassi, G. Maga, L. Botta and R. Saladino. Molecules. 2022.

- Efficacy of Licensed Monoclonal Antibodies and Antiviral Agents against the SARS-CoV-2 Omicron Sublineages BA.1 and BA.2. L. Fiaschi, F. Dragoni, E. Schiaroli, A. Bergna, B. Rossetti, F. Giammarino, C. Biba, A. Gidari, A. Lai, C. Nencioni, D. Francisci, M. Zazzi and I. Vicenti. Viruses. 2022.

In vitro cross-resistance to doravirine in a panel of HIV-1 clones harbouring multiple NNRTI resistance mutations

Francesco Saladini (ORCID) [1]*, Federica Giammarino[1], Behnaz A. Hosseini[1], Alessia Giannini[1], Adele Boccuto[1], Filippo Dragoni[1], Ilaria Vicenti (ORCID) [1], Robert W. Shafer[2] and Maurizio Zazzi[1]

¹Department of Medical Biotechnologies, University of Siena, Siena, Italy; ²Stanford University, Stanford, CA, USA

*Corresponding author. E-mail: saladini6@unisi.it

Objectives: Doravirine is a recently licensed HIV-1 NNRTI with improved efficacy, pharmacokinetics and safety profile compared with efavirenz and limited cross-resistance with rilpivirine and etravirine. In this *in vitro* study, cross-resistance to doravirine was analysed in a representative panel of NNRTI-resistant clones.

Methods: *In vitro* phenotypic susceptibility to doravirine was assessed in 10 clinically derived infectious clones with intermediate- to high-level resistance to rilpivirine, etravirine, efavirenz and nevirapine, and in NL4-3 site-directed mutants harbouring K103N, Y181C, M230L or K103N/Y181C NNRTI mutations.

Results: Although none of the infectious clones harboured any of the major doravirine resistance-associated mutations (RAMs) included in the IAS-USA reference list, doravirine fold change (FC) values were comparable to or higher than those calculated for other NNRTIs, particularly etravirine and rilpivirine. As expected, single NNRTI mutations K103N and Y181C did not impair doravirine susceptibility (FC 1.4 and 1.8, respectively), while reduced activity was observed with the single M230L or double K103N/Y181C mutations (FC 7.6 and 4.9, respectively). Median FC values increased significantly with increasing numbers of NNRTI RAMs ($P = 0.005$) and were >10 in 4/4 and 1/4 clones harbouring four and three NNRTI RAMs, respectively. FC values correlated well with predicted susceptibility as inferred by Stanford HIV Drug Resistance Database (HIVdb) and ANRS algorithms (both $P < 0.001$).

Conclusions: Substantial cross-resistance to doravirine was detected in NNRTI-resistant viruses harbouring complex mutational patterns, even in the absence of major IAS-USA doravirine RAMs. Therefore, based on the simple IAS-USA reference list, doravirine resistance may be underestimated in viruses harbouring multiple NNRTI mutations.

Introduction

Doravirine (formerly MK-1439) is a novel once-daily NNRTI approved by the US FDA for the treatment of HIV-1 in therapy-naive patients or as a switch option in virologically suppressed patients with no history of treatment failure and no known substitutions associated with resistance to doravirine.[1] The approval label of the EMA provided slightly different therapeutic indications, recommending the use of doravirine for the treatment of adults infected with HIV-1 without past or present evidence of resistance to the NNRTI class.[2] In clinical studies, doravirine showed non-inferior efficacy and improved pharmacokinetics and/or safety profile, both as a switch option in virologically suppressed patients[3] and as part of a first-line regimen, when compared with efavirenz and darunavir.[4,5] Moreover, doravirine was effective in halting viral replication even in the presence of transmitted NNRTI mutations, such as K103N and G190A, in a small group of treatment-naive patients.[6] Based on *in vitro* and *in vivo* data, the last update of the

IAS-USA HIV-1 drug resistance mutations list indicates V106A/M and Y188L as major doravirine mutations and V106I/T, Y188C/H, G190E, P225H, F227C/L/R, M230L and L234I as minor mutations.[7] Indeed, *in vitro* studies demonstrated that doravirine retained full activity against most of the single resistance-associated mutations (RAMs) selected by older NNRTIs, except for V106A, Y188L and M230L, as well as against some combinations of multiple NNRTI RAMs.[8,9] A recent study conducted on a large panel of clinical isolates collected from treatment-naive patients revealed that 92.5% of samples were susceptible to doravirine, as indicated by a fold change (FC) value lower than the biological cut-off of 3-fold.[10] *In vitro* resistance selection experiments revealed the emergence of V106A/M/I, V108I, F227C/I/L and L234I, with minimal HIV-1 subtype-related differences,[11] resulting in a limited cross-resistance with rilpivirine and possibly with etravirine.[12] Although three recent large surveys showed a low prevalence of doravirine RAMs in NNRTI-exposed individuals,[13–15] the impact of various combinations of NNRTI RAMs and the possible cross-resistance with other

NNRTIs have been poorly investigated. Importantly, one clinical trial (NCT04233216) has recently started to recruit heavily treatment-experienced patients with multidrug-resistant viruses harbouring NNRTI and NRTI RAMs to evaluate the efficacy of the doravirine/islatravir combination plus optimized background therapy. In this study, we aimed to evaluate the activity of doravirine in a reference panel of NNRTI-resistant infectious clones and in site-directed mutants including relevant NNRTI mutations.

Materials and methods

Cell lines

Lenti-X 293 T cells (Takara Bio, Kusatsu, Japan) and TZM-bl cells were cultured in high-glucose DMEM with L-glutamine, supplemented with 10% FBS, 100 U/mL penicillin and 100 µg/mL streptomycin. The MT-2 cell line was cultured in RPMI supplemented with 2 mM L-glutamine, 10% FBS, 100 U/mL penicillin and 100 µg/mL streptomycin. TZM-bl and MT-2 cell lines were obtained from the Centre for AIDS Reagent of the National Institute for Biological Standards and Control. All cell culture media and relevant reagents were obtained from EuroClone (Italy).

NNRTI-resistant infectious clones

A reference panel of HIV-1 infectious clones harbouring combinations of major NNRTI RAMs was obtained from the NIH AIDS Reagent Program. These clinically derived recombinant viruses were characterized by intermediate- to high-level resistance to rilpivirine, etravirine, efavirenz and nevirapine as determined by the Phenosense Assay.[16] Reverse transcriptase sequences of NNRTI-resistant clones were submitted to GenBank under accession numbers JQ814884–JQ814893. In addition, we introduced the individual NNRTI mutations K103N, Y181C, M230L and the combination of K103N/Y181C into the HIV-1 NL4-3 backbone through the QuikChange® Multi Site-Directed Mutagenesis Kit (Agilent Technologies, Santa Clara, CA, USA). The NL4-3 plasmid was obtained from the NIH AIDS Reagent Program. NL4-3 and all clones with NNRTI mutations were transfected into Lenti-X 293 T cells, propagated in MT-2 cells and titrated in TZM-bl cells as previously described.[17]

Phenotypic determination of susceptibility to doravirine

In vitro susceptibility to doravirine was determined in duplicate through a TZM-bl cell-based assay previously shown to correlate well with the reference phenotypic Phenosense Assay in the measurement of susceptibility to HIV-1 protease, reverse transcriptase and integrase inhibitors.[17] Briefly, 10 000 TZM-bl cells/well were infected with the WT NL4-3 strain or NNRTI-resistant viruses at a multiplicity of infection of 0.03 in the presence of 5-fold dilutions of doravirine (MedChemExpress, Monmouth Junction, NJ, USA) ranging from 10 µM to 0.00512 nM. After 48 h, cells were treated with the Glo-Lysis buffer (Promega, Madison, WI, USA) and the Bright-Glo Luciferase Assay (Promega), then relative luminescence units were measured through the GloMax Discover instrument (Promega) and elaborated with GraphPad software to calculate IC_{50} values. FC values were calculated with respect to the IC_{50} value obtained with the NL4-3 WT strain.

Results and discussion

According to the IAS-USA drug resistance mutations list,[7] none of the clones harboured any major doravirine RAMs (namely V106A/M and Y188L), while two clones included the minor doravirine RAM M230L. As described in Table 1, 8 out of the 10 NNRTI-resistant clones and the mutant K103N/Y181C NL4-3 clone have an FC value higher than the biological cut-off. The highest FC values (>100)

were found in samples 12225 and 12237, harbouring mutations E138G/H221Y/F227L/M230L and V106I/Y181C/G190A/H221Y, respectively, while the other sample harbouring M230L together with L100I and V179D (ID 12243) showed an FC value of 6.2. Other clones with Y181C and additional NNRTI RAMs (ID 12231, 12235 and 12239) had FC values of 14.2–31.8, suggesting a considerably reduced susceptibility to doravirine, while the absence of Y181C and doravirine RAMs (clones 12227, 12229, 12233 and 12241) resulted in FC values from 0.4 to 3.1, suggesting no or minimal impact on doravirine susceptibility. The single K103N or Y181C mutations within the NL4-3 backbone did not reduce doravirine susceptibility (FC values 1.4 and 1.8, respectively), while the double mutant K103N/Y181C showed a reduced susceptibility (FC 4.9). These data were comparable to those already described for viruses harbouring single K103N or Y181C and the K103N/Y181C mutations, showing mean FC values of 1.5, 2.5 and 4.3, respectively.[8] Interestingly, clone 12231 harbouring mutations K103N/V179F/Y181C showed an FC value of 22.1, suggesting that the non-polymorphic V179F substitution by itself or in combination with other uncharacterized amino acid variations can further decrease doravirine susceptibility. Similarly, the site-directed NL4-3/M230L mutant showed an FC value of 7.6, comparable to those observed in clone 12243 but significantly lower than in clone 12225, harbouring the additional doravirine RAM F227L together with NNRTI RAMs E138G and H221Y. Overall, doravirine FC values were comparable to or lower than those calculated with other licensed NNRTIs in clones 12227, 12229, 12233, 12241 and 12243, while in the remaining five clones doravirine FC values were higher than those of other NNRTIs, particularly etravirine and rilpivirine. Irrespective of the type of NNRTI RAMs, a higher number of NNRTI RAMs correlated significantly with increasing median FC values (linear test for trend, $P = 0.005$) (Figure 1a). Indeed, all of the eight viruses with ≥3 NNRTI mutations showed FC values >3, including clones 12231, 12235, 12237 and 12239 with no canonical doravirine mutations. By comparing FC values and predicted susceptibility to doravirine, both the HIV Drug Resistance Database (HIVdb; version 8.9-1) and the ANRS algorithm (version 30) could estimate doravirine activity with good accuracy, indicating that these two algorithms can be reliably used to evaluate doravirine susceptibility for possible use in patients harbouring NNRTI RAMs (Figure 1b and c).

The 10 clinically derived NNRTI-resistant clones were originally conceived to include combinations of NNRTI mutations commonly observed among sequences stored in the Stanford HIVdb and causing intermediate- to high-level resistance to nevirapine, efavirenz, rilpivirine and etravirine.[16] This study completes the NNRTI susceptibility profile for this reference panel of clones, which is publicly available and ideal to inform further NNRTI development. Partly contrary to expectations, we found that doravirine activity was overall similar to that of the second-generation NNRTIs etravirine and rilpivirine, indicating that doravirine may only partially overcome NNRTI resistance. While previous *in vitro* testing had been mostly carried out on viruses harbouring one or two NNRTI mutations,[8,9] the key result of this study is that multiple mutations selected by older NNRTIs can confer substantial cross-resistance to doravirine even in the absence of major IAS-USA doravirine RAMs. It must also be noted that clones derived from clinical isolates accommodate *in vivo* selected minor or compensatory changes which cannot be recapitulated in site-directed mutants,

Table 1. Mean IC$_{50}$ ± SD, fold change values for doravirine and other licensed NNRTIs against infectious clones harbouring NNRTI resistance-associated mutations (RAMs) and levels of doravirine activity predicted by the Stanford HIVdb and ANRS prediction algorithms

| Virus ID | NNRTI RAMs | NRTI RAMs | Other mutations | Mean doravirine IC$_{50}$ ± SD (nM) | Fold change (FC) | | | | | Predicted doravirine activity[d] | |
					Doravirine[b]	Nevirapine[c]	Efavirenz[c]	Etravirine[c]	Rilpivirine[c]	Stanford HIVdb	ANRS
12225[a]	E138G, H221Y, F227L, M230L	M41L, L210W, T215Y	K122E, D177E, I178L, R211K, V245M, I293V	>100	>100	>200	15	21	18	R	R
12227[a]	K101P, K103N	M41L, T215Y	A98S, K102Q, D123E, K166R, D177E, D192N, R211K, V245K, K277R, R284K, T286A, E297K	0.4 ± 0.1	0.4	>200	>200	5.8	92	S	S
12229[a]	L100I, K103N, H221Y	M41L, L74V, M184V, T215Y	R83K, D177E, T200A, R211Q, K281R, R284K, I293V, E297A	4.8 ± 0.3	4.0	>200	>200	6.8	6.3	I	R
12231[a]	K103N, V179F, Y181C	M41L, T215F	K49R, K82R, A98S, D177E, G196E, Q207R, R211A, L228R, A272P, I293V, K311R	26.5 ± 14.4	22.1	>200	90	8.8	2.3	I	R
12233[a]	K101E, Y181V	K70R, M184V, T215F	T27S, E28K, K32E, V60I, T69N, R83K, V179I, T200A, Q207D, L228R, V245E, T286A, E297K	3.3 ± 0.5	2.8	>200	2.1	27	24	I	I
12235[a]	A98G, K101E, Y181C, G190A	M41L, E44D, D67N, T69D, L74I, L210W, T215Y	T39E, V118I, K122E, I135T, G196E, E203K, R211K, A272S, V276T, K277R, Q278E, L283I, I293V, E297K	38.2 ± 5.8	31.8	>200	>200	15	22	R	R
12237[a]	V106I, Y181C, G190A, H221Y	none	V35I, S68G, A98S, D121E, K122E, I135V, R211K, F214L, V245E, D250E, A272P, E297K	>100	>100	>200	26	6	3.5	R	R
12239[a]	A98G, K101E, E138K, Y181C	M41L, T215D	K122E, I135T, S162Y, T200A, L210F, P243T, V245E, D250E, A272P, I274V, Q278H, K281R, T286A, A288S, K311R	17.0 ± 4.0	14.2	>200	3.6	10	9.2	I	R
12241[a]	K101E, E138G, G190S	none	V35M, R211K, V245E, S251I	3.8 ± 1.4	3.1	>200	>200	3.2	2.6	I	R
12243[a]	L100I, V179D, M230L	M41L, D67G, L74I, M184V, T215Y	V35I, K103R, K122E, I202V, R211K, T240K	7.5 ± 0.6	6.2	>200	>200	95	13	R	R
NL4-3/103N	K103N			2.0 ± 1.2	1.4	NA	NA	NA	NA	S	S
NL4-3/181C	Y181C			2.6 ± 1.1	1.8	NA	NA	NA	NA	S	S
NL4-3/103N/181C	K103N, Y181C			6.9 ± 2.8	4.9	NA	NA	NA	NA	I	R
NL4-3/230L	M230L			10.6 ± 4.7	7.6	NA	NA	NA	NA	R	R

NA, not available.
[a]NIH AIDS Reagent Program catalogue number.
[b]Doravirine FC values calculated according to the NL4-3 strain IC$_{50}$ value of 1.4±0.7 nM.
[c]FC values determined through the Phenosense Assay.[16]
[d]The HIVdb five-level grading was collapsed to three levels as indicated by the HIValg release notes at https://hivdb.stanford.edu/page/release-notes/. S, susceptible; I, intermediate resistance; R, high-level resistance.
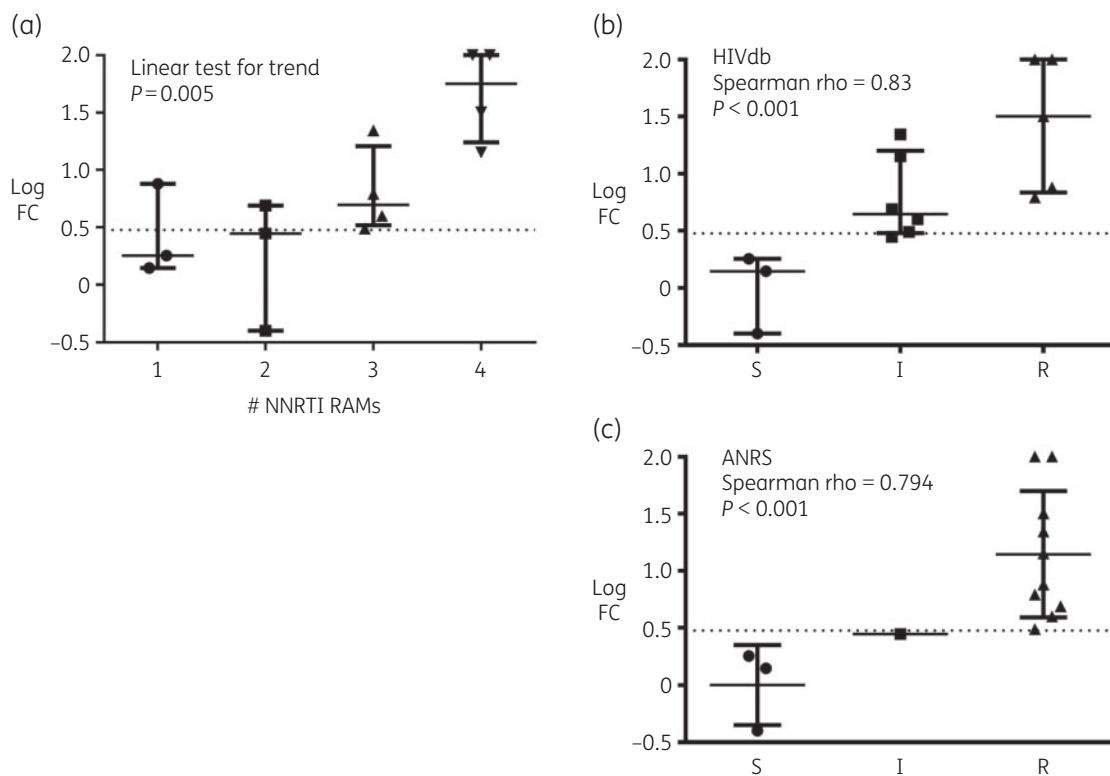
JAC

Figure 1. Distribution of doravirine fold change (FC) values measured with clones harbouring NNRTI resistance-associated mutations (RAMs), as grouped by (a) number of NNRTI RAMs (linear test for trend, $P=0.005$); (b) predicted doravirine susceptibility by the Stanford HIVdb algorithm; (c) predicted doravirine susceptibility by the ANRS algorithm. S, susceptible; I, intermediate resistance; R, high-level resistance. The dotted line indicates the biological FC cut-off (3-fold) recently established for doravirine.[10]

yet may play a relevant role in modulating resistance. For example, patient-derived viruses harbouring G190S or L100I + K103N without any canonical doravirine mutation showed FC values in the range of 1.5–11 and 2.7–19, respectively.[8]

A relevant consequence of these findings is that prediction of resistance simply based on the presence of IAS-USA doravirine RAMs may overestimate doravirine activity. Genotypic interpretation systems such as the Stanford HIVdb or ANRS should be preferred in the context of multiple NNRTI mutations. Indeed, a recent study showed that the Stanford HIVdb detected more transmitted resistance to doravirine with respect to the IAS-USA list.[15] Importantly, clinical use of doravirine as part of salvage therapy in heavily treatment-experienced patients still needs to be informed by expanded *in vitro* genotype–phenotype correlation analysis, coupled with *in vivo* data allowing the establishment of clinical FC cut-offs.

Acknowledgements

Funding

Transparency declarations

M.Z. reports consultancy fees for ViiV Healthcare, Gilead Sciences and Janssen-Cilag, and grants for his institution from ViiV Healthcare and Gilead outside the submitted work. R.W.S. received research funding from Janssen Pharmaceuticals and Vela Diagnostics outside the submitted work. All other authors have none to declare.

References

1 US Food and Drug Administration. *PIFELTRO (Doravirine) Prescribing Information.* https://www.accessdata.fda.gov/drugsatfda_docs/label/2019/210806s003lbl.pdf.

2 European Medicines Agency. *Pifeltro Product Information, Annex I—Summary of Product Characteristics.* https://www.ema.europa.eu/en/documents/product-information/pifeltro-epar-product-information_en.pdf.

3 Johnson M, Kumar P, Molina JM *et al.* Switching to doravirine/lamivudine/tenofovir disoproxil fumarate (DOR/3TC/TDF) maintains HIV-1 virologic suppression through 48 weeks: results of the DRIVE-SHIFT trial. *J Acquir Immune Defic Syndr* 2019; **81**: 463–72.

4 Orkin C, Squires KE, Molina JM *et al.* Doravirine/lamivudine/tenofovir disoproxil fumarate is non-inferior to efavirenz/emtricitabine/tenofovir disoproxil fumarate in treatment-naive adults with human immunodeficiency virus-1

infection: week 48 results of the DRIVE-AHEAD trial. *Clin Infect Dis* 2019; **68**: 535–44.

5 Molina JM, Squires K, Sax PE *et al.* Doravirine versus ritonavir-boosted darunavir in antiretroviral-naive adults with HIV-1 (DRIVE-FORWARD): 96-week results of a randomised, double-blind, non-inferiority, phase 3 trial. *Lancet HIV* 2020; **7**: e16–26.

6 Wong A, Goldstein D, Mallolas J *et al.* Efficacy and safety of doravirine/lamivudine/tenofovir disoproxil fumarate (DOR/3TC/TDF) in treatment-naive adults with HIV-1 and transmitted nonnucleoside reverse transcriptase inhibitor resistance mutations. *J Acquir Immune Defic Syndr* 2019; **82**: e47–9.

7 Wensing AM, Calvez V, Ceccherini-Silberstein F *et al.* 2019 Update of the drug resistance mutations in HIV-1. *Top Antivir Med* 2019; **27**: 111–21.

8 Lai MT, Feng M, Falgueyret JP *et al.* In vitro characterization of MK-1439, a novel HIV-1 nonnucleoside reverse transcriptase inhibitor. *Antimicrob Agents Chemother* 2014; **58**: 1652–63.

9 Feng M, Sachs NA, Xu M *et al.* Doravirine suppresses common nonnucleoside reverse transcriptase inhibitor-associated mutants at clinically relevant concentrations. *Antimicrob Agents Chemother* 2016; **60**: 2241–7.

10 Asante-Appiah E, Lai J, Li Q *et al.* Doravirine resistance profile in clinical isolates and impact of baseline NNRTI resistance-associated mutations observed in treatment-naïve participants from phase 3 clinical trials. *Oral Abstracts from the 23rd International AIDS Conference, 6–10 July 2020.* Abstract PDB0406. https://onlinelibrary.wiley.com/doi/10.1002/jia2.25547.

11 Feng M, Wang D, Grobler JA *et al.* In vitro resistance selection with doravirine (MK-1439), a novel nonnucleoside reverse transcriptase inhibitor with distinct mutation development pathways. *Antimicrob Agents Chemother* 2015; **59**: 590–8.

12 Smith SJ, Pauly GT, Akram A *et al.* Rilpivirine and doravirine have complementary efficacies against NNRTI-resistant HIV-1 mutants. *J Acquir Immune Defic Syndr* 2016; **72**: 485–91.

13 Sterrantino G, Borghi V, Callegaro AP *et al.* Prevalence of predicted resistance to doravirine in HIV-1-positive patients after exposure to nonnucleoside reverse transcriptase inhibitors. *Int J Antimicrob Agents* 2019; **53**: 515–19.

14 Soulie C, Santoro MM, Storto A *et al.* Prevalence of doravirine-associated resistance mutations in HIV-1-infected antiretroviral-experienced patients from two large databases in France and Italy. *J Antimicrob Chemother* 2020; **75**: 1026–30.

15 Guerrero-Beltrán C, Martínez-Sanz J, Álvarez M *et al.* The algorithm used for the interpretation of doravirine transmitted drug resistance strongly influences clinical practice and guideline recommendations. *J Antimicrob Chemother* 2020; **75**: 1294–300.

16 Balamane M, Varghese V, Melikian GL *et al.* Panel of prototypical recombinant infectious molecular clones resistant to nevirapine, efavirenz, etravirine, and rilpivirine. *Antimicrob Agents Chemother* 2012; **56**: 4522–4.

17 Saladini F, Giannini A, Boccuto A *et al.* Agreement between an in-house replication competent and a reference replication defective recombinant virus assay for measuring phenotypic resistance to HIV-1 protease, reverse transcriptase, and integrase inhibitors. *J Clin Lab Anal* 2018; **32**: e22206.

1   **Residual phenotypic susceptibility to doravirine in multidrug resistant HIV-1 from subjects enrolled in the**

2   **PRESTIGIO Registry**

3

4   Francesco SALADINI[1*‡], Federica GIAMMARINO[1‡], Franco MAGGIOLO[2], Micol FERRARA[3], Giovanni CENDERELLO[4],

5   Benedetto M. CELESIA[5], Ferdinando MARTELLOTTA[6], Vincenzo SPAGNUOLO[7], Giulio M. CORBELLI[8†], Nicola

6   GIANOTTI[7], Maria M. SANTORO[10], Stefano RUSCONI[11], Maurizio ZAZZI[1], Antonella CASTAGNA[7,9], for the

7   PRESTIGIO STUDY GROUP

8

9   [1]Department of Medical Biotechnologies, University of Siena, Siena, Italy; [2]Azienda Ospedaliera Papa Giovanni

10   XXIII, Bergamo, Italy; [3]Unit of Infectious Diseases, Department of Medical Sciences, University of Turin, Turin,

11   Italy; [4]Galliera Hospital, Genoa, Italy; [5]Garibaldi Hospital, Catania, Italy; [6]Centro di riferimento oncologico, Aviano,

12   Italy; [7]San Raffaele Scientific Institute, Milan, Italy; [8]Plus, Bologna, Italy; [9]San Raffaele Vita-Salute University,

13   Milan, Italy; [10]University of Rome Tor Vergata, Rome, Italy; [11]DIBIC Luigi Sacco, University of Milan, Italy

14

15   Running title: *In vitro* susceptibility to second-generation NNRTI in MDR HIV-1

16

18

19   *Corresponding author:

20   Francesco Saladini, PhD

21   Telephone: +39 0577233855

22   Fax: +39 0577233870

23   Email: saladini6@unisi.it

24

25   [‡]Contributed equally to this work. [†]Deceased.

26 **Abstract**

27

28 **Background**

29 Doravirine showed a rather distinct resistance profile within the NNRTI class. This study aimed to evaluate the

30 phenotypic susceptibility to doravirine, rilpivirine and etravirine in a panel of multidrug resistant (MDR) HIV-1

31 isolates collected from people living with HIV (PLWH) enrolled in the PRESTIGIO Registry.

32 **Methods**

33 Recombinant viruses expressing PLWH derived protease-reverse transcriptase coding region were generated

34 from plasma samples at virological failure with documented resistance to PIs, NRTIs, NNRTIs and INSTIs. *In vitro*

35 susceptibility was assessed through a phenotypic assay measuring fold-change values with respect to the

36 reference NL4-3 virus. Genotypic susceptibility was computed by the Stanford HIVdb algorithm 8.9-1.

37 **Results**

38 Plasma samples were collected from 22 PLWH, twenty (91%) were male, median age 55 years (IQR 50-58), time

39 since HIV-1 diagnosis 27 years (23-31), time on ART 23 years (22-26). Median doravirine, etravirine and rilpivirine

40 fold-change values were 9.8 (2.9-40.4), 42.9 (3.1-100.0) and 100.0 (17.9-100.0), respectively. According to the

41 fold-change cut-offs, full susceptibility was observed in 5 (23%), 4 (18%) and 1 (5%) cases with doravirine,

42 etravirine and rilpivirine, respectively. Irrespective of the presence of specific doravirine mutations, higher

43 numbers of NNRTI mutations correlated with higher fold-change values for doravirine. By comparing the

44 distribution of fold-change values with the Stanford HIVdb predicted susceptibility, a significant correlation was

45 detected for doravirine and rilpivirine but not etravirine.

46 **Conclusion**

47 Despite extensive cross-resistance among NNRTIs, doravirine can be a valid option in a proportion of PLWH with

48 MDR HIV-1. Doravirine activity appeared to be inferred with fair accuracy by HIVdb algorithm.

49

50 **Highlights**

51   •   Doravirine showed higher activity compared to etravirine and rilpivirine in MDR HIV-1

52   •   Full susceptibility to doravirine was retained in 23% of NNRTI resistant viruses

53   •   The higher the number of NNRTI mutations, the higher the resistance to doravirine

54   •   Resistance to doravirine has been detected even in the absence of doravirine RAMs

55   •   Stanford HIVdb algorithm predicted doravirine activity with fair accuracy

56

1. Introduction

Doravirine is the latest nonnucleoside reverse transcriptase inhibitor (NNRTI) approved for the treatment of HIV-1-infected therapy naïve people living with HIV (PLWH) or as a switch option in virologically suppressed PLWH without past or present evidence of resistance to the NNRTI class [1,2]. Clinical studies showed that doravirine had non-inferior efficacy, improved pharmacokinetics and/or safety profile both in first-line therapy and as switch option in virologically suppressed PLWH, compared with the standard of care [3-5]. In addition, doravirine efficacy was documented in a small group of therapy naïve individuals with the transmitted NNRTI mutations K103N and G190A [6].

Emergent resistance to doravirine in clinical trials led to different combinations of the mutations A98G, V106A/I/M, V108I, Y188L, H221Y, P225H, F227C, Y318F [7], while the individual NNRTI mutations G190E/S and M230L were found to reduce doravirine activity *in vitro* [8-10]. This pattern is relatively distinct from those involved in resistance to the other NNRTIs. Indeed, doravirine has shown full activity against 92.5% of viruses included in a large panel of clinical isolates, even in presence of the most common single NNRTI mutations except for Y188L and Y318F. In addition, doravirine has shown to retain full activity in presence of multiple NNRTI mutations and in more than half of isolates resistant to the other NNRTIs [11]. Considering the low prevalence of doravirine resistance associated mutations (RAMs) in both treatment naïve and experienced individuals [12-14], together with the limited cross-resistance with etravirine and rilpivirine [9,11], the use of doravirine in combination with the investigational nucleoside reverse transcriptase translocation inhibitor islatravir and an optimized background therapy is under clinical evaluation in subjects harboring NNRTI and nucleoside reverse transcriptase inhibitor (NRTI) RAMs (NCT04233216). This clinical trial was further supported by *in vitro* experiments where the combination of doravirine and islatravir exhibited a higher genetic barrier to resistance with respect to the combination of doravirine/lamivudine and dolutegravir/lamivudine [15]. However, a previous *in vitro* study on a small panel of NNRTI resistant clones showed that doravirine susceptibility was affected by

82   multiple NNRTI RAMs, suggesting that phenotypic investigation might be needed to support treatment decision

83   with complex resistance patterns [16]. Aiming to add further data on doravirine activity and on the cross-

84   resistance with the other second-generation NNRTIs, we evaluated the phenotypic susceptibility to doravirine,

85   etravirine and rilpivirine in a panel of multidrug resistant HIV-1 isolates collected from heavily treatment

86   experienced individuals enrolled in the Italian PRESTIGIO Registry.

87

88   **2. Materials and Methods**

89

90   **2.1 Patients and samples**

91

92   Plasma samples were collected from individuals enrolled in the Italian PRESTIGIO Registry (NCT04098315), which

93   includes PLWH with documented genotypic resistance to NRTIs, NNRTIs and protease inhibitors (PIs) plus either

94   genotypic resistance to integrase strand transfer inhibitors (INSTIs) or virological failure to an INSTI regimen

95   without an integrase genotype. Genotypic resistance to a drug class was defined as at least intermediate

96   resistance to at least one drug in the class, according to the Stanford HIVdb algorithm, version 8.9-1.

97

98   The PRESTIGIO Registry was approved by the San Raffaele Scientific Institute Ethical Committee with protocol

99   number 41/int/December_2017 and the use of residual, anonymized clinical samples for research studies was

100   regulated by patient informed consent. The collection of clinical information and biological samples is allowed

101   once the Ethics Committee of each participating centers has approved the participation in the Registry.

102   Demographic, clinical, and virological data of multidrug resistant PLWH were retrieved from the PRESTIGIO

103   Registry database. The Prestigio Registry has generated studies aiming to evaluate the effectiveness of different

104   antiretroviral regimens and the evolution of the genotype and phenotypic susceptibility of antiretroviral drugs

105   used in highly treatment experienced PLWH with virological failure [17-21].

106

107 **2.2 Cells and reagents**

108

109 293T Lenti-X cells (Takara Bio, Kusatsu, Japan) were cultured in DMEM high glucose with L-glutamine,

110 supplemented with 10% fetal bovine serum, 100 U/mL penicillin, and 100 µg/mL streptomycin. The TZM-bl cell

111 line was obtained from the Centre for AIDS Reagent of the National Institute for Biological Standards and Control

112 and cultured in DMEM high glucose with L-glutamine, supplemented with 10% fetal bovine serum, 100 U/mL

113 penicillin and 100 µg/mL streptomycin. All cell culture media and reagents were obtained from EuroClone (Italy).

114

115 **2.3 Antiviral drugs**

116

117 The NNRTI etravirine and rilpivirine were obtained through the NIH AIDS Reagent Program, while doravirine was

118 purchased from MedChemExpress (Monmouth Junction, NJ, USA).

119

120 **2.4 Generation of recombinant viruses**

121

122 The protocol for the generation of recombinant viruses consisted in a homologous recombination between a

123 modified NL4-3 vector lacking the region encompassing the GAG cleavage sites, the protease and the first 290

124 aminoacids of reverse transcriptase (pNL4-3ΔPR-RT, HXB2 nucleotide coordinates of deletion 1850-3420) and a

125 clinically derived PCR fragment corresponding to the deletion [22]. The plasmid was generated by reverse PCR

126 using primers including the SacII restriction enzyme sequences, while the PCR fragment had a 109- and 171-base

127 pair overlap with the ends of linearized pNL4-3ΔPR-RT. For the amplification of the target region, viral RNA was

128 extracted from the bottom 0.4 mL of plasma following centrifugation at 20,000 xg for 90 minutes, by using the

129 EZ1 automatic system and the DSP Virus Kit (Qiagen) according to the manufacturer's instructions. The reverse

130 transcription and first-round PCR were performed using the SuperScript III One-Step RT-PCR System with

131 Platinum Taq High Fidelity (Invitrogen) using the primers P210 (5'-ACCCTTCAGGAACAAATAGSATGGA-3', HXB2

132 nucleotide coordinates 1513-1537) and P220 (5'-TTCTGCTATTAAGTCTTTTGMTGGGTCRTA-3', HXB2 3504-3533).

133 Two microliters of the first-round PCR were used as the template for a nested PCR including the Q5 Hot Start

134 High-Fidelity   DNA   Polymerase   (New   England   Biolabs)   and   the   primers   P240   (5'-

135 CAAAGGAACCCTTYAGAGAYTATGT-3', HXB2 1655-1679) and P533 (5'- GCTAYTAARTCTTTTGWTGGGTCATA-3',

136 HXB2 3502-3529). Triplicate nested PCRs of each sample were purified, combined with 10 μg of linearized pNL4-

137 3ΔPR-RT and co-transfected in 293T Lenti-X cells through a calcium phosphate method as previously described

138 [22]. Supernatants harboring recombinant viruses were harvested 48 hours post transfection and expanded in

139 MT-2 cells to increase viral titers. In presence of large cellular syncytia, supernatants were harvested and stored

140 at -80°C.

141

142 **2.5 Determination of the *in vitro* susceptibility to doravirine, rilpivirine and etravirine**

143

144 *In vitro* susceptibility to doravirine, rilpivirine and etravirine was determined in duplicate through a TZM-bl cell-

145 based assay previously shown to correlate well with the reference phenotypic Phenosense Assay in the

146 measurement of susceptibility to HIV-1 protease, reverse transcriptase, and integrase inhibitors [22]. Briefly,

147 10,000 TZM-bl cells/well were infected with the wild-type NL4-3 strain or NNRTI resistant viruses at multiplicity

148 of infection of 0.03 in the presence of five-fold dilution of doravirine, rilpivirine (range 10 μM – 0.00512 nM) and

149 etravirine (range 5 μM – 0.00256 nM). After 48 hours, cells were treated with the Glo-Lysis buffer (Promega,

150 Madison, WI, USA) and the Bright-Glo Luciferase Assay (Promega), then relative luminescence units were

151 measured through the GloMax Discover instrument (Promega) and elaborated with GraphPad software to

152 calculate half-maximal inhibitory concentration (IC_{50}) values. Fold-change (FC) values were calculated with

153 respect to the IC_{50} value obtained with the NL4-3 wild-type strain. Viruses with FC >100 were considered as FC =

154 100 for statistical analyses. To infer drug activity based on phenotypic FC values, available drug-specific cut-offs

155 from Monogram Biosciences were considered including 3-fold and 2.5-fold as biological cut-off for doravirine

156 and rilpivirine, respectively, and 2.9-fold and 10-fold as the lower and upper clinical cut-off for etravirine,

157 respectively.

158

159 **2.6 HIV-1 sequencing, subtyping and genotypic prediction of drug activity**

160

161 The reverse transcriptase sequences within PCR amplicons generated to produce recombinant viruses were

162 obtained by Sanger population sequencing using primers P214 (5'-TTTGCCAGGAAAATGGAAACCAAAAATGAT-3',

163 HXB2 2363-2392) and P533. The HIV-1 subtype was assigned by using the COMET HIV-1 subtyping tool [23].

164 According to the rules of Stanford HIVdb algorithm, the following NNRTI mutations with score equal to or higher

165 than 15 were considered as associated with resistance to doravirine: A98G, L100I, K101E, V106A/M, Y181I/V,

166 Y188F/L, G190E/S/Q, P225H, F227C/I/L/V, M230I/L, L234I.

167

168 **2.7 Statistical analysis**

169

170 FC values calculated for the three NNRTIs were compared by Friedman test followed by pairwise comparisons by

171 Dunn's test with Bonferroni correction. The Spearman test was used to test the correlation between FC values

172 for each pair of drugs. The Jonckheere-Terpstra test was used to analyze the association of the phenotypic drug

173 susceptibility with the number of NNRTIs used and with the Stanford HIVdb susceptibility level. The Mann-

174 Whitney test was used to compare phenotypic susceptibility values depending on exposure to the different

175 NNRTIs. All statistical analyses were performed by SPSS (IBM Corporation) version 20.

176

177 **3. Results**

178

179 **3.1 Characteristics of the study population**

180

181 Samples were collected from 22 PLWH with a median age of 55 years (IQR 50-58), 20 (91%) males, a median time

182 since HIV-1 diagnosis of 27 years (IQR 23-31) and a median time on antiretroviral therapy of 23 years (IQR 22-26)

183 (Table 1). At sample collection, 9, 5 and 8 PLWH had been exposed to 1, 2 and 3 NNRTIs, respectively, with a

184 median time of cumulative exposure to NNRTIs of 47 months (IQR 10-71). At the time of sampling, 10 and 1

185 PLWH were on treatment with etravirine and rilpivirine, respectively. Viral sequences were attributed to subtype

186 B in 20 cases and subtype F1 in two cases.

187

188 **3.2 Phenotypic susceptibility to doravirine, etravirine and rilpivirine**

189

190 Recombinant viruses had different NNRTI RAM burdens, ranging from one (3/22 cases, 14%), two (5/22, 23%),

191 three (9/22, 41%), four (4/22, 18%) to five (1/22, 5%) mutations, while major Stanford HIVdb doravirine RAMs

192 were detected in 17/22 (77%) viruses (table 2). NRTI and PI RAMs included in the recombinant viruses have been

193 described in the supplementary table 2. Doravirine, etravirine and rilpivirine showed the lowest FC value in 14/22

194 (64%), 6/22 (27%) and 0/22 (0%) cases, respectively (Figure 1). Indeed, the median doravirine FC value (9.8, IQR

195 2.9-40.4) was significantly lower than the median rilpivirine FC value (100.0, IQR 17.9-100.0) (P <0.001) but not

196 than the median etravirine FC value (42.9, IQR 3.1-100.0) (P = 0.211), while etravirine and rilpivirine did not differ

197 from each other (P = 0.071). However, there was a significant correlation between the FC values for any pair of

198 drugs (doravirine vs. etravirine: rho = 0.517, P = 0.014; doravirine vs. rilpivirine: rho = 0.762, P <0.001; etravirine

199 vs. rilpivirine: rho = 0.785, P <0.001).

200

201 Cases with FC >100 were common for rilpivirine and etravirine but infrequent for doravirine (15, 10 and 4,

202 respectively). In two cases, all the drugs showed an FC value higher than 100, indicating complete lack of NNRTI

203 activity. One of these recombinant viruses (RV-14) had a complex pattern of NNRTI mutations but none of them

204 was considered as a major doravirine RAM, although alternative mutations occurred at positions involved in

205 doravirine resistance such as 100, 101 and 190. The other virus (RV-16) harboured mutations E138K and G190E,

206   the latter being among the individual NNRTI mutations able to cause a substantial reduction of doravirine

207   susceptibility [10].

208

209   Despite sharing the same NNRTI RAMs, RV-13 and RV-15 showed substantially different levels of phenotypic

210   resistance to all the drugs, with RV-13 more resistant to doravirine (4.1-fold), etravirine (10.3-fold) and rilpivirine

211   (>6.9-fold) compared with RV-15. These two viruses differed also for the viral subtype (F1 for RV-13 and B for

212   RV-15)   and   for   the   accompanying   NRTI   RAMs   (D67N,   K70R,   T215L,   K219E   for   RV-13;

213   M41L, A62AV, D67N, K70G, V75I, M184MV, L210W, T215Y, K219Q for RV-15).

214

215   Based on currently available biological or clinical cut-offs, predicted full in vivo susceptibility was observed in few

216   cases, namely 5 (23%), 4 (18%) and 1 (5%) cases with doravirine, etravirine and rilpivirine, respectively, while an

217   additional 3 cases had intermediate susceptibility to etravirine. Notably, full susceptibility to all the three NNRTIs

218   was predicted only for RV-17, harbouring the singleton K103N mutation. The other cases with predicted

219   susceptibility to multiple NNRTIs included RV-11 and RV-15, both susceptible to doravirine and etravirine. One

220   isolate with the uncommon singleton A98G mutation (RV-9) retained full susceptibility to etravirine and FC values

221   slightly above the biological cut-offs for doravirine and rilpivirine.

222

223   The cumulative number of NNRTIs included in the current plus past treatments did not correlate with the FC

224   value measured to any of the three NNRTIs (supplementary table 1). Similarly, FC values calculated for doravirine

225   did not correlate with the time of exposure to NNRTI (rho = 0.082, P = 0.718), with the time elapsed since last

226   exposure to NNRTI (rho = -0.237, P = 0.288). The inclusion of etravirine (n=10) or rilpivirine (n=1) in the failing

227   regimen at sample collection was associated with higher median FC values for etravirine (100.0, IQR 48.0-100.0

228   with vs. 4.0, IQR 0.5-26.0 without; P = 0.004) and rilpivirine (100.0, IQR 100.0-100.0 with vs. 30.6, IQR 3.9-100.0

229   without; P = 0.029) but not for doravirine (17.9, IQR 7.4-80.1 with vs. 4.4, IQR 0.9-27.1 without; P = 0.145).

230   Notably,   only   2/10   cases   where   etravirine   was   included   in   the   failing   regimen   showed   full   phenotypic

231   susceptibility to doravirine and all the three cases of exposure to both etravirine and rilpivirine were associated

232   with high levels of phenotypic resistance to doravirine (RV-8, RV-14, RV-16).

233

234   **3.3 Comparison of genotypic and phenotypic resistance**

235

236   When analyzing the distribution of FC values according to the predicted susceptibility as determined by Stanford

237   HIVdb, a significant correlation was detected for doravirine and rilpivirine (P <0.001 and P = 0.001, respectively),

238   but not for etravirine (P = 0.131) (Figure 2). Interestingly, higher numbers of Stanford HIVdb major NNRTI RAMs

239   positively correlated with higher FC values calculated for doravirine (P = 0.001), with viruses harboring two or

240   more NNRTI RAMs showing FC values higher than the biological cut-off irrespective of the presence of major

241   doravirine RAMs (figure 3).

242

243   **4. Discussion**

244

245   Clinical trials have demonstrated that doravirine may represent a valuable treatment option for both naïve and

246   virologically suppressed PLWH due to improved genetic barrier to resistance compared with past NNRTIs,

247   excellent tolerability, and low potential for drug-drug interactions [24]. However, clinical studies are still needed

248   to better define the role of doravirine, both in naïve and treatment experienced individuals. Firstly, clinical data

249   are required to compare the efficacy and safety profile of doravirine with respect to second-generation INSTI

250   based regimens, which are mostly recommended as first-line treatment. Second, clinical studies addressing the

251   role of doravirine in the presence of transmitted or acquired resistance to past NNRTIs are eagerly awaited to

252   complete the assessment of drug profile, particularly in low-middle income countries. For example, a recent

253   analysis revealed that the prevalence of predicted doravirine resistance in NNRTI-experienced individuals is

254   higher in a South African cohort than in two European study populations (84.8% vs. 42.0% and 18.8%,

255   respectively) [12,13,25].

256

As previously reported [11], the improved antiviral activity of doravirine with respect to etravirine and rilpivirine against NNRTI-resistant isolates was confirmed in this study, with a panel of 22 recombinant viruses from PLWH with resistance to the four main antiretroviral classes. When considering the provisional 3-fold biological cut-off, full susceptibility to doravirine was observed in 5 (23%) of NNRTI resistant viruses, as compared with 4 (18%) to etravirine and only 1 (5%) to rilpivirine. Although doravirine had the lowest reduction in FC values compared to the other NNRTIs, it must be noted that the pairwise difference was significant with respect to rilpivirine but not to etravirine. As a further caveat, it must be emphasized that almost all the isolates (19/22) had been exposed to etravirine, including concomitant exposure at the time of sampling in 10 cases, as opposed to none to doravirine. Thus, the sample panel was strongly biased towards selection of RAMs by etravirine which may have favored disproportionally loss of phenotypic activity with etravirine, while saving activity for doravirine. Analysis of a complementary panel of viruses, i.e. isolates with emergent resistance to doravirine and with no exposure to etravirine, is needed to complete the assessment of cross-resistance between doravirine and etravirine. Preliminary data from the few cases of first-line doravirine failures in clinical trials suggest maintenance of full or partial etravirine activity [10]. In addition, the prediction of in vivo activity could be based on clinical cut-offs for etravirine but not for doravirine which is currently interpreted based on a provisional biological cut-off. Determining a clinical cut-off for doravirine may be helpful to better compare the role of these two NNRTIs in the context of prior exposure and resistance to this class of drugs.

274

Each isolate had a unique set of NNRTI RAMs, with one exception. RV-13 and RV-15 shared the same RAM pattern, however FC values were significantly different from each other for all the three drugs. This highlights the possibility that additional mutations not currently acknowledged as NNRTI RAMs modulate susceptibility to NNRTIs. Alternatively, the genetic background of the different subtypes involved (B and F1) and/or some effects of NRTI RAMs [11,26] may have played a role.

280

281   It must be noted that recombinant viruses harbored a clinically derived fragment including the first 290

282   aminoacids of the reverse transcriptase, thus excluding mutation Y318F which has been shown to be associated

283   with significant reduction of doravirine susceptibility *in vitro* [11]. However, according to the HIV Stanford

284   database, Y318F mutation has been detected in only 1% of individuals receiving efavirenz or nevirapine.

285

286   In agreement with previous studies [11,16], this work showed that the accumulation of NNRTI RAMs due to past

287   or current exposure to NNRTIs decreased doravirine susceptibility, with substantially reduced activity in most

288   viruses harboring ≥3 major NNRTI RAMs. The time of exposure to NNRTI and the number of previously

289   experienced NNRTI did not significantly affect the susceptibility to doravirine, indicating that the previous

290   exposure to NNRTI do not predict the residual activity of doravirine. Importantly, high-level doravirine resistance

291   was detected in viruses without major doravirine resistance mutations, suggesting that cross resistance is quite

292   common among NNRTI resistant strains [27]. By comparing genotypic and phenotypic data, we observed that

293   the activity of doravirine and rilpivirine, but not etravirine, could be predicted with good accuracy by Stanford

294   HIVdb. Indeed, predicted resistance to etravirine was underestimated, particularly in six cases with predicted

295   intermediate resistance which showed FC values >100. On the other hand, two isolates with FC values below or

296   equal to the lower clinical cut-off, indicating full or partial susceptibility to etravirine, were classified as highly

297   resistant by HIVdb. This highlights the remaining uncertainties in inferring susceptibility to etravirine by

298   genotyping, despite frequent updates of multiple interpretation algorithms [28].

299

300   **5. Conclusions**

301

302   Although doravirine remains the most active NNRTI against isolates exposed to previous drugs of the same class,

303   its activity in salvage therapy may be compromised by the accumulation of NNRTI mutations, including cases

304   without major doravirine RAMs. These data suggest that doravirine might be properly considered in salvage

305   regimens following the genotypic resistance testing in a proportion of PLWH with 4-drug class resistant HIV-1

and limited treatment options to achieve the suppression of viral replication. Overall, doravirine may have a significant role in the management of difficult to treat PLWH as a fully active drug or a partially active drug particularly when novel antiretroviral classes are available.

Funding

Transparency declaration

364

365   **References**

366

367   [1] U.S. Food and Drug Administration. PIFELTRO (doravirine) prescribing information,

368   https://www.accessdata.fda.gov/drugsatfda_docs/label/2019/210806s003lbl.pdf; 2019 [accessed 09

369   August 2022]

370   [2] European Medicines Agency. Pifeltro product information, Annex I – Summary of product characteristics,

371   https://www.ema.europa.eu/en/documents/product-information/pifeltro-epar-product-

372   information_en.pdf; 2022 [accessed 09 August 2022]

373   [3] Molina JM, Squires K, Sax PE, Cahn P, Lombaard J, DeJesus E, et al; DRIVE-FORWARD trial group.

374   Doravirine versus ritonavir-boosted darunavir in antiretroviral-naive adults with HIV-1 (DRIVE-

375   FORWARD): 96-week results of a randomised, double-blind, non-inferiority, phase 3 trial. Lancet HIV

376   2020;7:e16-e26. doi: 10.1016/S2352-3018(19)30336-4.

377   [4] Orkin C, Squires KE, Molina JM, Sax PE, Sussmann O, Lin G, et al. Doravirine/Lamivudine/Tenofovir

378   Disoproxil Fumarate (TDF) Versus Efavirenz/Emtricitabine/TDF in Treatment-naive Adults With Human

379   Immunodeficiency Virus Type 1 Infection: Week 96 Results of the Randomized, Double-blind, Phase 3

380   DRIVE-AHEAD Noninferiority Trial. Clin Infect Dis 2021;73:33-42. doi: 10.1093/cid/ciaa822.

381   [5] Kumar P, Johnson M, Molina JM, Rizzardini G, Cahn P, Bickel M, et al; DRIVE-SHIFT Study Group. Brief

382   Report: Switching to DOR/3TC/TDF Maintains HIV-1 Virologic Suppression Through Week 144 in the

383   DRIVE-SHIFT Trial. J Acquir Immune Defic Syndr 2021;87:801-805. doi: 10.1097/QAI.0000000000002642.

384   [6] Wong A, Goldstein D, Mallolas J, DeJesus E, Johnson M, Molina JM, et al. Efficacy and Safety of

385   Doravirine/Lamivudine/Tenofovir Disoproxil Fumarate (DOR/3TC/TDF) in Treatment-Naïve Adults With

386   HIV-1 and Transmitted Nonnucleoside Reverse Transcriptase Inhibitor Resistance Mutations. J Acquir

387   Immune Defic Syndr 2019;82:e47-e49. doi: 10.1097/QAI.0000000000002153.

388   [7] Martin EA, Lai MT, Ngo W, Feng M, Graham D, Hazuda DJ, et al. Review of Doravirine Resistance Patterns

389   Identified in Participants During Clinical Development. J Acquir Immune Defic Syndr 2020;85:635-642.

390   doi: 10.1097/QAI.0000000000002496.

391   [8] Lai MT, Feng M, Falgueyret JP, Tawa P, Witmer M, DiStefano D, et al. In vitro characterization of MK-

392   1439, a novel HIV-1 nonnucleoside reverse transcriptase inhibitor. Antimicrob Agents Chemother

393   2014;58:1652-63. doi: 10.1128/AAC.02403-13.

394   [9] Smith SJ, Pauly GT, Akram A, Melody K, Ambrose Z, Schneider JP, Hughes SH. Rilpivirine and Doravirine

395   Have Complementary Efficacies Against NNRTI-Resistant HIV-1 Mutants. J Acquir Immune Defic Syndr

396   2016;72:485-91. doi: 10.1097/QAI.0000000000001031.

397 [10] Lai MT, Xu M, Ngo W, Feng M, Hazuda D, Hanna G, et al. Characterization of doravirine-selected

398   resistance patterns from participants in treatment-naïve Phase 3 clinical trials. Oral abstracts of the 22nd

399   International AIDS Conference, 23–27 July 2018, Amsterdam, the Netherlands. J Int AIDS Soc 2018;

400   21:e25148. doi: 10.1002/jia2.25148

401 [11] Asante-Appiah E, Lai J, Wan H, Yang D, Martin EA, Sklar P, et al. Impact of HIV-1 Resistance-Associated

402   Mutations on Susceptibility to Doravirine: Analysis of Real-World Clinical Isolates. Antimicrob Agents

403   Chemother 2021;65:e0121621. doi: 10.1128/AAC.01216-21.

404   [12] Soulie C, Santoro MM, Storto A, Abdi B, Charpentier C, Armenia D, et al. Prevalence of doravirine-

405   associated resistance mutations in HIV-1-infected antiretroviral-experienced patients from two large

406   databases in France and Italy. J Antimicrob Chemother 2020;75:1026-1030. doi: 10.1093/jac/dkz553.

407   [13] Sterrantino G, Borghi V, Callegaro AP, Bruzzone B, Saladini F, Maggiolo F, et al; ARCA Study Group.

408   Prevalence of predicted resistance to doravirine in HIV-1-positive patients after exposure to non-

409   nucleoside reverse transcriptase inhibitors. Int J Antimicrob Agents 2019;53:515-519. doi:

410   10.1016/j.ijantimicag.2019.02.007.

411   [14] Guerrero-Beltrán C, Martínez-Sanz J, Álvarez M, Olalla J, García-Álvarez M, Iribarren JA, et al; CoRIS. The

412   algorithm used for the interpretation of doravirine transmitted drug resistance strongly influences

413   clinical practice and guideline recommendations. J Antimicrob Chemother 2020;75:1294-1300. doi:

414   10.1093/jac/dkaa009.

415   [15] Lai MT, Feng M, Xu M, Ngo W, Diamond TL, Hwang C, et al. Doravirine and Islatravir Have

416   Complementary Resistance Profiles and Create a Combination with a High Barrier to Resistance.

417   Antimicrob Agents Chemother 2022;66:e0222321. doi: 10.1128/aac.02223-21.

418   [16] Saladini F, Giammarino F, Hosseini BA, Giannini A, Boccuto A, Dragoni F, et al. In vitro cross-resistance

419   to doravirine in a panel of HIV-1 clones harbouring multiple NNRTI resistance mutations. J Antimicrob

420   Chemother 2021;76:130-134. doi: 10.1093/jac/dkaa401.

421   [17] Castagna A, Ferrara M, Galli L, Comi L, Sterrantino G, Cenderello G, et al. Long-term efficacy of

422   dolutegravir in treatment-experienced subjects failing therapy with HIV-1 integrase strand inhibitor-

423   resistant virus. J Antimicrob Chemother 2018;73:177-182. doi: 10.1093/jac/dkx371.

424   [18] Saladini F, Giannini A, Giammarino F, Maggiolo F, Vichi F, Corbelli GM, et al. In vitro susceptibility to

425   fostemsavir is not affected by long-term exposure to antiviral therapy in MDR HIV-1-infected patients. J

426   Antimicrob Chemother 2020;75:2547-2553. doi: 10.1093/jac/dkaa178.

427   [19] Galli L, Parisi MR, Poli A, Menozzi M, Fiscon M, Garlassi E, et al. Burden of Disease in PWH Harboring a

428   Multidrug-Resistant Virus: Data From the PRESTIGIO Registry. Open Forum Infect Dis 2020;7:ofaa456.

429   doi: 10.1093/ofid/ofaa456.

430   [20] Armenia D, Santoro MM, Bellocchi MC, Carioti L, Galli L, Galli A, et al. Viral resistance burden and APOBEC

431   editing correlate with virological response in heavily treatment-experienced people living with multi-

432   drug resistant HIV. Int J Antimicrob Agents 2022;59:106492. doi: 10.1016/j.ijantimicag.2021.106492.

433   [21] Rusconi S, Saladini F, Bellocchi MC, Galli L, Gagliardini R, Gazzola L, et al. Leronlimab (PRO 140) in vitro

434   activity against 4-class drug resistant HIV-1 from heavily treatment experienced subjects. Pharmacol Res

435   2022;176:106064. doi: 10.1016/j.phrs.2022.106064.

436   [22] Saladini F, Giannini A, Boccuto A, Vicenti I, Zazzi M. Agreement between an in-house replication

437   competent and a reference replication defective recombinant virus assay for measuring phenotypic

438   resistance to HIV-1 protease, reverse transcriptase, and integrase inhibitors. J Clin Lab Anal

439   2018;32:e22206. doi: 10.1002/jcla.22206.

440   [23] Struck D, Lawyer G, Ternes AM, Schmit JC, Bercoff DP. COMET: adaptive context-based modeling for

441   ultrafast HIV-1 subtype identification. Nucleic Acids Res 2014;42:e144. doi: 10.1093/nar/gku739.

442   [24] Stockdale AJ, Khoo S. Doravirine: its role in HIV treatment. Curr Opin HIV AIDS 2022;17:4-14. doi:

443   10.1097/COH.0000000000000709.

444   [25] Steegen K, Moorhouse M, Wensing AM, Venter WD, Hans L. Is there a role for doravirine in African HIV

445   treatment programmes? A large observational resistance study in South Africa. J Int AIDS Soc

446   2021;24:e25706. doi: 10.1002/jia2.25706.

447   [26] Whitcomb JM, Huang W, Limoli K, Paxinos E, Wrin T, Skowron G, et al. Hypersusceptibility to non-

448   nucleoside reverse transcriptase inhibitors in HIV-1: clinical, phenotypic and genotypic correlates. AIDS

449   2002;16:F41-7. doi: 10.1097/00002030-200210180-00002.

450   [27] Wang Y, De Clercq E, Li G. Current and emerging non-nucleoside reverse transcriptase inhibitors

451   (NNRTIs) for HIV-1 treatment. Expert Opin Drug Metab Toxicol 2019;15:813-829. doi:

452   10.1080/17425255.2019.1673367.

453   [28] Vingerhoets J, Nijs S, Tambuyzer L, Hoogstoel A, Anderson D, Picchio G. Similar predictions of etravirine

454   sensitivity regardless of genotypic testing method used: comparison of available scoring systems. Antivir

455   Ther 2012;17:1571-9. doi: 10.3851/IMP2275.

456 **Table 1**. Patients characteristics at the time of sampling. Data are described as median (IQR) or number of
457 cases (%)

|	
Number of PLWH	22
Male gender	20 (91%)
Age, years	55 (50-58)
Time since HIV-1 diagnosis, years	27 (23-31)
Time on ART, years	23 (22-26)
Occurrence of previous AIDS events	12 (52%)
Nadir CD4+ cell count, cells/mm^3	50 (10-147)
HIV-1 RNA, log$_{10}$ copies/mL	4.30 (3.35-5.14)
CD4+ cell count, cells/mm^3	195 (80-279)
CD8+ cell count, cells/mm^3	1012 (358-1448)
CD4/CD8 ratio	0.2 (0.1-0.5)
Number of drugs included in the current regimen: 2 3 4 5	 4 (18%) 9 (41%) 6 (27%) 3 (14%)
Number of drug resistance mutations for each drug class: PI NRTI NNRTI INSTI	 6 (1-8) 5 (3-7) 3 (2-3) 2 (2-3)

458
459 **Table 2**. Phenotypic and genotypic susceptibility of recombinant viruses (RV) harboring NNRTI resistance
460 associated mutations (RAMs) according to current or past exposure to NNRTIs. Mutations associated with
461 reduced susceptibility to doravirine are in bold.
462

RV	Major Stanford HIVdb NNRTI RAMs	Subtype	NNRTI exposure at sample collection	Previous exposure to NNRTI	IC$_{50}$ fold-change values			Stanford HIVdb predicted susceptibility		
					Doravirine	Etravirine	Rilpivirine	Doravirine	Etravirine	Rilpivirine
1	**A98G**, K103N, Y181C, **P225H**	B	Etravirine	Efavirenz, nevirapine	17.9	>100	>100	R	I	R
2	**L100I**, K103N, K238N	B	Etravirine	Efavirenz	12.2	37.8	>100	I	I	R
3	K103N, **Y181V**	B	Etravirine	Nevirapine	7.4	>100	>100	LLR	R	R
4	K103KNRS, Y181C, **G190S, H221HY**	B	Etravirine	None	22.5	48.0	>100	R	R	R
5	E138Q, V179E, Y181C	B	None	Efavirenz, nevirapine	0.9	26.0	12.2	PLLR	I	R
6	V108I, Y181C	B	None	Efavirenz,	3.7	3.2	30.6	LLR	I	I

#	Mutations				IC50			Resistance		
			etravirine, nevirapine							
7	V106I, **Y188L**, K238N	B	None	Efavirenz	>100	2.9	>100	R	LLR	R
8	Y181C, **H221Y**, **M230I**	B	Rilpivirine	Etravirine	80.1	>100	>100	I	I	R
9	**A98G**	B	None	Nevirapine	3.4	0.5	3.7	LLR	PLLR	LLR
10	**L100I**, E138R, V179L	B	Etravirine	None	21.9	>100	>100	LLR	I	R
11	K103N, **Y181I**	B	None	Efavirenz, etravirine, nevirapine	0.2	0.4	3.9	LLR	R	R
12	K103N, E138A, **P225H**, **M230L**	B	None	Etravirine	>100	14.1	>100	R	I	R
13	**K101E**, Y181C, G190A	F1	None	Efavirenz, etravirine	5.3	22.7	>100	I	R	R
14	L100V, K101H, V179F, Y181C, G190A	B	Etravirine	Nevirapine, rilpivirine	>100	>100	>100	I	R	R
15	**K101E**, Y181C, G190A	B	Etravirine	None	1.3	2.2	14.4	I	R	R
16	E138K, **G190E**	B	Etravirine	Efavirenz, rilpivirine	>100	>100	>100	R	I	R
17	K103N	F1	None	Efavirenz, etravirine, nevirapine	0.4	0.2	0.6	S	S	S
18	V108I, E138A, **Y181V**	B	Etravirine	Efavirenz, nevirapine	14.9	>100	>100	I	R	R
19	**Y181I**	B	Etravirine	None	1.2	>100	>100	LLR	R	R
20	**L100I**, K103N, E138G	B	None	Efavirenz, etravirine	7.0	>100	>100	I	I	R
21	**A98G**, **L100I**, K103N, E138Q	B	None	Etravirine	27.1	>100	>100	I	I	R
22	K103N, Y181C	B	None	Etravirine	4.4	4.0	19.1	LLR	I	I
			Median IC50 fold-change (IQR)		**9.8 (2.9-40.4)**	**42.9 (3.1-100)**	**100 (17.9-100)**			

Legend. S = susceptible; PLLR = potential low-level resistance; LLR = low-level resistance; I = intermediate resistance; R = high-level resistance.

465 **Figure 1**. Doravirine (DOR), etravirine (ETR) and rilpivirine (RPV) IC_{50} fold-change values of recombinant viruses

466 harbouring NNRTI RAMs.
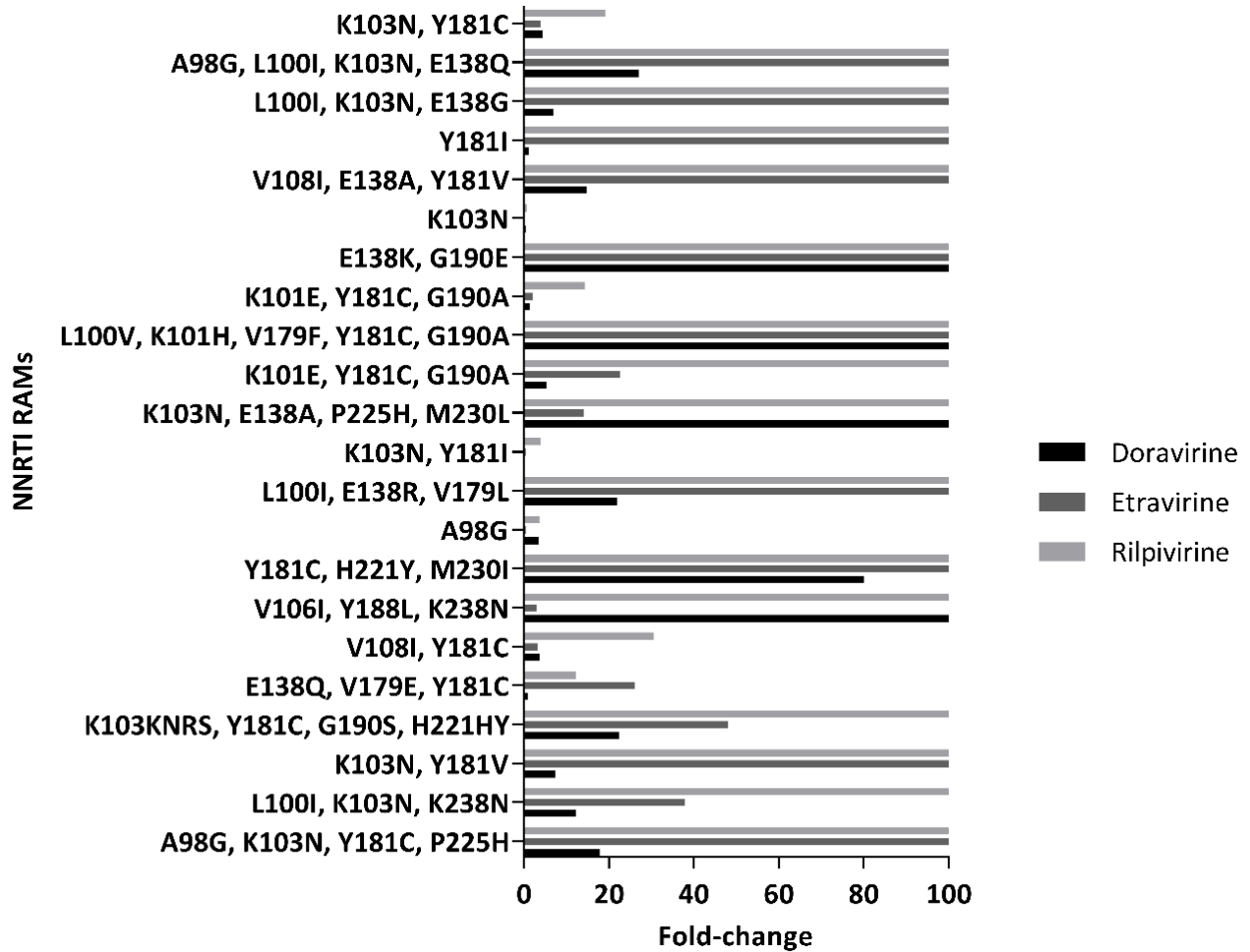
467

468

469

470

471

472 **Figure 2**. Distribution of (A) doravirine (DOR), (B) etravirine (ETR) and (C) rilpivirine (RPV) IC_{50} fold-change values

473 according to the predicted susceptibility levels as determined by the Stanford HIVdb algorithm.

A. **DOR**

p=0.0001

Fold-change (y-axis): 100, 80, 60, 40, 30, 20, 10, BCO 3

	S	PLLR	LLR	I	R
N	1	1	7	8	5
Median	0.4	0.9	3.7	13.6	100
IQR			1.2-7.4	5.7-66.9	20.2-100

B **ETR**

p=0.131

Fold-change (y-axis): 100, 90, 80, 70, 50, 40, 30, 20, UCO 10, LCO 2.9

	S	PLLR	LLR	I	R
N	1	1	1	11	8
Median	0.2	0.5	2.9	100	74.0
IQR				14.1-100	7.3-100

C **RPV**

p=0.001

Fold-change (y-axis): 100, 90, 40, 30, 20, 10, BCO 2.5

	S	PLLR	LLR	I	R
N	1	0	1	2	18
Median	0.6		3.7	24.9	100
IQR				19.1-30.6	100-100

474
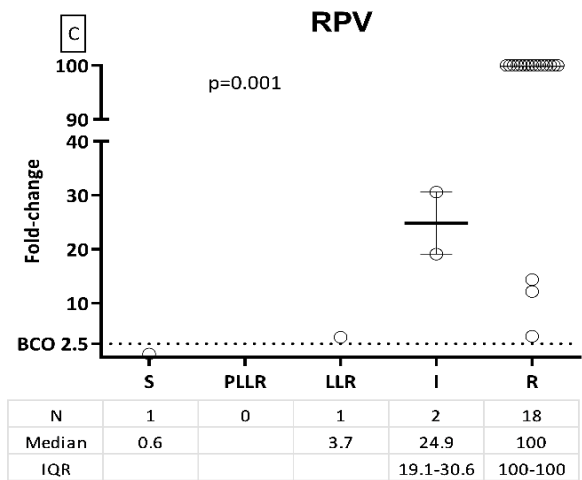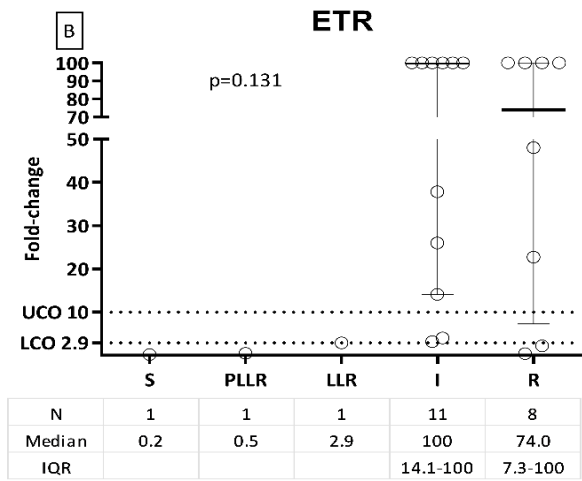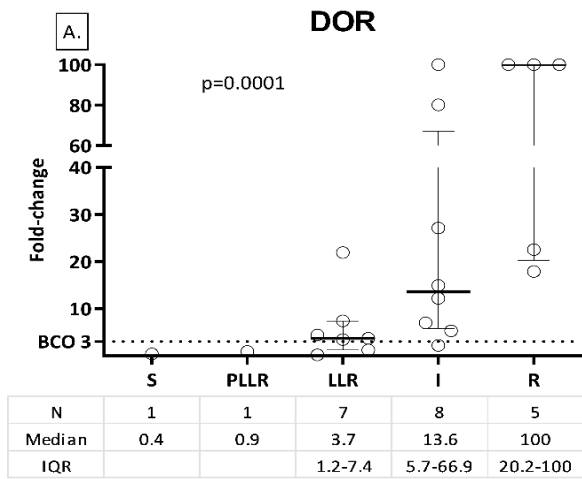
475   Legend. S = susceptible; PLLR = potential low-level resistance; LLR = low-level resistance; I = intermediate

476   resistance; R = high-level resistance; BCO = biological fold-change cut-off value; LCO = lower clinical fold-change

477   cut-off value; UCO = upper clinical fold-change cut-off value.

478

479   **Figure 3**. Distribution of doravirine fold-change values according to the presence of major NNRTI resistance

480   associated mutations (RAMs) as defined by Stanford HIVdb. Black circles indicate fold-change values associated

481   with viruses harboring doravirine RAMs.
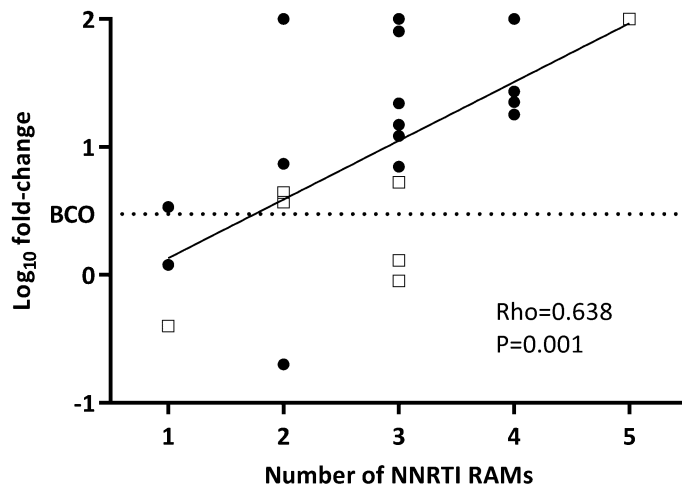
482

483   Legend. BCO = doravirine biological fold-change cut-off (= 3-fold). Black circles indicate fold-change values

484   associated with viruses harboring doravirine RAMs.

ABSTRACT PRESENTED AS ORAL PRESENTATION AT THE EUROPEAN MEETING OF HIV AND HEPATITIS in 2021

HIV-1 reverse transcriptase natural polymorphism V106I does not alter the susceptibility and the genetic barrier to resistance to doravirine *in vitro.*

Federica Giammarino[1], Alessia Giannini[1], Gaetana Sterrantino[2], Grazia Colao[3], Valeria Micheli[4], Adele Boccuto[1], Filippo Dragoni[1], Niccolò Bartolini[1], Ilaria Vicenti[1], Maurizio Zazzi[1], Francesco Saladini[1]

1 Department of Medical Biotechnologies, University of Siena, Italy.
2 Department of Clinical and Experimental Medicine, University of Florence, Italy.
3 Laboratory of Virology, Careggi Hospital, Florence, Italy.
4 Department of Clinical Microbiology, Virology and Bioemergencies, Sacco University Hospital, Milan, Italy.

Background

Doravirine (DOR, MK-1439) is a newly licensed NNRTI demonstrating a superior genetic barrier to resistance and partial cross-resistance as compared to older NNRTI. This study aimed to evaluate the *in vitro* susceptibility to DOR in a panel of HIV-1 recombinant viruses harbouring the RT natural polymorphism V106I. In addition, V106I was compared to the NNRTI resistance variants V106A and V106M for its impact on the genetic barrier to DOR resistance in the reference NL4-3 and HXB2 genetic background.

Materials and methods

Twelve plasma samples from HIV-1 infected patients were used to generate NL4-3-based recombinant viruses harboring clinically derived RT-RNaseH coding region including V106I polymorphism and no other major NNRTI mutations. *In vitro* susceptibility to DOR was assessed through a TZM-bl cell based phenotypic assay and fold-change (FC) values were calculated with respect to the NL4-3 IC_{50} value. V106I, V106A and V106M mutations were introduced by site-directed mutagenesis in the NL4-3 and HXB2 genomes and the resulting viruses were used to infect MT-2 cells and exposed to 2X, 4X, 8X and 16X DOR IC_{90} in quadruplicate. The time of viral breakthrough was defined by the day of the appearance of cytopathic effect and viral RNA was sequenced to detect possible emerging mutations.

Results

Recombinant viruses with clinically derived RT-RNaseH coding region showed a median DOR FC of 1.6 (IQR 1.2-2.0), while in 3/12 cases FC values were equal to or higher than the DOR FC biological cut-off (FC 3.0, 3.7 and 3.9 vs. 3.0). V106I, V106A and V106M mutants in NL4-3 and HXB2 backbones showed FC values of 0.7, 1.4, 9.4 and 1.5, 14.9, 14.7, respectively. Linear regression indicated that the times of viral breakthrough for wild type NL4-3 and NL4-3_106I viruses were comparable and higher than those of NL4-3_106A and NL4-3_106M viruses at all DOR concentrations, while the times for HXB2 were wild-type>106I>106A>106M. By comparing the ratio between the time of viral breakthrough and DOR concentration, statistically significant differences were observed with both NL4-3 and HXB2 based viruses (p=0.0309 and p=0.0072, respectively; Kruskal-Wallis test). No emerging mutations were identified in DOR 2X and 4X IC_{90} cultures, while mixed I106IM population were detected in 1/4 cultures of both NL4-3_106I and HXB2_106I at 8X $IC_{90.}$ At DOR 16X

IC$_{90}$, mutations V108I or F227L emerged in two NL4-3_106M cultures, L205LV+F227L+P236L emerged in one HXB2_106A, I106M in one HXB2_106I, K102Q in two HXB2_106I, L205LV+P236PL in one wild type HXB2.

Conclusions

Natural polymorphism V106I seems to minimally affect the susceptibility to DOR in clinical isolates and the genetic barrier to resistance as compared to reference wild-type viruses and V106A or V106M mutants. However, the genetic background may affect the susceptibility to DOR, as shown by (i) higher FC values observed in three recombinant viruses and (ii) the notably different FC values measured with NL4-3 and HXB2 harboring V106A (FC 1.4 and 14.9, respectively).
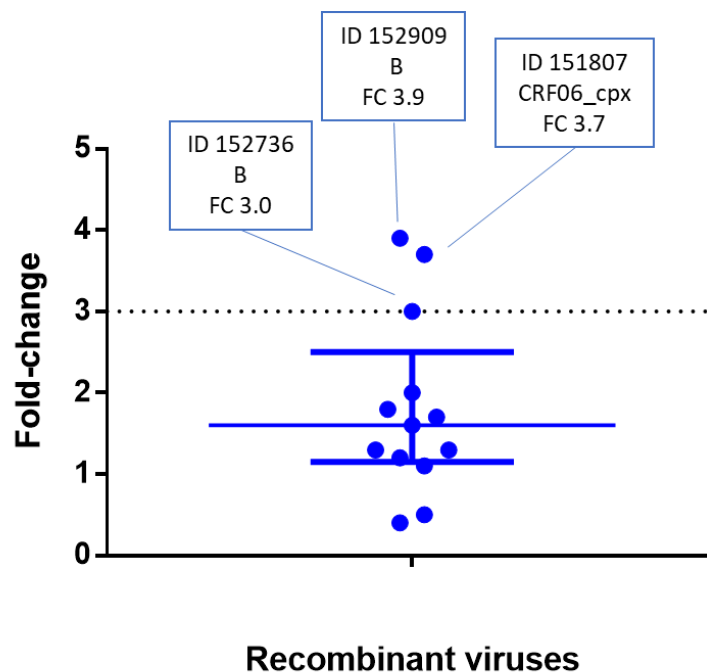
Figure 1: *Most of the viral isolated used for the construction of recombinant viruses belong to subtype B, one to sub-subtype A1 and one to CRF06_cpx. The median DOR fold change of recombinant viruses was 1.6, while in 3/13 cases fold change values were equal to or higher than the DOR fold change biological cut-off. Two of these viruses belong to subtype B and one to CRF06_cpx.*
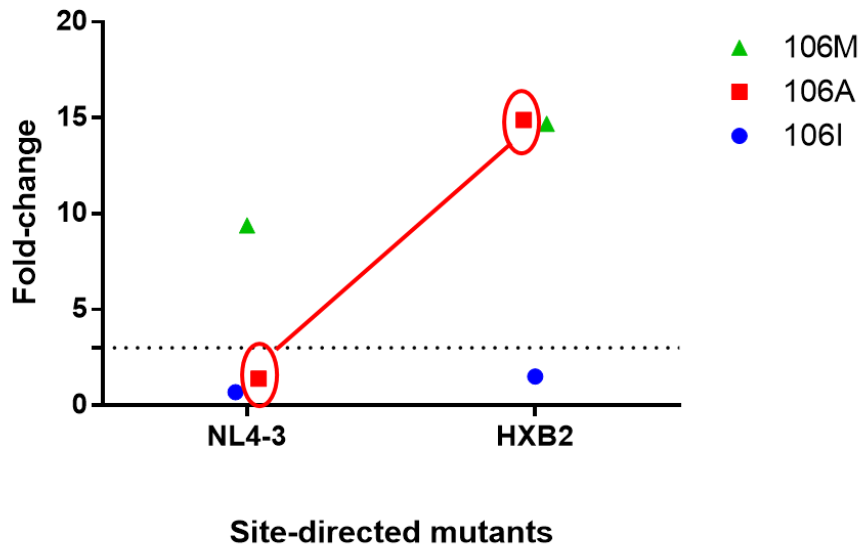
Figure 2: *Fold-change values of viruses harboring V106I, V106A and V106M mutations in NL4-3 and HXB2 backbones were 0.7, 1.4, 9.4 and 1.5, 14.9, 14.7, respectively. In particular, V106A mutant gives a different susceptibility depending on the NL4-3 and HXB2 genetic background.*
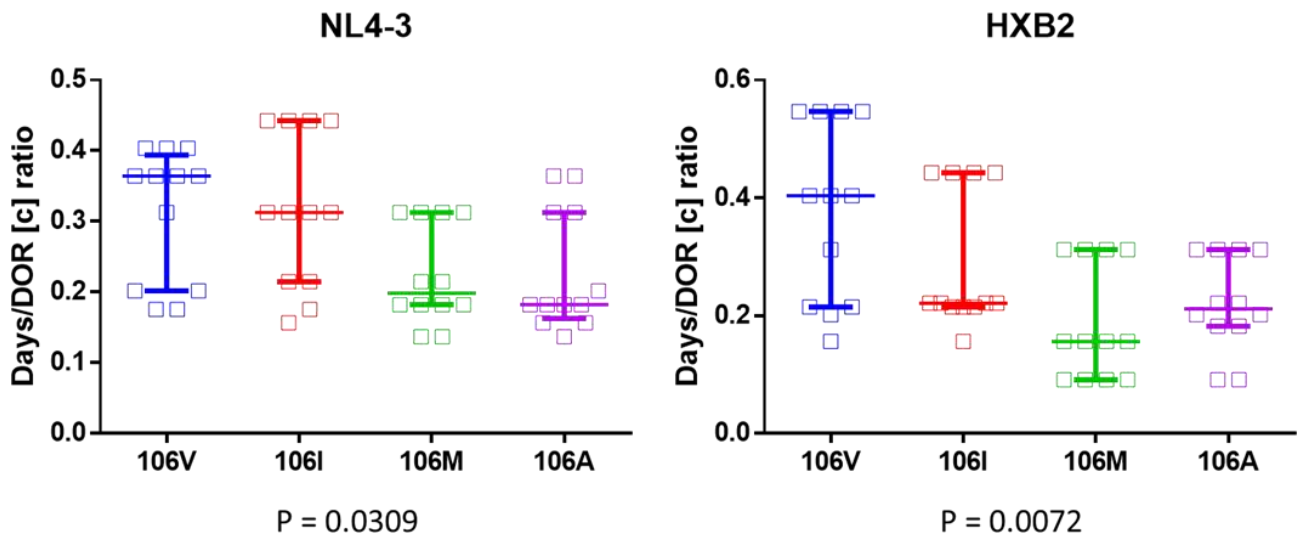

Figure 3: *By comparing the ratio between the time of viral breakthrough and DOR concentration, we observed statistically significant differences among mutant and wild-type viruses with both NL4-3 and HXB2. Wild-type NL4-3 and NL4-3_106I showed a similar median ratio and higher than those observed with 106A and M. In the case of HXB2, there was a significant difference in the comparation of the viral breakthrough between HXB2 and V106M. In both cases we can see that V106I did not significantly decrease the genetic barrier to DOR.*

POSTER PRESENTED AT HIV DRUG THERAPY GLASGOW in 2022

Phenotypic analysis of the impact of V106I in HIV-1 reverse transcriptase on resistance to Doravirine

Francesco Saladini, Adolfo de Salazar, Ana Fuentes, Laura Viñuela, Federica Giammarino, Niccolò Bartolini, Charlotte Charpentier, Sidonie Lambert-Niclot, Gaetana Sterrantino, Grazia Colao, Veleria Micheli, Ada Berloti, Lavinia Fabeni, Isabelle Malet, Elisa Teyssou, Perpetua Gomes, Dimitrios Paraskevis, Maria M. Santoro, Anne-Genevieve Marcelin, Francesca Ceccherini-Silberstein, Maurizio Zazzi, Federico García

Aim

To evaluate the impact of V106I mutation on phenotypic resistance to doravirine in the background of B and non-B subtypes; in addition, we describe its prevalence in MeditRes HIV.

Methods

MeditRes HIV is a consortium that includes ART naïve people living with HIV newly diagnosed in France, Greece, Italy, Portugal and Spain during the years 2018-2021. We evaluated the impact of V106I on susceptibility to doravirine (a) in site directed mutants containing V106I, V106A, V106M & Y188L mutations in subtype B (NL4.3, HXB2) and CRF02_AG background and (b) in a subset of recombinant viruses with clinically derived RT-RNAseH coding region harboring V106I and no other major NNRTI RAMs. Phenotypic susceptibility to doravirine was determined through a TZM-bl cell-based assay and expressed as fold-change (FC) with respect to the reference wild type virus.

Results

MeditRes HIV includes 2705 patients. The prevalence of V106I in the dataset was 2.85%. FC values for site directed mutants in the NL4.3, HXB2 and CRF02_AG background were 0.7, 2.0 and 2.5 with V106I, respectively; 3.4, 19.9 and na (not available) with V106A; 9.4, 27.3 and 13.5 with V106M; >100, na, and >100 with Y188L. The panel of clinically derived viruses tested so far includes 20 subtypes B and 15 non-B subtypes (2 A1, 2 CRF02_AG, 3 CRF06_cpx, 1 CRF44_BF, 2 D, 4 F1 and 1 URF). The median doravirine FC values were 1.5 (range 0.3-6.5) in the whole data set, 1.2 (range 0.3-1.9) for the B subtypes, and 2.45 (range 0.5-6.5) for non-Bs; only three non B clinical isolates showed FC values higher than doravirine biological cutoff (3.0) (CRF06_cpx, FC=3.7; A1; FC=5.5; F1, FC=6.5).

Conclusions

Pretreatment drug resistance to doravirine through the years 2018-2021 remains low in the MeditRes HIV countries. Using site directed mutagenesis on a B and CRF02_AG background, there was no impact of V106I mutation on resistance to doravirine.

Likewise, clinical isolates harboring V106I and no other major NNRTI RAMs retained in vitro susceptibility to doravirine.
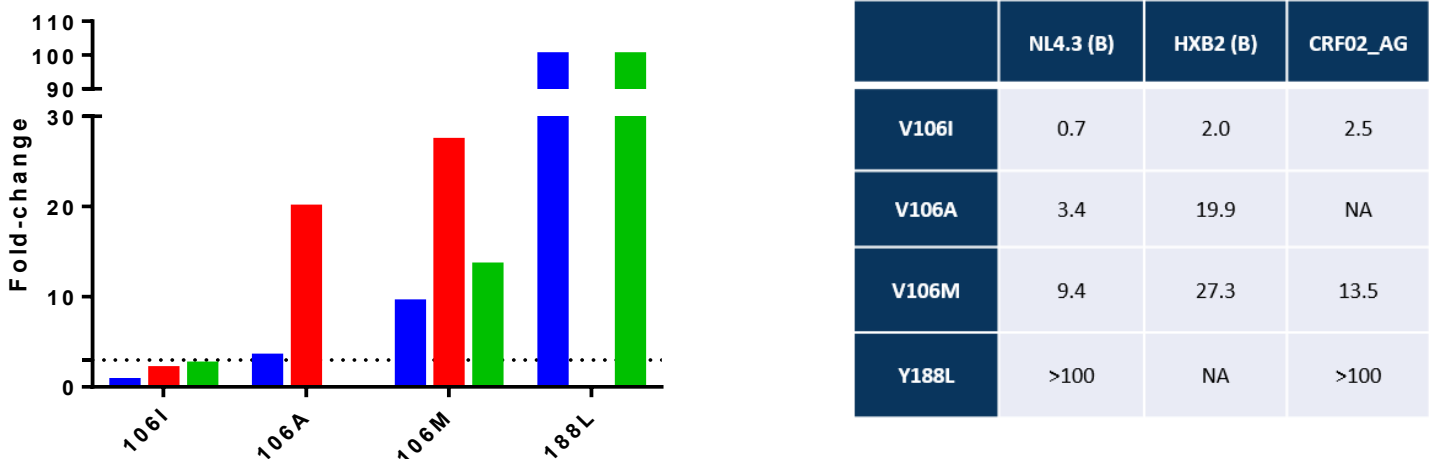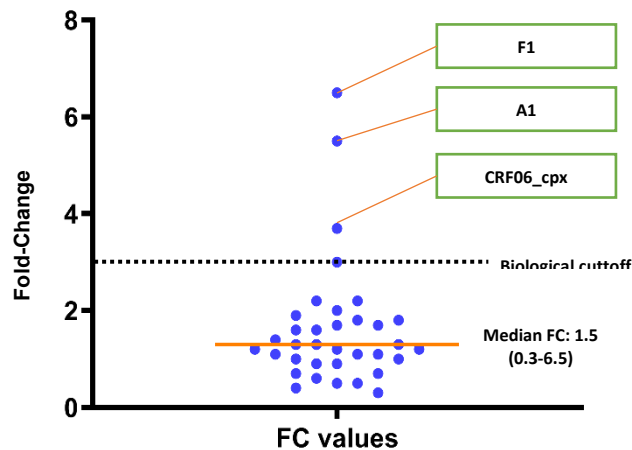

	NL4.3 (B)	HXB2 (B)	CRF02_AG
V106I	0.7	2.0	2.5
V106A	3.4	19.9	NA
V106M	9.4	27.3	13.5
Y188L	>100	NA	>100

Figure 1 and Table 1: *MeditRes HIV includes 2705 patients from 2018 to 2021. The prevalence of V106I in the dataset was 2.85%. Representation of fold-change values for site directed mutants in the NL4.3, HXB2 and CRF02_AG background.*

Figure 2: *The panel of clinically derived viruses tested includes 20 subtypes B and 15 non-B subtypes (2 A1, 2 CRF02_AG, 3 CRF06_cpx, 1 CRF44_BF, 2 D, 4 F1 and 1 URF). The median Doravirine FC values were 1.5 (range 0.3-6.5), 1.2 (range 0.3-1.9), and 2.5 (range 0.5-6.5) in the whole data set, in the B and non-B subtypes, respectively. Only three non-B clinical isolates showed FC values higher than Doravirine biological cutoff (3.0) (CRF06_cpx, FC=3.7; A1, FC=5.5; F1, FC=6.5).*

Federica Giammarino, Niccolò Bartolini, Maurizio Zazzi, Francesco Saladini:
Department of Medical Biotechnologies, University of Siena, Italy

Maria Mercedes Santoro, Francesca Ceccherini-Silberstein:
Department of Experimental Medicine, University of Rome "Tor Vergata", Rome, Italy

Gaetana Sterrantino
Department of Clinical and Experimental Medicine, University of Florence, Italy

Grazia Colao
Laboratory of Virology, Careggi Hospital, Florence, Italy

Valeria Micheli
Department of Clinical Microbiology, Virology and Bioemergencies, Sacco University Hospital, Milan, Italy

Ada Bertoli
Microbiology and Virology Unit, University Hospital of Rome Tor Vergata, Rome, Italy

Lavinia Fabeni
Virology and Biosafety Laboratories Unit, "Lazzaro Spallanzani"-IRCCS, National Institute for Infectious Diseases, Rome, Italy

Isabelle Malet, Elisa Teyssou, Anne-Genevieve Marcelin:
Sorbonne Université, INSERM, Institut Pierre Louis d'Epidémiologie et de Santé Publique, AP-HP, Hôpitaux Universitaires Pitié-Salpêtrière – Charles Foix, laboratoire de virologie, F75013 Paris, France

Charlotte Charpentier
Université de Paris, IAME, UMR1137, INSERM, Laboratoire de Virologie, Hôpital Bichat-Claude Bernard, AP-HP, Paris, France

Sidonie Lambert-Niclot
Sorbonne Université, INSERM, Institut Pierre Louis d'Epidémiologie et de Santé Publique, AP-HP, Hôpital Saint-Antoine, laboratoire de virologie, F75012 Paris, France

Adolfo de Salazar, Ana Fuentes, Laura Viñuela, Federico García:
1. Department of Clinical Microbiology, Hospital Universitario Clínico San Cecilio, Instituto de Investigación Ibs, Granada, Spain
2. CIBER de Enfermedades Infecciosas (CIBERINFEC), ISCIII, Madrid, Spain

Perpetua Gomes
1. Centro de Investigação Interdisciplinar Egas Moniz (CiiEM), Instituto Universitário Egas Moniz, Lisboa, Portugal

2. Laboratório de Biología Molecular, LMCBM, SPC, Centro Hospitalar Lisboa Ocidental – HEM, Lisboa, Portugal

Dimitrios Paraskevis
Department of Hygiene, Epidemiology and Medical Statistics, Medical School, National and Kapodistrian University of Athens, Athens, Greece

Original Research

Development of a Cell-Based Immunodetection Assay for Simultaneous Screening of Antiviral Compounds Inhibiting Zika and Dengue Virus Replication

Ilaria Vicenti[1] (iD), Filippo Dragoni[1], Alessia Giannini[1], Federica Giammarino[1], Michele Spinicci[2], Francesco Saladini[1], Adele Boccuto[1], and Maurizio Zazzi[1]

Abstract

Practical cell-based assays can accelerate anti-Zika (ZIKV) and anti-dengue (DENV) virus drug discovery. We developed an immunodetection assay (IA), using a pan-flaviviral monoclonal antibody recognizing a conserved envelope domain. The final protocol includes a direct virus yield reduction assay (YRA) carried out in the human Huh7 cell line, followed by transfer of the supernatant to a secondary Huh7 culture to characterize late antiviral effects. Sofosbuvir and ribavirin were used to validate the assay, while celgosivir was used to evaluate the ability to discriminate between early and late antiviral activity. In the direct YRA, at 100, 50, and 25 $TCID_{50}$, sofosbuvir IC_{50} values were 5.0 ± 1.5, 2.7 ± 0.5, 2.5 ± 1.1 μM against ZIKV and 16.6 ± 2.8, 4.6 ± 1.4, 2.6 ± 2.2 μM against DENV; ribavirin IC_{50} values were 6.8 ± 4.0, 3.8 ± 0.6, 4.5 ± 1.4 μM against ZIKV and 17.3 ± 4.6, 7.6 ± 1.2, 4.1 ± 2.3 μM against DENV. Sofosbuvir and ribavirin IC_{50} values determined in the secondary YRA were reproducible and comparable with those obtained by direct YRA and plaque reduction assay (PRA). In agreement with the proposed mechanism of late action, celgosivir was active against DENV only in the secondary YRA (IC_{50} 11.0 ± 1.0 μM) and in PRA (IC_{50} 10.1 ± 1.1 μM). The assay format overcomes relevant limitations of the gold standard PRA, allowing concurrent analysis of candidate antiviral compounds against different viruses and providing preliminary information about early versus late antiviral activity.

Introduction

Dengue (DENV) and Zika (ZIKV) viruses are related members of the Flaviviridae family, transmitted by mosquitoes of the *Aedes* genus.[1–3] Multiple factors, such as globalization,[4] environmental changes favoring reproduction of the vector,[5] and viral adaptation to the urban setting,[6] have recently spread these viruses to novel areas. DENV is the most prevalent arboviral infection in humans, as indicated by the World Health Organization (WHO) (https://www.who.int/dengue-control/disease/en/), causing severe flu-like illness and occasionally lethal dengue hemorrhagic fever or dengue shock syndrome. Over the last 50 years, the incidence of DENV has increased dramatically with an estimated 400 million new infections per year occurring mainly in tropical and subtropical areas.[1] Since the first recognized large outbreak of ZIKV in Micronesia in 2007, ZIKV has also spread rapidly to many countries in the Americas affecting millions of individuals. The association of ZIKV infection with Guillain-Barré syndrome in adults and congenital brain abnormalities in newborn infants,[7] established during the last Brazilian

outbreak, has renewed the interest in ZIKV. Consequently, the WHO has ranked DENV as the most critical mosquito-borne viral disease and ZIKV as an international public health emergency.

Despite the urgent need for effective treatment, no specific antiviral therapy is available to control ZIKV or DENV infection and transmission.[8,9] In addition, increasing rates of co-infections with different flaviviruses co-circulating within the same vector complicate the clinical outcome and

[1]Department of Medical Biotechnologies, University of Siena, Siena, Italy
[2]Unit of Infectious Diseases, Careggi University Hospital, Florence, Toscana, Italy

Corresponding Author:
Ilaria Vicenti, Department of Medical Biotechnologies, University of Siena, Viale Bracci 16, Siena, 53100, Italy.
Email: ilariavicenti@gmail.com

treatment options.[10] Potential targets for antiflavivirus compounds include viral proteins, such as protease or polymerase, and host cell functions essential for virus replication, such as α-glucosidase and proteins involved in nucleoside biosynthesis.[11,12]

High-throughput screening (HTS) of libraries of small molecules is a powerful tool to identify novel flavivirus inhibitors;[13–15] however, measurement of virus replication can be cumbersome, expensive, and prone to inaccuracy. To date, a variety of methods have been developed, including the classical plaque reduction assay (PRA),[16–18] microscopy monitoring of cytopathic effect (CPE),[19] and immunofluorescence-based assays such as the fluorescence focus assay and the most advanced fluorescence-activated cell sorting assay.[20,21] Cell-based assays using live viruses, such as PRA or CPE, are indicated as the reference standard for antiviral screening, despite poor reproducibility, the requirement of experienced technicians, and high-turnaround times.[8] Consequently, the development of accurate, easy-to-perform, and fast cell-based assays is highly valuable to test candidate inhibitors of ZIKV and DENV replication.

In this study, we describe a fast and accurate cell-based flavivirus immunodetection assay (IA) allowing quantification of ZIKV and/or DENV antigen by a specific monoclonal antibody to the fusion loop of the E protein domain II, which is shared among different flaviviruses. The assay is applied as a readout of a direct yield reduction assay (YRA) measuring inhibition of virus replication in the initially infected cell culture. In addition, viral stocks generated in the direct YRA can be transferred to a second cell culture in the absence of drug, to better characterize antiviral activity exerted at steps occurring later than envelope expression. To validate the assay, sofosbuvir and ribavirin half-maximal inhibitory concentrations (IC$_{50}$) were determined and compared with values obtained by a standardized PRA[22] and with values previously reported in the literature.[23–26] To evaluate the ability of the system to discriminate between early and late antiviral effects, the IC$_{50}$ of celgosivir, an α-glucosidase inhibitor acting at late steps of DENV infection and recently evaluated in a phase Ib/IIa randomized clinical trial (NCT01619969),[27,28] was determined by both a direct and a secondary YRA, as well as by the reference PRA against both viruses. In the literature, celgosivir anti-DENV effects were also determined in vitro[29,30] and in animal models.[31] Even though a possible activity of celgosivir against ZIKV has been hypothesized based on the high similarity between ZIKV and DENV,[28] in a recently published work[32] celgosivir was not active in vitro against ZIKV when a monkey cell line (VERO) was used.

Materials and Methods

Cells

Vero E6 (African green monkey kidney cell line; ATCC, Manassas, VA, USA, CRL-1586), A549 (human lung carcinoma cell line; ATCC CCL-185), Huh7 (human hepatoma cell line; kindly provided by Istituto Toscano Tumori, Core Research Laboratory, Siena, Italy), and LN-18 (glioblastoma cell line; ATCC CRL-2610) cells were used to titrate ZIKV and DENV viral stocks by IA. The C6/36 (*Aedes albopictus* mosquito; ATCC CRL-1660) cell line was used to expand DENV, and the VERO E6 cell line was used to expand ZIKV. The cell propagation medium was Dulbecco's modified Eagle's medium (DMEM), high glucose with sodium pyruvate, and L-glutamine (Euroclone, Milan, Italy) supplemented with 10% fetal bovine serum (FBS; Euroclone) and 1% penicillin/streptomycin (pen/strep; Euroclone). Additional L-glutamine (2 mM) and HEPES (25 mM) were used only in C6/36 medium. The cell infection medium was the same as the propagation medium but with 1% FBS. The mammalian cells were incubated at 37 °C in a humidified incubator supplemented with 5% CO$_2$, whereas the mosquito cell line was maintained at 28 °C.

Viruses

The H/PF/2013 ZIKV strain, belonging to the Asian lineage, and the New Guinea C DENV serotype 2 strain were kindly provided by the Istituto Superiore di Sanità, Rome, Italy. Once expanded in VERO E6 (ZIKV) and C6/36 (DENV) cells, viral stocks were titrated by plaque assay[22] in A549 and VERO E6 cells, yielding viral titers of 400,000 and 20,000 plaque-forming units (PFU) per milliliter, respectively. Briefly, confluent cells in six-well plate format were infected with three 10-fold dilutions of viral stock, and after 1 h viral adsorption at 37 °C with 5% CO$_2$, cells were washed with PBS and infection medium with 0.75% Sea Plaque Agarose (Lonza, Rockland, ME, USA) was added to each well. After 5 days' incubation at 37 °C, the monolayers were fixed with 10% formaldehyde (Carlo Erba Chemicals, Milan, Italy) and stained with 0.1% crystal violet (Carlo Erba Chemicals). After at least 3 h of incubation, the agar overlay was removed by water washing and PFU were counted.

Antivirals

The FDA-approved anti-hepatitis C virus compounds sofosbuvir (β-D-2′-deoxy-2′-α-fluoro-2′-β-C-methyluridine; MedChemExpress, Monmouth Junction, NJ, USA, cat. HY-15005) and ribavirin (1-β-D-ribofuranosyl-1,2,4-triazole-3-carboxamide; Sigma Aldrich, St. Louis, MO, USA, cat. R9644) were used to validate the system. The inhibitor of viral protein glycosylation celgosivir (6-*O*-butanoyl castanospermine; Sigma Aldrich cat. SML2314), acting at the late stage of DENV replication, was used to evaluate the ability of the assay to discriminate between early and late antiviral effects. All reference compounds were supplied as powder; ribavirin and sofosbuvir were dissolved in 100% DMSO, while celgosivir was dissolved in bi-distilled sterile water.

Cytotoxicity Assay

Serial twofold dilutions of antivirals in infection medium (propagation medium supplemented with 1% FBS) were added to Huh7 cells seeded at 7000 cells/well in a 96-well plate. After 72 h of incubation, drug cytotoxicity was measured by using the CellTiter-Glo 2.0 Luminescent Cell Viability Assay (Promega, Madison, WI, USA) according to the manufacturer's protocol. The luminescent signal generated by cells treated with the test compound was compared with that generated by cells treated with DMSO/water to determine the half-maximal cytotoxic concentration (CC_{50}).

Setup of the Immunodetection Assay

Optimal experimental conditions for the detection of viral antigen by IA were defined by growing viral stocks in human cell lines (A549, Huh7, and LN-18) and in the reference monkey line (VERO E6) that were titrated at 48, 72, and 96 h. The day before infection, each cell line was seeded in a 96-well plate format at the appropriate concentration to obtain 90% confluence at the time of antigen detection. Serial twofold dilutions of viral stocks were adsorbed to target cells in quadruplicate for 1 h at 37 °C in a humidified incubator with 5% CO_2. After removal of the virus inoculum, DMEM infection medium with 1% or 3% FBS was added to cultures to be maintained for 48/72 h or 96 h, respectively.

For the immunodetection of virus antigen, the supernatant was removed and cells were fixed for 30 min with 10% formaldehyde (Carlo Erba Chemicals), rinsed with 1% PBS, and permeabilized for 10 min with 1% Triton X-100 (Carlo Erba). Following washing with PBS containing 0.05% Tween 20 (Carlo Erba Chemicals), cells were incubated for 1 h with monoclonal antiflavivirus mouse antibody (clone D1-4G2-4-15; Novus Biologicals, Centennial, CO, USA, NBP2-52709) diluted 1:400 in blocking buffer (PBS containing 1% BSA and 0.1% Tween 20). After washing four times, cells were incubated for 1 h with a polyclonal horseradish peroxidase (HRP)-coupled anti-mouse IgG secondary antibody (Novus Biologicals NB7570) diluted 1:10,000 in blocking buffer. Next, cells were washed five times and the 3,3′,5,5′-tetramethylbenzidine substrate (Sigma Aldrich) was added to each well. After 15 min of incubation in the dark, the reaction was stopped with one volume of 0.5 M sulfuric acid. All incubation steps were performed at room temperature. Absorbance was measured at 450 nm optical density (OD_{450}) using the Absorbance Module of the GloMax Discover Multimode Microplate Reader (Promega) and adjusted by subtracting the background value, established as twofold the mean OD_{450} value of quadruplicate uninfected cells. The 50% tissue culture infectious dose ($TCID_{50}$) of each virus was calculated according to Reed and Muench.[33]

Direct Yield Reduction Assay

The direct YRA is based on the infection of cells in the presence of serial drug dilutions followed by absorbance measurement by IA. Since the readout is based on the detection of the E protein, the system allows us to measure interference with the virus life cycle up to protein production but not at later steps. To define the optimal virus inoculum, 7000 Huh7 cells/well were infected with ZIKV or DENV at 100, 50, and 25 $TCID_{50}$, as determined by the IA described above. Viral adsorption was performed in 96-well plates for 1 h at 37 °C with 5% CO_2. After virus removal, serial dilutions of sofosbuvir or ribavirin were added to the cell media at final concentrations ranging from 0.03 to 100 μM and the plates were incubated at 37 °C with 5% CO_2. All drug concentrations were tested in triplicate and three independent experiments at each $TCID_{50}$ used were performed to determine the assay reproducibility. Infected and uninfected cells without antivirals were used to calculate 100% and 0% of viral replication, respectively. After 72 h, supernatants were harvested and stored at –80 °C for subsequent analysis, and IA was performed on cell monolayers as described above. Based on initial experiments, each IA run was validated when the OD_{450} value in the virus control culture was above 1. This value was taken as 100% replication and IC_{50} values were calculated based on this reference by a nonlinear regression analysis of the dose–response curves generated with the GraphPad PRISM software version 6.01 (La Jolla, CA, USA). The activity of celgosivir against ZIKV and DENV was determined by YRA with 50 $TCID_{50}$ as described above.

Secondary Yield Reduction Assay

The secondary YRA is designed to measure viral protein production driven by the virus generated in the first round in the presence of drug. Thus, antiviral effects exerted at late steps of the virus life cycle, for example, virus glycosylation and assembly, not detected by the direct YRA, can be measured. The secondary YRA was carried out by infecting 7000 Huh7 cells/well in a 96-well plate with ZIKV and DENV viral supernatants generated by direct YRA with reference compounds. Triplicate viral stocks derived from the direct YRA were used and two independent runs of the secondary YRA were performed to assess the reproducibility of results. After 72 h of incubation at 37 °C with 5% CO_2, cells were fixed, and IA was performed to determine the IC_{50} value for each drug as described in the "Direct Yield Reduction Assay" section (**Suppl. Fig. S1**). The DENV glycosylation inhibitor celgosivir was chosen as a reference compound to assess the ability of assay to discriminate between early and late antiviral effects.
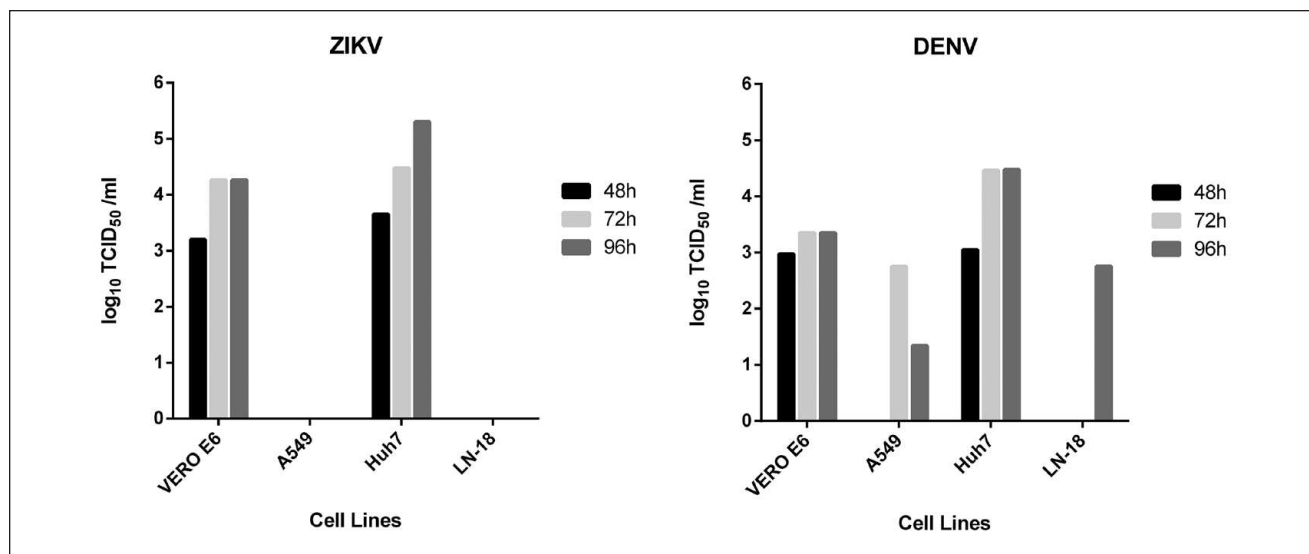
Figure 1. Titration of ZIKV and DENV viral stocks in Huh7, A549, LN-18, and VERO E6 cells at 48, 72, and 96 h by IA.

Plaque Reduction Assay of ZIKV and DENV on Reference Compounds

The PRA on reference compounds was performed as previously described.[22] Briefly, Huh7 cells were infected with ZIKV or DENV at 0.1 multiplicity of infection (MOI), as determined by plaque assay quantification, in the presence of serial fivefold drug dilutions, with a final drug concentration ranging from 0.03 to 100 μM for sofosbuvir and ribavirin and from 0.02 to 50 μM for celgosivir. After 72 h of incubation, three 10-fold dilutions of cell supernatant were used to infect in duplicate A549 (ZIKV) and VERO E6 (DENV) cells. Each experiment included a positive control (original viral stock) and a mock-infected well with infection medium only (**Suppl. Fig. S2**). Viral plaques were visualized 5 and 10 days following infection for ZIKV and DENV, respectively, and the viral titers were calculated by PFU counting. IC_{50} values were calculated by nonlinear regression analysis of the dose–response curves generated with the GraphPad PRISM software version 6.01.

Results

Choice of Cell System and Incubation Time for IA

Titration of ZIKV and DENV viral stocks by IA was possible at 48, 72, and 96 h in VERO E6 and Huh7 cell lines (**Fig. 1**). Despite a visible CPE at 48 h in A549 cells and the ability of both viruses to produce plaques in LN-18 cells (data not shown), ZIKV infection in these cell lines gave negative results by IA, while a weak signal of DENV infection was detected at 72 and 96 h in A549 cells (viral stock titrated as 564 and 22 $TCID_{50}$/mL, respectively) and at 96 h in LN-18

cells (566 $TCID_{50}$/mL). The increasing amount of FBS in infection medium (3% instead of 1%), required to keep cells healthy after 96 h of incubation, probably decreased viral infectivity, as also suggested by the lack of increase of ZIKV viral titers in VERO E6 cells and DENV viral titers in A549, Huh7, and VERO E6 cells. Although the ZIKV viral titer increased up to 96 h in Huh7 (6.6-fold increase with respect to 72 h), the virus yield assay was finally set at 72 h of incubation to maintain the infection medium at 1% FBS concentration and standardize the procedure with both viruses. Huh7 cells, rather than VERO E6 cells, were chosen since human-derived cell lines are more appropriate for the screening of antiviral compounds expected to be used for the treatment of human viral infections, particularly when cellular factors are targeted. The linear dynamic range in such experimental conditions covered 4 logs for both ZIKV and DENV. ZIKV and DENV stocks, titrated in Huh7 at 72 h and subsequently used by direct YRA, were 30,000 and 29,000 $TCID_{50}$/mL, respectively.

Performance of the Direct and Secondary YRA in Determining the Antiviral Activity of Reference Compounds

Reference compounds showed no cytotoxicity in the tested concentration range (0.78–200 μM) (**Suppl. Fig. S3**). The activity of the reference compounds against ZIKV and DENV was first assessed by PRA. Sofosbuvir IC_{50} values were 2.0 ± 1.1 μM against ZIKV and 3.8 ± 1.1 μM against DENV; ribavirin IC_{50} values were 2.2 ± 1.2 against ZIKV and 4.1 ± 1.1 μM against DENV. In PRA, the celgosivir IC_{50} value was 10.1 ± 1.1 μM against DENV, while the compound was not active against ZIKV (**Fig. 2**). The
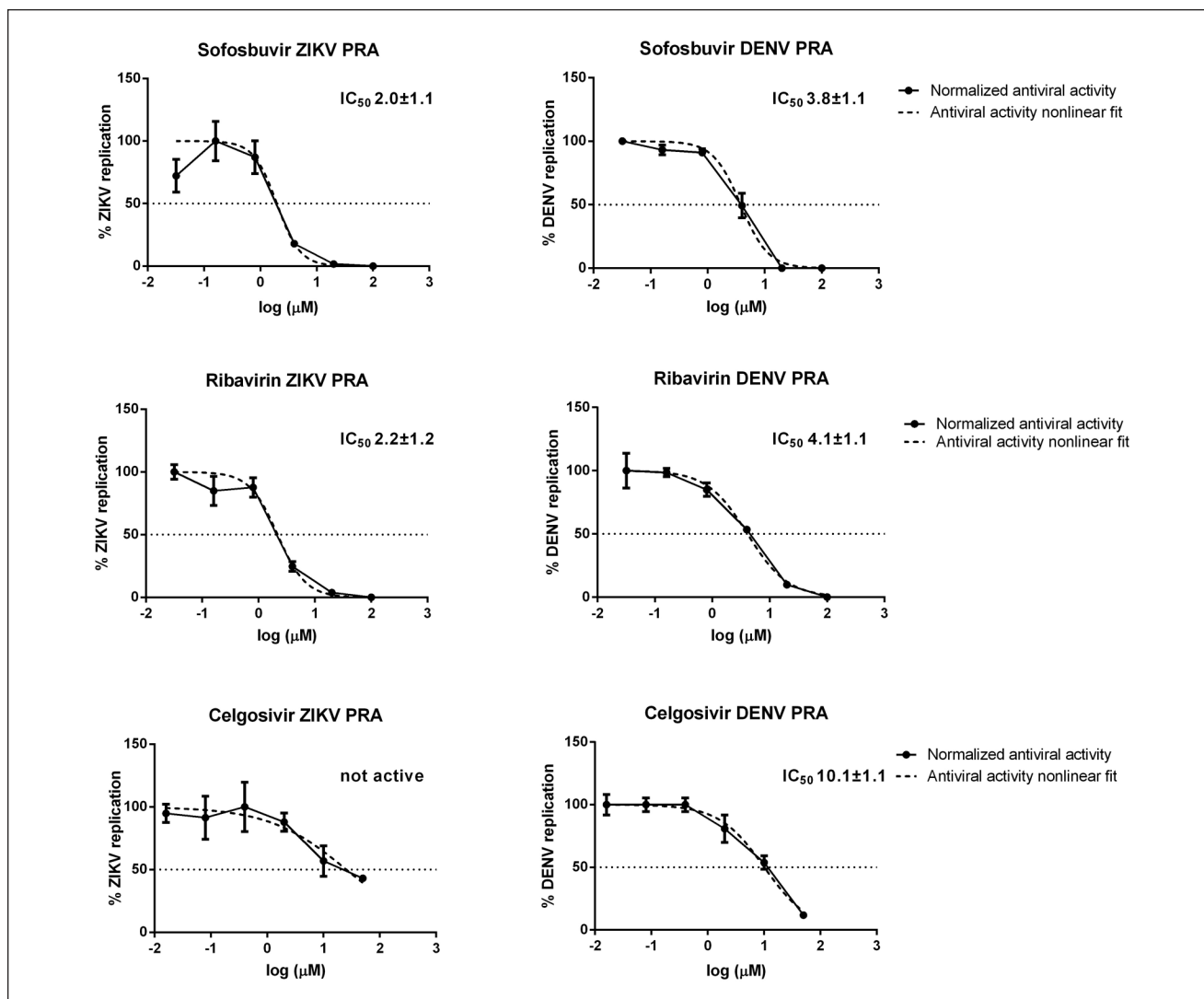
Figure 2. Activity of sofosbuvir and ribavirin against ZIKV and DENV as determined by PRA at 0.1 MOI.

Table 1. IC_{50} of Sofosbuvir and Ribavirin against ZIKV and DENV.

	Sofosbuvir						Ribavirin					
	ZIKV			DENV			ZIKV			DENV		
$TCID_{50}$ viral input	100	50	25	100	50	25	100	50	25	100	50	25
IC_{50}, mean ± SD (µM)[a]	5.0 ± 1.5	2.7 ± 0.5	2.5 ± 1.1	16.6 ± 2.8	4.6 ± 1.4	2.6 ± 2.2	6.8 ± 4.0	3.8 ± 0.6	4.5 ± 1.4	17.3 ± 4.6	7.6 ± 1.2	4.1 ± 2.3
IC_{50} direct YRA/PRA	2.6	1.4	1.3	4.4	1.2	0.7	3.1	1.7	2.1	4.2	1.9	1.0

[a]Values are derived from three independent experiments.

antiviral activities of sofosbuvir and ribavirin for each virus as determined by the direct YRA are shown in **Table 1**. Based on reproducibility within replicates (i.e., lowest coefficient of variation) and correlation with PRA (i.e., ratio of direct YRA IC_{50} to PRA IC_{50} closest to 1), 50

$TCID_{50}$ was set as the optimal amount of viral input to perform the YRA. In the direct YRA, celgosivir was inactive not only against ZIKV but also against DENV, since the step expected to be targeted in the virus life cycle occurs after synthesis of the viral E protein that is detected by IA.
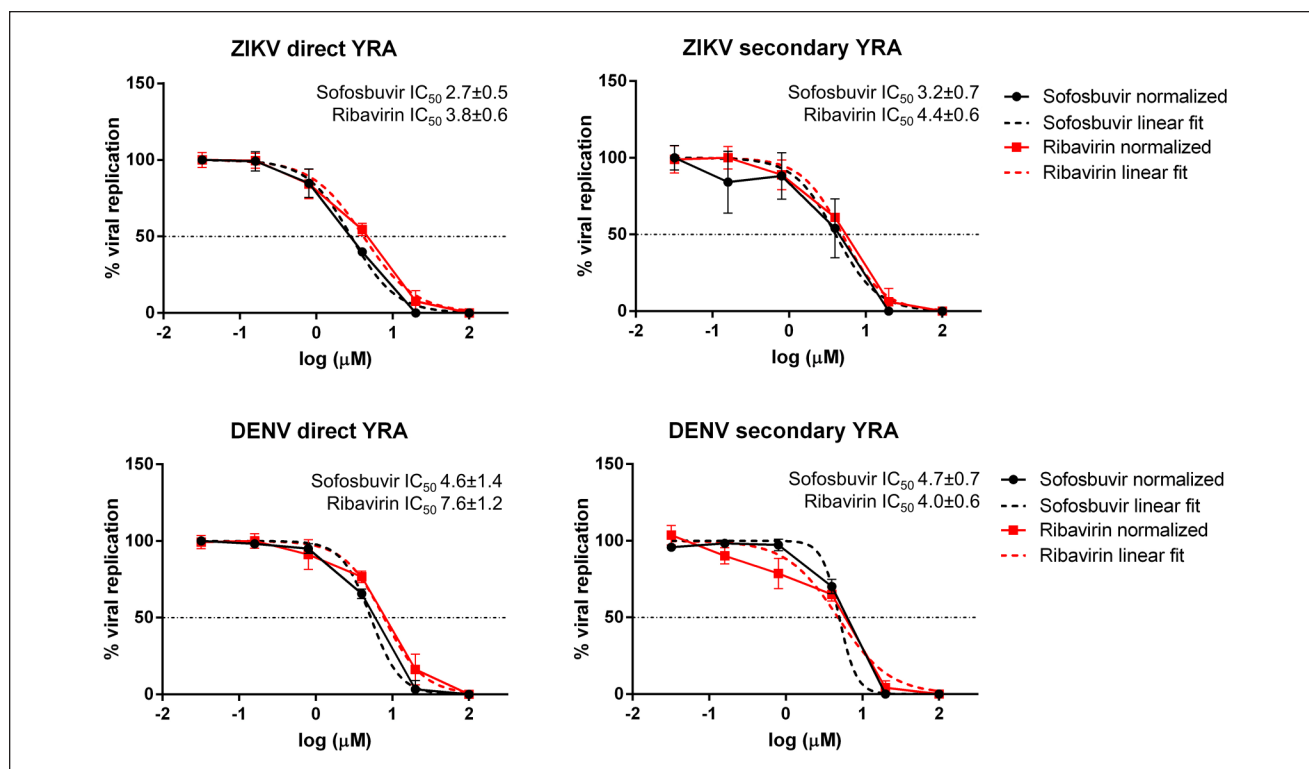
Figure 3. Activity of sofosbuvir and ribavirin against ZIKV and DENV in the direct and secondary YRA.

Table 2. IC$_{50}$ Values of Sofosbuvir, Ribavirin, and Celgosivir against ZIKV and DENV.

	Sofosbuvir		Ribavirin		Celgosivir	
	ZIKV	DENV	ZIKV	DENV	DENV	ZIKV
IC$_{50}$, mean ± SD (µM)[a]	3.2 ± 0.7	4.7 ± 0.7	4.4 ± 0.6	4.0 ± 0.6	11.0 ± 1	Not active
Secondary YRA IC$_{50}$/PRA IC$_{50}$ ratio[b]	1.6	1.2	2.0	1.0	1.1	NA
IC$_{50}$ secondary YRA/IC$_{50}$ direct YRA ratio[b]	1.2	0.8	1.2	0.5	NA	NA

NA, not applicable.
[a]Values are derived from three independent experiments.
[b]The ratio is expressed in fold of differences.

In the secondary YRA, using viral stocks generated in the direct YRA to reinfect Huh7 cell lines, sofosbuvir and ribavirin IC$_{50}$ values against ZIKV and DENV were reproducible and comparable to those obtained by direct YRA and PRA (**Fig. 3**). In addition, celgosivir was active against DENV with a mean IC$_{50}$ value comparable to those obtained in PRA (11.0 ± 1.0 µM and 10.1 ± 1.1 µM, respectively), confirming the value of the secondary YRA to preliminarily identify candidate compounds acting at late steps of viral replication (**Table 2 and Fig. 4**).

Discussion

In the absence of effective vaccines and therapeutic options, supportive care is the only available option for the treatment of flavivirus infections.[34] Assessment of antiviral effects in cultured cells is a key approach for screening candidate compounds. Several cell-based phenotypic assays have been developed, including assays using live virus, subgenomic viral replicons, or virus-like particles.[35] The main disadvantage of the live-virus assays is the obvious necessity for high-level biosafety containment. Subgenomic viral replicons and virus-like particles can overcome safety concerns and are prevalently based on convenient readouts, such as luminescence and fluorescence; however, they do not recapitulate the complete virus life cycle and thus are not amenable for the screening of compounds with unknown targets. Moreover, these assays must be validated carefully to avoid false-positive hits resulting from cytotoxicity or interaction with the luciferase readout.[8] Among live-virus
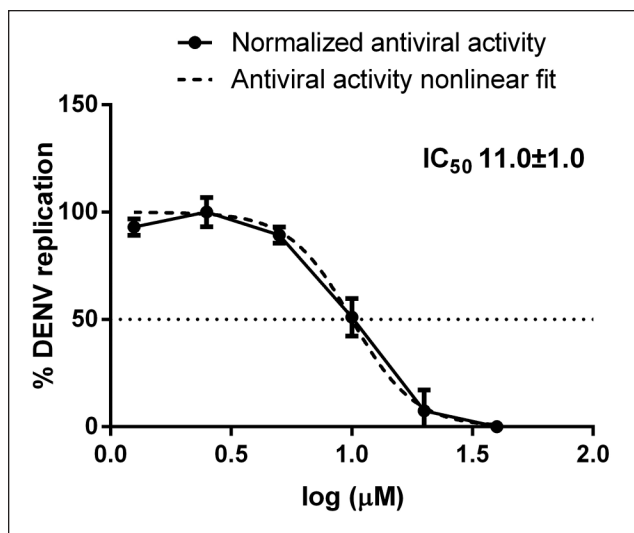
Figure 4. Activity of celgosivir against DENV as determined by the secondary YRA.

assays, PRA has long been considered the gold standard for antiviral screening and is commonly used for anti-DENV and anti-ZIKV antibody titration in plaque reduction neutralization tests.[36] However, PRA has several drawbacks, including high labor, long-turnaround time, and low throughput, making it not suitable for the analysis of large numbers of compounds or sera.

This study describes the development and validation of an IA-based yield reduction test to simultaneously determine the antiviral activity of candidate compounds against ZIKV and DENV in vitro. To define the best experimental conditions, both viruses were propagated in four different cell lines (Huh7, A549, LN-18, and VERO E6) and the viral titer was determined by IA at different time points. The most effective combination of shorter propagation time and better maintenance of cell health was obtained with Huh7 cells, a widely used human hepatoma cell line, and with VERO E6, the monkey cell line mostly used for the propagation and titration of flaviviruses. However, differences in drug metabolism in monkey cells with respect to human cells[37] impact the activity of sofosbuvir and ribavirin against ZIKV and DENV,[25,38] as well as West Nile virus (WNV).[39] Thus, Huh7 was chosen as the model cell line for assay validation. In addition, human cell lines are clearly preferred when assaying candidate host targeting agents for a possible antiviral effect.

The antiviral activity of sofosbuvir and ribavirin was determined by a direct YRA in which the immunodetection of the E protein is directly performed on cells infected with viral stocks and subjected to drug pressure. In the secondary YRA, the antiviral activity is determined by measuring the infectivity of viral stocks generated in the direct YRA. Both drugs were shown to be active against ZIKV and DENV in

the low-micromolar range with IC_{50} values that were comparable in both the direct and secondary YRA performed in this work and in previously reported studies.[11,23,24,26] The secondary YRA can additionally screen compounds exerting antiviral activity at the late stage of the viral cycle (i.e., assembly and maturation of viral particles) that would go undetected or only partially detected by direct YRA. For example, a similar two-step system is adopted to measure the anti-HIV activity of drugs acting at different steps of virus replication.[40,41] Thus, the combined use of the direct and secondary YRA can not only measure antiviral activity but also help characterize the mechanism of action. As proof of concept, we tested celgosivir, an inhibitor of endoplasmic reticulum (ER) α-glycosidases, found to be active against DENV both in vitro, with IC_{50} values ranging from the sub- (0.2 μM) to low- (5.7 μM) micromolar range,[30,42] and in vivo in a mouse model, demonstrating the reduction of viremia and inducement of protection against virus-induced mortality.[30,31] Celgosivir impairs viral protein glycosylation affecting virus assembly and egress, inducing ER stress and the unfolded protein response.[43] We observed that celgosivir did not interfere with the expression of viral E protein at each drug concentration tested in the direct YRA, while a dose-dependent effect of celgosivir on the expression of the E protein was detected in the secondary YRA (**Fig. 4**). The mean celgosivir IC_{50} values against DENV, calculated in the secondary YRA (11.0 μM) or PRA (10.1 μM), were comparable to the values obtained in primary human macrophages (5.2 μM) but significantly higher with respect to the IC_{50} values obtained in BHK-21 cells,[30] reinforcing the importance of antiviral testing in human cell lines for proper assessment of antiviral activity. Globally, these data support the ability of the direct and secondary YRA in the determination of antiviral activity according to the mechanism of action, suggesting that the secondary YRA can be successfully adopted when the mechanism of action of investigational compounds is expected to involve the late phase of viral replication or is unknown.

Importantly, the IA format overcomes relevant limitations of the gold standard PRA. The direct YRA and the secondary YRA are completed in 72 and 144 h, respectively, compared with 192 h for ZIKV and 312 h for DENV required by PRA. In addition, the readout is automated through microplate reading as opposed to manual and error-prone counting in PRA. The use of a pan-flaviviral monoclonal antibody allows use of the same system for different viruses, and indeed similar systems have been described for screening antiviral candidates against DENV.[26,44] However, several of these procedures rely on high-content fluorescence imaging, which may be not easily available, and none are designed to simultaneously screen multiple viruses or to distinguish between early and late antiviral effects.[44–46] Some published protocols were adapted to HTS of large libraries of compounds.[32,47] However, these systems are

based on CPE readout, an indirect measurement of viral infectivity possibly confounded by cell death caused by candidate compounds, as opposed to direct estimates of virus activity like PRA and IA. In terms of turnaround time (about 4 h for 12 compounds analyzed simultaneously for ZIKV and DENV), our system can be defined as a medium-throughput screening assay suitable for testing small to medium libraries of candidate compounds. In summary, the system described here combines several advantages with respect to previously published work, including (1) the use of the same protocol for two different viruses, (2) the ability to distinguish between early and late antiviral effects, (3) a readout directly proportional to virus production and consequently to virus inhibition, and (4) the completion of the assay within 6 days. Thus, the system provides an opportunity to expand the potential for fast cell-based screening of multiple compounds for antiflavivirus therapy.

Declaration of Conflicting Interests

The authors declared the following potential conflicts of interest with respect to the research, authorship, and/or publication of this article: M.Z. reports consultancy for ViiV Healthcare, Gilead Sciences, and Janssen-Cilag, and grants for his institution from ViiV Healthcare and Gilead outside the submitted work.

ORCID iD

Ilaria Vicenti　 https://orcid.org/0000-0002-4306-2960

References

1. Bhatt, S.; Gething, P.; Brady, O.; et al. The Global Distribution and Burden of Dengue. *Nature* **2013**, *496*, 504–507.
2. Marchette, N. J.; Garcia, R.; Rudnick, A. Isolation of Zika Virus from *Aedes aegypti* Mosquitoes in Malaysia. *Am. J. Trop. Med. Hyg.* **1969**, *18*, 411–415.
3. Suwanmanee, S.; Luplertlop, N. Dengue and Zika Viruses: Lessons Learned from the Similarities between These *Aedes* Mosquito-Vectored Arboviruses; *J. Microbiol.* **2017**, *55*, 81–89.
4. Imperato, P. J. The Convergence of a Virus, Mosquitoes, and Human Travel in Globalizing the Zika Epidemic. *J. Commun. Health* **2016**, *41*, 674–679.
5. Liang, G.; Gao, X.; Gould, E. A. Factors Responsible for the Emergence of Arboviruses, Strategies, Challenges and Limitations for Their Control. *Emerg. Microbes Infect.* **2015**, *4*, e18.
6. Vorou, R. Zika Virus, Vectors, Reservoirs, Amplifying Hosts, and Their Potential to Spread Worldwide: What We Know and What We Should Investigate Urgently. *Int. J. Infect. Dis.* **2016**, *48*, 85–90.
7. Krauer, F.; Riesen, M.; Reveiz, L.; et al. Zika Virus Infection as a Cause of Congenital Brain Abnormalities and Guillain–Barré Syndrome: Systematic Review. *PLoS Med.* **2017**, *14*, e1002203.
8. Boldescu, V.; Behnam, M. A. M.; Vasilakis, N.; et al. Broad-Spectrum Agents for Flaviviral Infections: Dengue, Zika and Beyond. *Nat. Rev. Drug Discov.* **2017**, *16*, 565–586.
9. Silva, J. V. J.; Lopes, T. R. R.; Oliveira-Filho, E. F.; et al. Current Status, Challenges and Perspectives in the Development of Vaccines against Yellow Fever, Dengue, Zika and Chikungunya Viruses. *Acta Trop.* **2018**, *182*, 257–263.
10. Estofolete, C. F.; Terzian, A. C. B.; Colombo, T. E.; et al. Co-Infection between Zika and Different Dengue Serotypes during DENV Outbreak in Brazil. *J. Infect. Public Health.* **2018**, *12*, 178–181.
11. Chang, J.; Schul, W.; Butters, T. D.; et al. Combination of α-Glucosidase Inhibitor and Ribavirin for the Treatment of Dengue Virus Infection In Vitro and In Vivo. *Antiviral Res.* **2011**, *89*, 26–34.
12. Munjal, A.; Khandia, R.; Dhama, K.; et al. Advances in Developing Therapies to Combat Zika Virus: Current Knowledge and Future Perspectives. *Front. Microbiol.* **2017**, *8*, 1469.
13. Lo, M. K.; Tilgner, M.; Shi, P. Y. Potential High-Throughput Assay for Screening Inhibitors of West Nile Virus Replication. *J. Virol.* **2003**, *77*, 12901–12906.
14. Puig-Basagoiti, F.; Deas, T. S.; Ren, P.; et al. High-Throughput Assays Using a Luciferase-Expressing Replicon, Virus-Like Particles, and Full-Length Virus for West Nile Virus Drug Discovery. *Antimicrob. Agents Chemother.* **2005**, *49*, 4980–4988.
15. Xie, X.; Zou, J.; Wang, Q. Y.; et al. Targeting Dengue Virus NS4B Protein for Drug Discovery. *Antiviral Res.* **2015**, *118*, 39–45.
16. Balasubramanian, A.; Manzano, M.; Teramoto, T.; et al. High-Throughput Screening for the Identification of Small-Molecule Inhibitors of the Flaviviral Protease. *Antiviral Res.* **2016**, *134*, 6–16.
17. Dulbecco, R. Production of Plaques in Monolayer Tissue Cultures by Single Particles of an Animal Virus. *Proc. Natl. Acad. Sci. U.S.A.* **1952**, *38*, 747–752.
18. Roehrig, J. T.; Hombach, J.; Barrett, A. D. T. Guidelines for Plaque-Reduction Neutralization Testing of Human Antibodies to Dengue Viruses. *Viral Immunol.* **2008**, *21*, 123–132.
19. Bernatchez, J. A.; Yang, Z.; Coste, M.; et al. Development and Validation of a Phenotypic High-Content Imaging Assay for Assessing the Antiviral Activity of Small-Molecule Inhibitors Targeting Zika Virus. *Antimicrob. Agents Chemother.* **2018**, *62*, e00725-18.
20. Kraus, A. A.; Messer, W.; Haymore, L. B.; et al. Comparison of Plaque- and Flow Cytometry-Based Methods for Measuring Dengue Virus Neutralization. *J. Clin. Microbiol.* **2007**, *45*, 3777–3780.

21. Payne, A. F.; Binduga-Gajewska, I.; Kauffman, E. B.; et al. Quantitation of Flaviviruses by Fluorescent Focus Assay. *J. Virol. Methods* **2006**, *134*, 183–189.

22. Vicenti, I.; Boccuto, A.; Giannini, A.; et al. Comparative Analysis of Different Cell Systems for Zika Virus (ZIKV) Propagation and Evaluation of Anti-ZIKV Compounds In Vitro. *Virus Res.* **2018**, *244*, 64–70.

23. Bullard-Feibelman, K. M.; Govero, J.; Zhu, Z.; et al. The FDA-Approved Drug Sofosbuvir Inhibits Zika Virus Infection. *Antiviral Res.* **2017**, *137*, 134–140.

24. Julander, J. G.; Siddharthan, V.; Evans, J.; et al. Efficacy of the Broad-Spectrum Antiviral Compound BCX4430 against Zika Virus in Cell Culture and in a Mouse Model. *Antiviral Res.* **2017**, *137*, 14–22.

25. Sacramento, C. Q.; de Melo, G. R.; de Freitas, C. S.; et al. The Clinically Approved Antiviral Drug Sofosbuvir Inhibits Zika Virus Replication. *Sci. Rep.* **2017**, *7*, 40920.

26. Xu, H. T.; Colby-Germinario, S. P.; Hassounah, S. A.; et al. Evaluation of Sofosbuvir (β-D-2′-Deoxy-2′-α-Fluoro-2′-β-C-Methyluridine) as an Inhibitor of Dengue Virus Replication. *Sci. Rep.* **2017**, *7*, 6345.

27. Low, J. G.; Sung, C.; Wijaya, L.; et al. Efficacy and Safety of Celgosivir in Patients with Dengue Fever (CELADEN): A Phase 1b, Randomised, Double-Blind, Placebo-Controlled, Proof-of-Concept Trial. *Lancet Infect. Dis.* **2014**, *14*, 706–715.

28. Sung, C.; Wei, Y.; Watanabe, S.; et al. Extended Evaluation of Virological, Immunological and Pharmacokinetic Endpoints of CELADEN: A Randomized, Placebo-Controlled Trial of Celgosivir in Dengue Fever Patients. *PLoS Negl. Trop. Dis.* **2016**, *10*, e0004851.

29. Courageot, M.-P.; Frenkiel, M.-P.; Duarte Dos Santos, C; et al. Alpha-Glucosidase Inhibitors Reduce Dengue Virus Production by Affecting the Initial Steps of Virion Morphogenesis in the Endoplasmic Reticulum. *J. Virol.* **2000**, *74*, 564–572.

30. Rathore, A. P. S.; Paradkar, P. N.; Watanabe, S.; et al. Celgosivir Treatment Misfolds Dengue Virus NS1 Protein, Induces Cellular Pro-Survival Genes and Protects against Lethal Challenge Mouse Model. *Antiviral Res.* **2011**, *92*, 453–460.

31. Watanabe, S.; Chan, K. W. K.; Dow, G.; et al. Optimizing Celgosivir Therapy in Mouse Models of Dengue Virus Infection of Serotypes 1 and 2: The Search for a Window for Potential Therapeutic Efficacy. *Antiviral Res.* **2016**, *127*, 10–19.

32. Adcock, R. S.; Chu, Y. K.; Golden, J. E.; et al. Evaluation of Anti-Zika Virus Activities of Broad-Spectrum Antivirals and NIH Clinical Collection Compounds Using a Cell-Based, High-Throughput Screen Assay. *Antiviral Res.* **2017**, *138*, 47–56.

33. Reed, L. J.; Muench, H. A Simple Method of Estimating Fifty Per Cent Endpoints. *Am. J. Epidemiol.* **1938**, *27*, 493–497.

34. Kok, W. M. New Developments in Flavivirus Drug Discovery. *Expert Opin. Drug Discov.* **2016**, *11*, 433–445.

35. Green, N.; Ott, R. D.; Isaacs, J.; et al. Cell-Based Assays to Identify Inhibitors of Viral Disease. *Expert Opin. Drug Discov.* **2008**, *3*, 671–676.

36. Cordeiro, M. T. Laboratory Diagnosis of Zika Virus. *Top. Magn. Reson. Imaging.* **2019**, *28*, 15–17.

37. Guo, D.; Zhu, Q.; Zhang, H.; et al. Proteomic Analysis of Membrane Proteins of Vero Cells: Exploration of Potential Proteins Responsible for Virus Entry. *DNA Cell Biol.* **2014**, *33*, 20–28.

38. Gan, C. S.; Lim, S. K.; Chee, C. F.; et al. Sofosbuvir as Treatment against Dengue? *Chem. Biol. Drug Des.* **2018**, *91*, 448–455.

39. Day, C. W.; Smee, D. F.; Julander, J. G.; et al. Error-Prone Replication of West Nile Virus Caused by Ribavirin. *Antiviral Res.* **2005**, *67*, 38–45.

40. Puertas, M. C.; Buzón, M. J.; Ballestero, M.; et al. Novel Two-Round Phenotypic Assay for Protease Inhibitor Susceptibility Testing of Recombinant and Primary HIV-1 Isolates. *J. Clin. Microbiol.* **2012**, *50*, 3909–3916.

41. Saladini, F.; Giannini, A.; Boccuto, A.; et al. Agreement between an In-House Replication Competent and a Reference Replication Defective Recombinant Virus Assay for Measuring Phenotypic Resistance to HIV-1 Protease, Reverse Transcriptase, and Integrase Inhibitors. *J. Clin. Lab. Anal.* **2017**, *32*, e22206.

42. Sayce, A. C.; Alonzi, D. S.; Killingbeck, S. S.; et al. Iminosugars Inhibit Dengue Virus Production via Inhibition of ER Alpha-Glucosidases—Not Glycolipid Processing Enzymes. *PLoS Negl. Trop. Dis.* **2016**, *10*, e0004524.

43. Zakaria, M. K.; Carletti, T.; Marcello, A. Cellular Targets for the Treatment of Flavivirus Infections. *Front. Cell. Infect. Microbiol.* **2018**, *8*, 398.

44. Tan, K. H.; Wing Ki, K. C.; Watanabe, S.; et al. Cell-Based Flavivirus Infection (CFI) Assay for the Evaluation of Dengue Antiviral Candidates Using High-Content Imaging. *Methods Mol. Biol.* **2014**, *1138*, 99–109.

45. Lee, E. M.; Titus, S. A.; Xu, M.; et al. High-Throughput Zika Viral Titer Assay for Rapid Screening of Antiviral Drugs. *Assay Drug Dev.* **2019**, *17*, 128–139.

46. Wang, Q. Y.; Patel, S. J.; Vangrevelinghe, E.; et al. A Small-Molecule Dengue Virus Entry Inhibitor. *Antimicrob. Agents Chemother.* **2009**, *53*, 1823–1831.

47. Han, Y.; Mesplède, T.; Xu, H.; et al. The Antimalarial Drug Amodiaquine Possesses Anti-ZIKA Virus Activities. *J Med Virol.* **2018**, *90*, 796–802.

Research paper

Evaluation of sofosbuvir activity and resistance profile against West Nile virus in vitro

Filippo Dragoni[a], Adele Boccuto[a], Francesca Picarazzi[b], Alessia Giannini[a], Federica Giammarino[a], Francesco Saladini[a], Mattia Mori[b], Eloise Mastrangelo[c], Maurizio Zazzi[a], Ilaria Vicenti[a,*]

[a] *Department of Medical Biotechnologies, University of Siena, Italy*
[b] *Department of Biotechnology, Chemistry and Pharmacy, University of Siena, Italy*
[c] *National Research Council, Biophysics Institute of Milano, Italy*

ABSTRACT

Sofosbuvir, a licensed nucleotide analog targeting hepatitis C virus (HCV) RNA-dependent RNA polymerase (RdRp), has been recently evaluated as a broad anti-Flavivirus lead candidate revealing activity against Zika and Dengue viruses both in vitro and in animal models. In this study, the in vitro antiviral activity of sofosbuvir against West Nile virus (WNV) was determined by plaque assay (PA) and Immunodetection Assay (IA) in human cell lines and by enzymatic RdRp assay. By PA, the sofosbuvir half-maximal inhibitory concentration (IC_{50}) was 1.2 ± 0.3 μM in Huh-7, 5.3 ± 0.9 μM in U87, 7.8 ± 2.5 μM in LN-18 and 63.4 ± 14.1 μM in A549 cells. By IA, anti-WNV activity was confirmed in both hepatic (Huh-7, 1.7 ± 0.5 μM) and neuronal (U87, 7.3 ± 2.0 μM) cell types. Sofosbuvir was confirmed to inhibit the purified WNV RdRp (IC_{50} 11.1 ± 4.6 μM). In vitro resistance selection experiments were performed by propagating WNV in the Huh-7 cell line with two-fold increasing concentrations of sofosbuvir. At 80 μM, a significantly longer time for viral breakthrough was observed compared with lower concentrations (18 vs. 7–9 days post infection; p = 0.029), along with the detection of the S604T mutation, corresponding to the well-known S282T substitution in the motif B of HCV NS5B, which confers resistance to sofosbuvir. Molecular docking experiments confirmed that the S604T mutation within the catalytic site of RdRp affected the binding mode of sofosbuvir. To our knowledge, this is the first report of the antiviral activity of sofosbuvir against WNV as well as of selection of mutants in vitro.

1. Introduction

West Nile virus (WNV) is a neurotropic Flavivirus preferentially transmitted by the Culex spp. Mosquitoes (Chancey et al., 2015). While most WNV infections are asymptomatic or paucisymptomatic, occasional patients experience severe neurological disease, including meningitis, encephalitis and flaccid paralysis (Sejvar, 2014). Due to lack of vaccine and specific antiviral drugs, only symptomatic treatment or supportive care is available for WNV disease (Kok, 2016).

Viral enzymes are attractive targets for the development of antiviral therapeutics against WNV and other flaviviruses (Acharya and Bai, 2016; Boldescu et al., 2017). The nonstructural protein 5 (NS5) is the key Flavivirus replication enzyme, about 900 amino acids in length, composed of two different domains: the N-terminal methyltransferase (MTase) and the C-terminal RNA dependent RNA-dependent RNA polymerase (RdRp). The MTase domain mediates both guanine-N7 and nucleoside-2′-O methylation of the cap structure, increasing the stability of newly synthesized RNA, facilitating the translation of the viral polyprotein and influencing the RdRp domain, which is essential for viral RNA replication. The structure of the WNV RdRp resembles the classical viral RdRp architecture with thumb, palm and fingers sub-domains and consists of six catalytic motifs (A-F), plus a G-loop (Malet et al., 2008, 2007; Zhang et al., 2008).

Given the high degree of structural homology observed among RdRp enzymes within the Flaviviridae family (Lim et al., 2013), sofosbuvir, a nucleotide analog licensed for hepatitis C virus (HCV) infection (Götte and Feld, 2016), has been recently evaluated as an anti-Flavivirus lead candidate. Indeed, the inhibitory activity of sofosbuvir has been documented in vitro against Zika virus (ZIKV) and Dengue virus (DENV) and in animal models against ZIKV (Mesci et al., 2018; Sacramento et al., 2017; H. T. Xu et al., 2017a). In addition, sofosbuvir has shown activity against the Alphavirus chikungunya (CHIKV), both in vitro and in an animal model (Ferreira et al., 2019). Since the NS5 amino acid residues predicted to interact with sofosbuvir show approximately 80% conservation among WNV, DENV and ZIKV (Appleby et al., 2015), sofosbuvir could also be active against WNV, providing a treatment option by itself or a lead structure for further development. The aim of this work was to determine for the first time sofosbuvir activity against the purified WNV RdRp and against WNV replication in a yield reduction system as measured by plaque assay (PA) and by Immunodetection Assay (IA) using different cell lines, as well as its resistance profile through in vitro resistance selection experiments.

---

* Corresponding author.
  E-mail address: ilariavicenti@gmail.com (I. Vicenti).

2. Materials and methods

2.1. Cells and virus

VERO E6 (African green monkey kidney cell line; ATCC® CRL-1586™), A549 (human lung carcinoma cell line; ATCC® CCL-185™), Huh-7 (human hepatoma cell line; kindly provided from Istituto Toscano Tumori, Core Research Laboratory, Siena, Italy), LN-18 (glioblastoma cell line; ATCC® CRL-2610™) and U87 (astroglioma cell line; NIBSC 044) were maintained in Dulbecco's Modified Eagle's Medium High Glucose with sodium pyruvate and L-Glutamine (DMEM; Euroclone) supplemented with 10% Fetal Bovine Serum (FBS; Euroclone) and 1% Penicillin/Streptomycin (Pen/Strep, Euroclone) at 37 °C with 5% CO_2. The same medium was used but with a lower FBS concentration for viral propagation and drug susceptibility testing (1%) and for in vitro selection experiments (3%). The WNV lineage 1 strain Italy/2009 (Magurano et al., 2012) was kindly provided by the Istituto Superiore di Sanità, Rome, Italy. Once expanded, WNV viral stock was titrated in VERO E6 cells by PA, as described below, yielding 4.2×10^7 PFU/ml.

2.2. Drugs and cytotoxicity assay

The FDA-approved anti-HCV compounds sofosbuvir (β-d-2′-deoxy-2′-α-fluoro-2′-β-C-methyluridine; MCE® cat. HY-15005), its active 5′-triphosphate metabolite (SOF-TP; MCE® cat. HY-15745), and ribavirin (1-β-D-Ribofuranosyl-1,2,4-Triazole-3-Carboxamide; Sigma Aldrich cat. R9644), used as reference compound, were supplied as powder and dissolved in 100% dimethyl sulfoxide (DMSO). Drug cytotoxicity was measured by the CellTiter-Glo 2.0 Luminescent Cell Viability Assay (Promega), according to the manufacturer's protocol. After 48 h incubation, the luminescent signal generated by the cells treated with the test compound was compared to that generated by the cells treated with DMSO to determine the 50% cytotoxic concentration (CC_{50}).

2.3. WNV propagation in different cell lines

Propagation of the titrated viral stock was tested in different cell lines and at different time points (24, 48 and 72 h).

For the PA readout, the day before infection each cell line (VERO E6, A549, Huh-7, LN-18 and U87) was seeded in 6-well plate to obtain 90% confluence at the time of collection of supernatants. Viral stock was diluted in infection medium and used to infect cells in duplicate for each time point at 0.1 multiplicity of infection (MOI). After 1 h adsorption at 37 °C, the viral stock was removed and replaced by infection medium, then the cells were incubated for 24, 48 and 72 h. For each time point, the PA was performed on harvested supernatants as previously described with minor modifications (Vicenti et al., 2018). Briefly, confluent cells in 6-well format were infected with three tenfold dilutions of viral stock and after 1 h adsorption at 37 °C, the cells were washed with PBS and 0.75% Sea Plaque Agarose (Lonza) was added to each well. After 3 days incubation at 37 °C, the monolayers were fixed with 10% formaldehyde (Carlo Erba Chemicals) and stained with 0.1% crystal violet (Carlo Erba Chemicals). After 3 h incubation, the agar overlay was removed by water washing and PFU were counted.

For the IA readout, the day before infection each cell line (Huh-7 and U87) was seeded in 96-well plate to obtain 90% confluence at the time of antigen detection. Serial two-fold dilutions of viral stocks were adsorbed to the target cells in quadruplicate for 1 h at 37 °C. After removal of the virus inoculum, DMEM infection medium was added to the cultures and the cells were incubated for 24, 48 and 72 h.

For the immunodetection of virus antigen, the supernatant was removed and the cells were fixed for 30 min with 10% formaldehyde (Carlo Erba), rinsed with 1% PBS and permeabilized for 10 min with 1% Triton X-100 (Carlo Erba). After washing with PBS containing 0.05% Tween 20 (Carlo Erba), the cells were incubated for 1 h with a

monoclonal anti-flavivirus mouse antibody (clone D1-4G2-4-15; Novus Bio NBP2-52709) diluted 1:400 in blocking buffer (PBS containing 1% BSA and 0.1% Tween 20). After washing, the cells were incubated for 1 h with a polyclonal HRP-coupled anti-mouse IgG secondary antibody (Novus Bio NB7570) diluted 1:10,000 in blocking buffer. Next, the cells were washed and the 3,3′,5,5′-Tetramethylbenzidine substrate (Sigma Aldrich) was added to each well. After 15 min incubation in the dark, the reaction was stopped with one volume of 0.5 M sulfuric acid. All the incubation steps were performed at room temperature. Absorbance was measured at 450 nm optical density (OD450) using the Absorbance Module of the GloMax® Discover Multimode Microplate Reader (Promega) and adjusted by subtracting the background value established as 2-fold the mean OD450 value of quadruplicate uninfected cells. The 50% tissue culture infectious dose ($TCID_{50}$) of each virus was calculated according to Reed and Munch (Reed and Muench, 1938).

2.4. Determination of sofosbuvir and ribavirin antiviral activity in cell line models

The antiviral activity of sofosbuvir and ribavirin against WNV was determined by PA in A549, Huh-7, U87 and LN-18 cells using 0.1 MOI based on published work (Escribano-Romero et al., 2017) and confirmed by IA in U87 and Huh-7 cells using 100, 50 and 25 $TCID_{50}$ to assess the reproducibility of the IC_{50} values using different virus inputs. For PA, the cells were pre-seeded in 96-well plate to obtain 90% confluence at the time of supernatant collection; for IA, the cells were pre-seeded in 96-well plate to obtain 10,000 cells for each well at the time of infection. The cells were then incubated in propagation medium at 37 °C. After 24 h, each cell line was infected with the specified input of viral stock and after 1 h adsorption the virus inoculum was removed and 5-fold dilutions of each drug (from 100 to 0.032 μM) were added to the cell monolayer. For PA, the viral supernatants were collected at 24 h for A549, at 48 h for Huh-7 and U87 and at 72 h for LN-18 cells according to the propagation experiments and PA was performed as previously indicated (paragraph 2.3). For the IA, the Huh-7 and U87 cell lines were incubated at 37 °C for 48 h, then the plates where fixed and stained as described in paragraph 2.3. Each drug concentration was tested in triplicate and infected and uninfected cells were tested as reference; three independent experiments were performed. IC_{50} values were calculated by a non-linear regression analysis of the dose-response curves generated with the Graphpad PRISM software version 6.01 (La Jolla, California, USA).

2.5. In vitro enzymatic inhibition assay with WNV RdRp

The WNV RdRp protein was expressed and purified as already described (Tarantino et al., 2016). RdRp activity was assessed following the synthesis of dsRNA from a single-stranded poly(C) template (10 μg) and 100 μM GTP in a reaction mixture containing 20 mM Tris/HCl (pH 7.5), 1 mM DTT, 25 mM NaCl, 5 mM $MgCl_2$, 0.3 mM $MnCl_2$, 2U RiboLock Ribonuclease inhibitor (Life technologies), 1 μl PicoGreen Quantitation Reagent (Life technologies) as already described (Gong et al., 2013; Tarantino et al., 2016; Van Dycke et al., 2018). WNV RdRp, at the concentration of 1 μM, was added to the reaction mixture together with SOF-TP (ranging from 0 to 250 μM). The PicoGreen fluorescence (excitation/emission = 485/530 nm) was measured at 30 °C for 30 min (Varian, Cary Eclipse Fluorescence Spectrophotometer). RdRp activity (i.e. linear slope of fluorescence increasing over time, Y) vs. inhibitor concentration (X) was used to estimate the IC_{50} of the SOF-TP using the equation $Y = (Range/(1 + (X/IC_{50}))$ where Range is the difference between the values observed for the uninhibited and completely inhibited RdRp.

2.6. In vitro selection experiments

In vitro selection experiments were performed in Huh-7 cells at 70%

confluence in T25 flasks with 0.05 and 0.01 MOI, each in duplicate. After 1 h adsorption at 37 °C, the virus inoculum was removed and the cells were incubated with 5 µM sofosbuvir, corresponding to about 4-fold IC50. The cell cultures were monitored every 24 h, and when 80% of viral cytopathic effect (CPE) was observed, the cells and supernatants were freeze-thawed, cleared by centrifugation and used to re-infect fresh pre-seeded Huh-7 in the presence of 2-fold higher sofosbuvir concentration. At each step, negative (cells with drug) and positive (cells with virus for each MOI) controls were included. Sanger sequencing of the WNV NS5 region was performed to detect emergent mutations at each drug increment. Mutant viruses were titrated by IA and sofosbuvir IC50 was measured as described above using 25 TCID50, in triplicate experiments. Fold changes (FC) values were calculated as the ratio between the IC50 of the mutant virus stock and the IC50 of the paired wild type control grown without drug pressure under the same experimental conditions (no-drug control).

2.7. Viral RNA amplification and sequencing

All the viral stocks collected during in vitro selection experiments were analyzed by population sequencing to detect emergent mutations in the NS5 region. Briefly, 150 µl of viral stocks were extracted using the ZR Viral RNA Kit (Zymo Research) according to the manufacturer's protocol. cDNA was generated by random hexamer-driven reverse transcription using 10 µl of RNA extract, 664 µM dNTPs, 6 µl of 5X ImProm-II TM Reaction Buffer, 50 ng Hexanucleotides, 1.5 mM MgCl2, 20U RNasin® Plus RNase Inhibitor and 1U of ImProm-II™ Reverse Transcriptase (Promega) in a final volume of 30 µl. The reactions included an initial 5-min step at 25 °C, followed by 30 min at 37 °C and a 5-min final step at 80 °C. cDNA was used as the template for PCR amplification of the whole NS5 gene, using the Q5 Hot Start High-Fidelity DNA Polymerase (NEB) protocol. To design primers with a high degree of conservation, the WNV alignment available at the NCBI web site was used (https://www.ncbi.nlm.nih.gov/genomes/VirusVariation); the primer sequences and coordinates, as referred to the WNV strain NY99 (GenBank accession no. DQ211652) are indicated in Table 1. Bidirectional DNA sequencing was performed using the BrilliantDye TM Terminator Kit v1.1 (Nimagen) with 8 different primers spanning the whole NS5 region (Table 1). The sequencing reactions were treated with the X-Terminator® Purification kit (Applied Biosystems) in a 96-well plate as suggested by the manufacturer, resolved by capillary electrophoresis on the 3130 XL Genetic Analyzer (Applied Biosystems) and analyzed with the DNAStar Lasergene 7.1.0 SeqMan Pro module.

2.8. Statistical analysis

Results of the replicate antiviral activity measurements were reported as mean and standard deviation (SD). The difference in time for viral growth under different experimental conditions was analyzed by Mann Whitney U test. Statistical analysis was performed using GraphPad PRISM software version 6.01.

2.9. Molecular docking experiments

Since the crystal structure of the whole WNV NS5 is not available, the crystallographic structures of RNA-free WNV RdRp (PDB-ID: 2HCN) (Malet et al., 2007) and RNA-bound HCV RdRp (PDB-ID: 4WTD) (Appleby et al., 2015) were used as structural templates to build a homology model of WNV RdRp according to Šebera (Šebera et al., 2018). WNV RdRp sequence was retrieved from UniProtKB (P06935). Chimeric homology models were generated by PrimeX software (Bell et al., 2012). The 793VPTGRTTWSIHAKGEWMTT810 loop was removed from the WNV RdRp template as it was overlapping with the RNA. Each model was solvated in TIP3P type water molecules and the total charge was neutralized by counter ions. The solvent was first energy minimized for 500 steps by the steepest descent algorithm (SDA) and 1500 steps by the conjugated gradient algorithm (CGA). Subsequently, the whole system was energy minimized for 1500 steps SDA and 8500 steps CGA. Amber18 software was used in energy minimization (Case et al., 2018), with the following force fields: i) ff14SB for the protein; ii) OL3 for RNA; iii) GAFF for ADP (partial charges and bond parameters were retrieved from the AMBER parameter database (Meagher et al., 2003).

Docking simulations were carried out with GOLD program (Jones et al., 1997), using the CHEMPLP as a scoring function. The binding site was centered on Tyr610 with a radius of 13 Å. The protonation state of sofosbuvir was assigned by FixpKa (OpenEye Scientific Software Santa Fe, NM) QUACPAC version 2.0.0.3 using default parameters and the molecule was energy minimized by Szybki (OpenEye Scientific Software Santa Fe, NM) version 1.10.0.3 using the MMFF94S force field (http://www.eyesopen.com).

3. Results

3.1. Viral propagation and determination of sofosbuvir and ribavirin antiviral activity

All the cell lines tested were permissive to WNV infection, as shown in Fig. 1a. By PA, the peak virus production was observed at 24 h in A549 cells ($1.7 \times 10^7 \pm 2.0 \times 10^6$ PFU/ml), at 48 h in Huh-7 ($4.4 \times 10^8 \pm 3.2 \times 10^7$ PFU/ml), VERO E6 ($2.7 \times 10^7 \pm 1.6 \times 10^6$ PFU/ml) and U87 ($1.7 \times 10^7 \pm 4.9 \times 10^5$ PFU/ml) cells, and at 72 h in LN-18 cells ($9.4 \times 10^6 \pm 8.8 \times 10^5$ PFU/ml). When WNV was quantified in Huh-7 and U87 cells by IA, a similar trend in viral growth was observed in both cell lines (Fig. 1b). Based on these results, the yield reduction assays to determine antiviral activity were specifically set at the peak of virus production of each cell line. Antiviral activity was tested only in the human cell lines, based on better ability to mimic the virus human tropism in different tissues.

In the range tested (0.78–400 µM), sofosbuvir and ribavirin showed no cytotoxicity in all the cell lines evaluated (Supplementary Fig. 1). The antiviral activity of sofosbuvir and ribavirin, measured by PA at 0.1 MOI, is shown in Fig. 2 and Table 2. Sofosbuvir was active in the low micromolar range in Huh-7 (1.2 ± 0.3 µM) cells and in both neuronal

Table 1
Primer used to sequence the whole NS5 region.

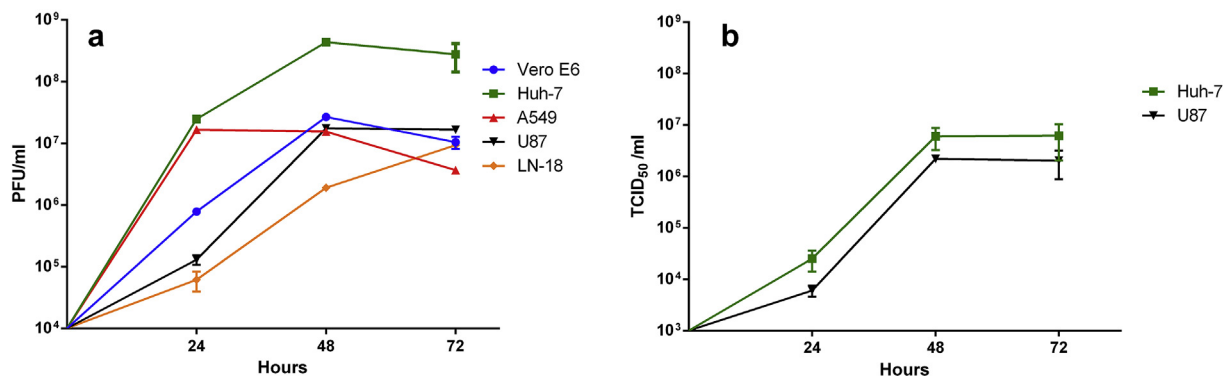| PRIMER	SEQUENCE	SENSE	GENE	From	To
P882	GACTYTGYCACATCATGCGTG	Forward	NS4B	7589	7609
P883	GCAGCACCGTCTACTCAACTTC	Reverse	3′UTR	10532	10553
P884	CAGCTGGTGAGRATGATGGAAGG	Forward	NS5	9541	9563
P885	GAGATGGTGGATGAGGAGCG	Forward	NS5	8983	9002
P886	TTGGTGAARGTGTTYAGGGCGTA	Reverse	NS5	9508	9530
P887	GAAGATGTMAACTTGGGAAGTGGAA	Forward	NS5	8446	8470
P888	CTRCCGTGRTAGTTCCAGGTTCT	Reverse	NS5	8587	8609
P890	CTCCRCTCTTCATGGTGACAATGTT	Reverse	NS5	8044	8068

Fig. 1. (a) WNV propagation as measured by Plaque Assay in four different human cell lines Huh-7, A549, U87 and LN-18 and in the monkey VERO E6 cell line; results were expressed as Plaque Forming Units per ml (PFU/ml). (b) WNV propagation as measured by Immunodetection Assay in Huh-7 and U87 cells; results were expressed as Tissue Culture Infectious Doses per milliliter (TCID50/ml).

cell lines U87 (5.3 $\pm$ 0.9 μM) and LN-18 (7.8 $\pm$ 2.5 μM), while a reduced activity was observed in A549 cells (63.4 $\pm$ 9.0 μM). Ribavirin was less active than sofosbuvir in Huh-7 (6.7 $\pm$ 0.6 μM), LN-18 (10.7 $\pm$ 0.5 μM) and U87 (60.5 $\pm$ 11.8 μM) cells, with 1.4- to 11.4-fold difference. Conversely, ribavirin was more active than sofosbuvir in A549 cells (6.2 vs. 63.4 μM, respectively). The antiviral activity of both compounds was also determined by IA in Huh-7 and U87 cells using three different viral inputs (Table 3). The IA IC_{50} was closest to the PA IC_{50} at the lowest viral input used, i.e. 25 $TCID_{50}$. Globally, IA confirmed the results obtained with PA showing the efficacy of sofosbuvir in inhibiting WNV replication in the human hepatic and neuronal cell lines in the low micromolar range.

The inhibitory effect of SOF-TP on WNV was determined also in vitro using the purified recombinant WNV RdRp in a *de novo* RdRp assay synthesizing dsRNA from the single-stranded poly(C) template. Sofosbuvir inhibited the WNV RdRp activity in a dose-dependent manner, with an IC_{50} of 11.1 $\pm$ 4.6 μM.

Table 2

Antiviral activity of sofosbuvir and ribavirin against WNV as measured by PA using the MOI of 0.1 in different human cell lines. Three independent experiments for each cell line were performed.

Cell line	Sofosbuvir	Ribavirin
	Mean IC_{50} (μM) $\pm$ SD	Mean IC_{50} (μM) $\pm$ SD
Huh-7	1.2 $\pm$ 0.3	6.7 $\pm$ 0.6
U87	5.3 $\pm$ 0.9	60.5 $\pm$ 11.8
A549	63.4 $\pm$ 9.0	6.2 $\pm$ 1.3
LN-18	7.8 $\pm$ 2.5	10.7 $\pm$ 0.5

IC_{50}: Half maximal inhibitory concentration; SD: Standard Deviation.

3.2. WNV In vitro selection experiments under sofosbuvir drug pressure

Two WNV inputs (0.01 and 0.05 MOI), each in duplicate, were used to infect Huh-7 cells in the presence of increasing concentration of
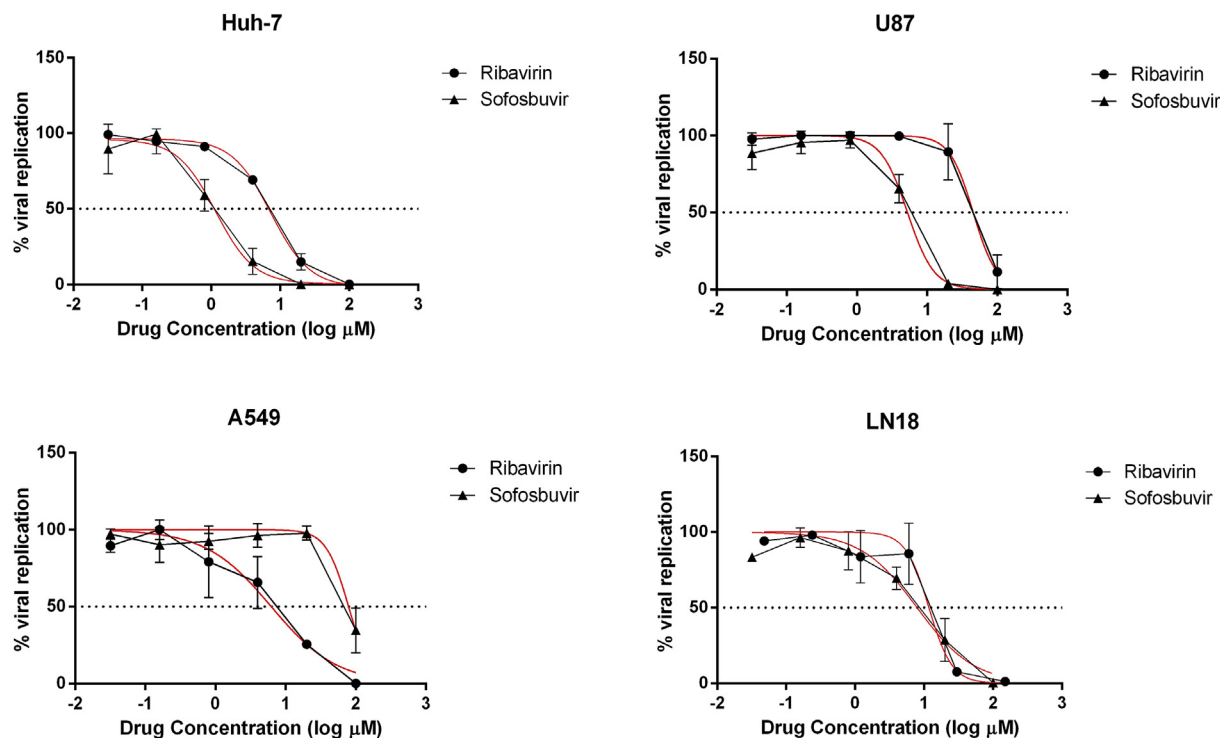

Fig. 2. Normalized antiviral activity of sofosbuvir and ribavirin as determined by Plaque Assay at 0.1 MOI in four different human cell lines (Huh-7, A549, U87 and LN-18). The non linear fitting curve as calculated by GraphPad Prism is depicted in red.

Table 3
Antiviral activity of sofosbuvir and ribavirin against WNV as measured by IA in Huh-7 and U87 cells using three different viral inputs in three independent experiments for each cell line.

Cell line	Sofosbuvir		Ribavirin	
	$TCID_{50}$	Mean IC_{50} (µM) ± SD	$TCID_{50}$	Mean IC_{50} (µM) ± SD
Huh-7	100	3.1 ± 0.6	100	14.4 ± 3.6
	50	2.0 ± 0.1	50	13.5 ± 3.1
	25	1.7 ± 0.5	25	9.5 ± 4.0
U87	100	15.1 ± 2.0	100	92.0 ± 13.8
	50	10.6 ± 2.1	50	73.0 ± 32.6
	25	7.3 ± 2.0	25	61.6 ± 13.7

$TCID_{50}$: Tissue Culture Infectious Dose; IC_{50}: Half maximal inhibitory concentration; SD: Standard Deviation.

sofosbuvir, starting from 5 µM, corresponding to about 4-fold the sofosbuvir IC_{50} as measured by PA in the same cells. Drug pressure significantly delayed viral growth with respect to the no-drug control. Indeed, around 80% of CPE was reached at 7–9 days post infection (dpi) with 5–40 µM sofosbuvir while the no-drug control virus was consistently collected at 3 dpi (p = 0.029). With 80 µM sofosbuvir, a significantly longer time for viral breakthrough was required (18 dpi for all experiments), with respect to lower concentrations, (p = 0.029) and several NS5 mutations emerged (Table 4). Notably, the S604T mutation, corresponding to the well-known S282T sofosbuvir resistance mutation in HCV NS5B (Wu et al., 2015; H. T. Xu et al., 2017b), was detected in three of four experiments, alone or in association with other mutations. Mutations detected in the MTase domain (Malet et al., 2008) included G2E, K76R and T216M, all occurring only once. The RdRp mutation A483G, detected in 2 experiments, is located in the finger domain, highly conserved among flaviviruses (Dubankova and Boura, 2019). In the experiment 4, the only without S604T, the A483G mutation was accompanied by M479K and L721M, located in a conserved domain of the motif F in the RdRp finger domain (Dubankova and Boura, 2019; Malet et al., 2007) and in the motif E of the RdRp thumb close to residues involved in the binding site of Zn_{2+} ion, respectively (Malet et al., 2008).

To assess whether emergent NS5 mutations were associated with drug resistance, sofosbuvir IC_{50} was measured against the mutant viruses collected at 80 µM as well as the wild type viruses collected at 40 µM sofosbuvir, to exclude FC variation independent by the NS5 substitutions. As indicated in Table 4, no changes in FC were observed in the absence of the NS5 mutations. In the presence of the NS5 mutations, IC_{50} values consistently increased with respect to the paired no-drug control virus (median FC 7.7, IQR 5.5–9.7). The maximum increase in FC was observed in experiment 1, where S604T was associated with the K76R and T216M MTase mutations.
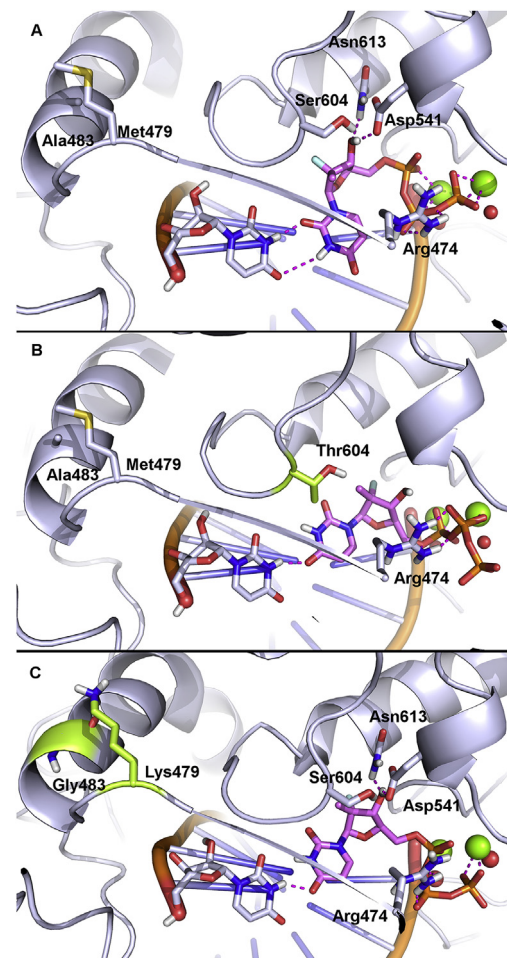

Fig. 3. Docking-based binding mode of sofosbuvir in the catalytic site of (a) wild type WNV RdRp, (b) S604T WNV RdRp, and (c) M479K/A483G/L721M WNV RdRp. Polar contacts are highlighted by magenta dashed lines. Residues involved in polar and non-polar interactions with sofosbuvir are shown as sticks and are labelled. Mg_{2+} ions and water molecules bound to Mg_{2+} ions are shown as green and red spheres, respectively. For the sake of clarity, in panel (c) only the M479K and A483G mutations, which are located near the catalytic site, are visible.

3.3. Molecular docking of sofosbuvir in wild type and mutant viruses

Available structures of RNA-free WNV RdRp and RNA-bound HCV RdRp were used as structural templates to generate the homology model of wild type, as well as S604T and M479K/A483G/L721M

Table 4
Changes in NS5 amino acid sequence detected at virus breakthrough with increasing sofosbuvir concentration in duplicate sample at MOI of 0.01 and of 0.05. The sofosbuvir half maximal inhibitory concentration (IC_{50}) of viral strains growth at the selective pressure of 40 and 80 µM was determined by IA in three independent assays for each experiment.

Experiment	MOI	Increasing sofosbuvir concentration						
		[5,10,20 µM]	[40 µM]			[80 µM]		
		Mutations	Mutations	Mean IC_{50} (µM) ± SD	FC	Mutations	Mean IC_{50} (µM) ± SD	FC
1	0.01	None	None	3.3 ± 0.7	1.4	K76RK, T216MT, S604T	20.1 ± 2.9	10.3
2	0.01	None	None	2.3 ± 0.2	1.0	G2EG, A483GA, S604T	10.4 ± 2.7	5.3
3[a]WT	0.01	None	None	2.3 ± 1.1	1.0	None	2.0 ± 0.4	1.0
4	0.05	None	None	2.2 ± 0.4	1.0	M479KM, A483G, L721M	14.4 ± 1.8	6.5
5	0.05	None	None	1.6 ± 0.9	0.7	S604T	19.5 ± 6.2	8.8
6[a]WT	0.05	None	None	2.2 ± 1.5	1.0	None	2.2 ± 0.4	1.0

FC: Fold-change with respect to the wild type control virus (WT); NM: None.

[a] WT were not subjected to sofosbuvir drug pressure.

variants of WNV RdRp. Docking results showed that the bioactive triphosphate form of sofosbuvir (Murakami et al., 2010) binds the catalytic site of WNV RdRp wild type by pairing the uracil from RNA template in a wobble-like conformation. The hydroxyl group of the drug establishes two H-bonds with Asp541 and Asn613, while phosphate groups are H-bonded to Arg474 and coordinated to catalytic Mg^{2+} ions (Fig. 3a). Probably, because of the steric hindrance of Thr604, which partially occludes the catalytic pocket, in WNV RdRp S604T sofosbuvir establishes only one H-bond with the uracil from the RNA template, while phosphate groups are H-bonded to Arg474. Moreover, only α and β phosphate groups coordinate to Mg^{2+} ions (Fig. 3b). Similarly, docking to the WNV M479K/A483G/L721M triple RdRp mutant showed that sofosbuvir binds within the catalytic site by establishing only one H-bond with the uracil from RNA template and losing the wobble base pairing. The hydroxyl group is H-bonded to Asp541 and Asn613, while phosphate groups are H-bonded to Arg474, although only α and γ phosphate groups coordinate to Mg^{2+} ions (Fig. 3c). Overall, docking results suggest that mutations within the catalytic site affect its overall shape and pharmacophoric features, and impair the binding mode of sofosbuvir particularly with respect to the base pairing with uracil from RNA template. This latter interaction seems to play a crucial role in the inhibition of WNV RdRp catalytic activity by sofosbuvir.

4. Discussion

WNV spreading, together with expanded transmission (Chancey et al., 2015) and increased virulence (Patel et al., 2015), prompts for intensive antiviral drug discovery efforts. Repurposing of licensed drugs can dramatically reduce the developing time for drug testing and validation. Sofosbuvir, a key agent in HCV treatment, has already been considered for the treatment of ZIKV and DENV infection, showing efficacy in vitro and in mouse models (Mesci et al., 2018; Sacramento et al., 2017; H. T. Xu et al., 2017a). We investigated the anti-WNV sofosbuvir activity in vitro in multiple human cell lines. Considering WNV tropism and pathogenesis, we included astroglioma (U87) and glioblastoma (LN-18) cell lines, in addition to epithelial and hepatic cells commonly used for WNV propagation (Ma et al., 2009; Urbanowski and Hobman, 2013). Sofosbuvir was active in the low micromolar range in all human cell lines tested except for the A549 cell line (around one log lower activity). These data, measured by the gold standard PA, were confirmed by the more convenient IA performed in the representative Huh-7 and U87 cells. On the other hand, the lack of sofosbuvir and ribavirin activity in A549 and U87 cells, respectively, underlines the need to choose a suitable cell substrate when testing candidate antiviral agents. The inhibitory activity of sofosbuvir against the purified WNV RdRp measured in a *de novo* enzymatic assay (Tarantino et al., 2016) was in the low micromolar range, comparable to the results previously reported with ZIKV (Xu et al., 2017b).

In vitro sofosbuvir resistance selection experiments have been performed with HCV (Lam et al., 2012; Xu et al., 2017), but not with any flavivirus. Based on homology with the HCV NS5B S282T selected by sofosbuvir, Xu et al. (H. T. Xu et al., 2017b) introduced the S604T mutation in ZIKV NS5 and documented 4.9-fold resistance to sofosbuvir in a biochemical assay. Our work definitely demonstrates that S604T is a major pathway of WNV escape to sofosbuvir pressure in vitro. Indeed, the S604T mutation emerged in three of four resistance selection experiments, resulting in 5.3- to 10.3-fold resistance which is comparable to the extent of sofosbuvir resistance described for the HCV replicons harboring S282T (Han et al., 2019). Both Ser604 and Gly605 are highly conserved residues among flaviviruses, located in the motif B of the RdRp palm (Dubankova and Boura, 2019). Despite limited sequence identity between Flavivirus and HCV RdRp (Malet et al., 2008), these residues are also conserved in HCV, corresponding to S282 and G283 (Appleby et al., 2015; Wu et al., 2015). In addition, a homolog S600T substitution in DENV RdRp has been reported to be involved in

resistance to nucleotide inhibitors in vitro (Latour et al., 2010).

Few other mutations were detected in association with the S604T (Table 4) mutation, all as mixtures with the wild type codon, possibly reflecting adaptation of the enzyme to compensate for loss of fitness consequent to selection of the key S604T resistance mutation, with minimal impact on resistance level. Of note, one experiment generated a 6.5-fold resistant mutant without S604T but harboring three mutations (M479K, A483G, L721M) which have no known counterpart in HCV. This highlights that alternative sofosbuvir escape pathways may occasionally occur.

An atomistic picture of the interaction between sofosbuvir and WNV RdRp was described by molecular modeling. Given the lack of experimental structural information, the 3D structures of catalytically competent wild type and mutant WNV RdRp forms in complex with RNA, metals and ADP were generated by homology modeling, and used as receptors in molecular docking simulations. Compared to the wild type WNV RdRp, in both mutant forms sofosbuvir loses the wobble-like base pairing with the uracil from the RNA template, as well as additional interactions with the catalytic Mg^{2+} ions. These binding modes might account for the different efficacy of sofosbuvir against the three variants of WNV RdRp and highlight the key pharmacophores in WNV RdRp inhibition by small molecules.

To our knowledge, these data show for the first time that sofosbuvir is active against WNV in vitro in human hepatic and neuronal cell lines in the low micromolar range, at levels comparable to those reported for ZIKV and DENV. Based on selection of the S604T mutation, sofosbuvir appears to interact with the same conserved domain across Flavivirus and Hepacivirus RdRp. Studies in animal models are required to confirm the relevance of these findings and better define opportunities for sofosbuvir use or further development against multiple flaviviral infections.

Appendix A. Supplementary data

Supplementary data to this article can be found online at https://doi.org/10.1016/j.antiviral.2020.104708.

References

Acharya, D., Bai, F., 2016. An overview of current approaches toward the treatment and prevention of west Nile virus infection. Methods Mol. Biol. 1435, 249–291. https://doi.org/10.1007/978-1-4939-3670-0_19.

Appleby, T.C., Perry, J.K., Murakami, E., Barauskas, O., Feng, J., Cho, A., Fox, D., Wetmore, D.R., McGrath, M.E., Ray, A.S., Sofia, M.J., Swaminathan, S., Edwards, T.E., 2015. Structural basis for RNA replication by the hepatitis C virus polymerase. Science 347, 771–775. https://doi.org/10.1126/science.1259210.

Bell, J.A., Cao, Y., Gunn, J.R., Day, T., Gallicchio, E., Zhou, Z., Levy, R., Farid, R., 2012. PrimeX and the Schrödinger Computational Chemistry Suite of Programs 534–538. https://doi.org/10.1107/97809553602060000864.

Boldescu, V., Behnam, M.A.M., Vasilakis, N., Klein, C.D., 2017. Broad-spectrum agents for flaviviral infections: dengue, Zika and beyond. Nat. Rev. Drug Discov. 16, 565–586. https://doi.org/10.1038/nrd.2017.33.

Case, D.A., Ben-Shalom, I.Y., Brozell, S.R., Cerutti, D.S., Cheatham III, T.E., Cruzeiro, V.W.D., Darden, T.A., Duke, R.E., Ghoreishi, D., Gilson, M.K., Gohlke, H., Goetz, A.W., Greene, D., Harris, R., Homeyer, N., Izadi, S., Kovalenko, A., Kurtzman, T., Lee, T.S., LeGrand, S., Li, P., Lin, C., Liu, J., Luchko, T., Luo, R., Mermelstein, D.J., Merz, K.M., Miao, Y., Monard, G., Nguyen, C., Nguyen, H., Omelyan, I., Onufriev, A., Pan, F., Qi, R., Roe, D.R., Roitberg, A., Sagui, C., Schott-Verdugo, S., Shen, J., Simmerling, C.L., Smith, J., Salomon-Ferrer, R., Swails, J., Walker, R.C., Wang, J., Wei, H., Wolf, R.M., Wu, X., Xiao, L., York, D.M., Kollman, P.A., 2018. AMBER 2018. University of California, San Francisco.

Chancey, C., Grinev, A., Volkova, E., Rios, M., 2015. The global ecology and epidemiology of west nile virus. BioMed Res. Int. 2015, 376230. https://doi.org/10.1155/2015/376230.

Dubankova, A., Boura, E., 2019. Structure of the yellow fever NS5 protein reveals conserved drug targets shared among flaviviruses. Antivir. Res. 169, 104536. https://doi.org/10.1016/j.antiviral.2019.104536.

Escribano-Romero, E., De Oya, N.J., Domingo, E., Saiza, J.C., 2017. Extinction of west nile virus by favipiravir through lethal mutagenesis. Antimicrob. Agents Chemother. 61, 1–9. https://doi.org/10.1128/AAC.01400-17.

Ferreira, A.C., Reis, P.A., de Freitas, C.S., Sacramento, C.Q., Hoelz, L.V.B., Bastos, M.M., Mattos, M., Rocha, N., de Azevedo Quintanilha, I.G., da Silva Gouveia Pedrosa, C., Souza, L.R.Q., Loiola, E.C., Trindade, P., Vieira, Y.R., Barbosa-Lima, G., de Castro Faria Neto, H.C., Boechat, N., Rehen, S.K., Brüning, K., Bozza, F.A., Bozza, P.T., Souza, T.M.L., 2019. Beyond members of the Flaviviridae family, sofosbuvir also inhibits chikungunya virus replication. Antimicrob. Agents Chemother. 63, 18. https://doi.org/10.1128/AAC.01389-18. e01389.

Gong, E.Y., Kenens, H., Ivens, T., Dockx, K., Vermeiren, K., Vandercruyssen, G., Devogelaere, B., Lory, P., Kraus, G., 2013. Expression and purification of dengue virus NS5 polymerase and development of a high-throughput enzymatic assay for screening inhibitors of dengue polymerase. Methods Mol. Biol. 1030, 237–247. https://doi.org/10.1007/978-1-62703-484-5_19. PubMed PMID: 23821273.

Götte, M., Feld, J.J., 2016. Direct-acting antiviral agents for hepatitis C: structural and mechanistic insights. Nat. Rev. Gastroenterol. Hepatol. 13, 338–351. https://doi.org/10.1038/nrgastro.2016.60.

Han, B., Martin, R., Xu, S., Parvangada, A., Svarovskaia, E.S., Mo, H., Dvory-Sobol, H., 2019. Sofosbuvir susceptibility of genotype 1 to 6 HCV from DAA-naïve subjects. Antivir. Res. 170, 104574. https://doi.org/10.1016/j.antiviral.2019.104574.

Jones, G., Willett, P., Glen, R.C., Leach, A.R., Taylor, R., 1997. Development and validation of a genetic algorithm for flexible docking. J. Mol. Biol. https://doi.org/10.1006/jmbi.1996.0897.

Kok, W.M., 2016. New developments in flavivirus drug discovery. Expert Opin. Drug Discov. 11, 433–445. https://doi.org/10.1517/17460441.2016.1160887.

Lam, A.M., Espiritu, C., Bansal, S., Micolochick Steuer, H.M., Niu, C., Zennou, V., Keilman, M., Zhu, Y., Lan, S., Otto, M.J., Furman, P.A., 2012. Genotype and subtype profiling of PSI-7977 as a nucleotide inhibitor of hepatitis C virus. Antimicrob. Agents Chemother. 56, 3359–3368. https://doi.org/10.1128/AAC.00054-12.

Latour, D.R., Jekle, A., Javanbakht, H., Henningsen, R., Gee, P., Lee, I., Tran, P., Ren, S., Kutach, A.K., Harris, S.F., Wang, S.M., Lok, S.J., Shaw, D., Li, J., Heilek, G., Klumpp, K., Swinney, D.C., Deval, J., 2010. Biochemical characterization of the inhibition of the dengue virus RNA polymerase by beta-d-2'-ethynyl-7-deaza-adenosine triphosphate. Antivir. Res. 87, 213–222. https://doi.org/10.1016/j.antiviral.2010.05.003.

Lim, S.P., Koh, J.H.K., Seh, C.C., Liew, C.W., Davidson, A.D., Chua, L.S., Chandrasekaran, R., Cornvik, T.C., Shi, P.Y., Lescar, J., 2013. A crystal structure of the dengue virus non-structural protein 5 (NS5) polymerase delineates interdomain amino acid residues that enhance its thermostability and de novo initiation activities. J. Biol. Chem. 288, 31105–31114. https://doi.org/10.1074/jbc.M113.508606.

Ma, D., Jiang, D., Qing, M., Weidner, J.M., Qu, X., Guo, H., Chang, J., Gu, B., Shi, P.Y., Block, T.M., Guo, J.T., 2009. Antiviral effect of interferon lambda against West Nile virus. Antivir. Res. 83, 53–60. https://doi.org/10.1016/j.antiviral.2009.03.006.

Magurano, F., Remoli, M.E., Baggieri, M., Fortuna, C., Marchi, A., Fiorentini, C., Bucci, P., Benedetti, E., Ciufolini, M.G., Rizzo, C., Piga, S., Salcuni, P., Rezza, G., Nicoletti, L., 2012. Circulation of West Nile virus lineage 1 and 2 during an outbreak in Italy. Clin. Microbiol. Infect. 18, E545–E547. https://doi.org/10.1111/1469-0691.12018.

Malet, H., Egloff, M.P., Selisko, B., Butcher, R.E., Wright, P.J., Roberts, M., Gruez, A., Sulzenbacher, G., Vonrhein, C., Bricogne, G., Mackenzie, J.M., Khromykh, A.A., Davidson, A.D., Canard, B., 2007. Crystal structure of the RNA polymerase domain of the West Nile virus non-structural protein 5. J. Biol. Chem. 282, 10678–10689. https://doi.org/10.1074/jbc.M607273200.

Malet, H., Massé, N., Selisko, B., Romette, J.L., Alvarez, K., Guillemot, J.C., Tolou, H., Yap, T.L., Vasudevan, S.G., Lescar, J., Canard, B., 2008. The flavivirus polymerase as a target for drug discovery. Antivir. Res. 80, 23–35. https://doi.org/10.1016/j.antiviral.2008.06.007.

Meagher, K.L., Redman, L.T., Carlson, H.A., 2003. Development of polyphosphate parameters for use with the AMBER force field. J. Comput. Chem. 24, 1016–1025. https://doi.org/10.1002/jcc.10262.

Mesci, P., Macia, A., Moore, S.M., Shiryaev, S.A., Pinto, A., Huang, C.T., Tejwani, L., Fernandes, I.R., Suarez, N.A., Kolar, M.J., Montefusco, S., Rosenberg, S.C., Herai, R.H., Cugola, F.R., Russo, F.B., Sheets, N., Saghatelian, A., Shresta, S., Momper, J.D., Siqueira-Neto, J.L., Corbett, K.D., Beltrão-Braga, P.C.B., Terskikh, A.V., Muotri, A.R., 2018. Blocking Zika virus vertical transmission. Sci. Rep. 8, 1218. https://doi.org/10.1038/s41598-018-19526-4.

Murakami, E., Tolstykh, T., Bao, H., Niu, C., Micolochick Steuer, H.M., Bao, D., Chang, W., Espiritu, C., Bansal, S., Lam, A.M., Otto, M.J., Sofia, M.J., Furman, P.A., 2010. Mechanism of activation of PSI-7851 and its diastereoisomer PSI-7977. J. Biol. Chem. 285, 34337–34347. https://doi.org/10.1074/jbc.M110.161802.

Patel, H., Sander, B., Nelder, M.P., 2015. Long-term sequelae of West Nile virus-related illness: a systematic review. Lancet Infect. Dis. 15, 951–959. https://doi.org/10.1016/S1473-3099(15)00134-6.

Reed, L.J., Muench, H., 1938. A simple method of estimating fifty per cent endpoints. Am. J. Epidemiol. 27, 493–497. https://doi.org/10.1093/oxfordjournals.aje.a118408.

Sacramento, C.Q., de Melo, G.R., de Freitas, C.S., Rocha, N., Hoelz, L.V.B., Miranda, M., Fintelman-Rodrigues, N., Marttorelli, A., Ferreira, A.C., Barbosa-Lima, G., Abrantes, J.L., Vieira, Y.R., Bastos, M.M., de Mello Volotão, E., Nunes, E.P., Tschoeke, D.A., Leomil, L., Loiola, E.C., Trindade, P., Rehen, S.K., Bozza, F.A., Bozza, P.T., Boechat, N., Thompson, F.L., de Filippis, A.M.B., Brüning, K., Souza, T.M.L., 2017. The clinically approved antiviral drug sofosbuvir inhibits Zika virus replication. Sci. Rep. 7, 40920. https://doi.org/10.1038/srep40920.

Šebera, J., Dubankova, A., Sychrovský, V., Ruzek, D., Boura, E., Nencka, R., 2018. The structural model of Zika virus RNA-dependent RNA polymerase in complex with RNA for rational design of novel nucleotide inhibitors. Sci. Rep. 8, 1–13. https://doi.org/10.1038/s41598-018-29459-7.

Sejvar, J.J., 2014. Clinical manifestations and outcomes of West Nile virus infection. Viruses 6, 606–623. https://doi.org/10.3390/v6020606.

Tarantino, D., Cannalire, R., Mastrangelo, E., Croci, R., Querat, G., Barreca, M.L., Bolognesi, M., Manfroni, G., Cecchetti, V., Milani, M., 2016. Targeting flavivirus RNA dependent RNA polymerase through a pyridobenzothiazole inhibitor. Antivir. Res. 134, 226–235. https://doi.org/10.1016/j.antiviral.2016.09.007.

Urbanowski, M.D., Hobman, T.C., 2013. The West Nile virus capsid protein blocks apoptosis through a phosphatidylinositol 3-kinase-dependent mechanism. J. Virol. 87, 872–881. https://doi.org/10.1128/jvi.02030-12.

Van Dycke, J., Arnoldi, F., Papa, G., Vandepoele, J., Burrone, O.R., Mastrangelo, E., Tarantino, D., Heylen, E., Neyts, J., Rocha-Pereira, J., 2018. A single nucleoside viral polymerase inhibitor against norovirus, rotavirus, and sapovirus-induced diarrhea. J. Infect. Dis. 218, 1753–1758. https://doi.org/10.1093/infdis/jiy398.

Vicenti, I., Boccuto, A., Giannini, A., Dragoni, F., Saladini, F., Zazzi, M., 2018. Comparative analysis of different cell systems for Zika virus (ZIKV) propagation and evaluation of anti-ZIKV compounds in vitro. Virus Res. 244, 64–70. https://doi.org/10.1016/j.virusres.2017.11.003.

Wu, J., Liu, W., Gong, P., Gong, P., 2015. A structural overview of RNA-dependent RNA polymerases from the Flaviviridae family. Int. J. Mol. Sci. 16, 12943–12957. https://doi.org/10.3390/ijms160612943.

Xu, H.T., Colby-Germinario, S.P., Hassounah, S.A., Fogarty, C., Osman, N., Palanisamy, N., Han, Y., Oliveira, M., Quan, Y., Wainberg, M.A., 2017a. Evaluation of Sofosbuvir (β-D-2'-deoxy-2'-α-fluoro-2'-β-C-methyluridine) as an inhibitor of Dengue virus replication. Sci. Rep. 7, 6345. https://doi.org/10.1038/s41598-017-06612-2.

Xu, H.T., Hassounah, S.A., Colby-Germinario, S.P., Oliveira, M., Fogarty, C., Quan, Y., Han, Y., Golubkov, O., Ibanescu, I., Brenner, B., Stranix, B.R., Wainberg, M.A., 2017b. Purification of Zika virus RNA-dependent RNA polymerase and its use to identify small-molecule Zika inhibitors. J. Antimicrob. Chemother. 72, 727–734. https://doi.org/10.1093/jac/dkw514.

Xu, S., Doehle, B., Rajyaguru, S., Han, B., Barauskas, O., Feng, J., Perry, J., Dvory-Sobol, H., Svarovskaia, E.S., Miller, M.D., Mo, H., 2017. In vitro selection of resistance to sofosbuvir in HCV replicons of genotype-1 to -6. Antivir. Ther. 22, 587–597. https://doi.org/10.3851/IMP3149.

Zhang, B., Dong, H., Zhou, Y., Shi, P.-Y., 2008. Genetic interactions among the West Nile virus methyltransferase, the RNA-dependent RNA polymerase, and the 5' stem-loop of genomic RNA. J. Virol. 82, 7047–7058. https://doi.org/10.1128/jvi.00654-08.

Privileged Scaffold Decoration for the Identification of the First Trisubstituted Triazine with Anti-SARS-CoV-2 Activity

Silvia Cesarini [1,†], **Ilaria Vicenti** [2,†], **Federica Poggialini** [3,†], **Massimiliano Secchi** [4,†], **Federica Giammarino** [2], **Ilenia Varasi** [2], **Camilla Lodola** [4], **Maurizio Zazzi** [2], **Elena Dreassi** [3], **Giovanni Maga** [4], **Lorenzo Botta** [1,*] and **Raffaele Saladino** [1]

[1] Department of Biological and Ecological Sciences, University of Viterbo, Via S.C. De Lellis s.n.c., 01100 Viterbo, Italy
[2] Department of Medical Biotechnologies, University of Siena, 53100 Siena, Italy
[3] Department of Biotechnology, Chemistry, and Pharmacy (DBCF), University of Siena, 53100 Siena, Italy
[4] Institute of Molecular Genetics, IGM CNR "Luigi Luca Cavalli-Sforza", Via Abbiategrasso 207, 27100 Pavia, Italy
[*] Correspondence: lorenzo.botta@unitus.it (L.B.)
[†] These authors contributed equally to this work.

Abstract: Current therapy against severe acute respiratory syndrome coronavirus type 2 (SARS-CoV-2) are based on the use of Remdesivir **1**, Molnupiravir **2**, and the recently identified Nirmatrelvir **3**. Unfortunately, these three drugs showed some limitations regarding potency and possible drug–drug interactions. A series of derivatives coming from a decoration approach of the privileged scaffold s-triazines were synthesized and evaluated against SAR-CoV-2. One derivative emerged as the hit of the series for its micromolar antiviral activity and low cytotoxicity. Mode of action and pharmacokinetic in vitro preliminary studies further confirm the role as candidates for a future optimization campaign of the most active derivative identified with this work.

Keywords: SARS-CoV-2; DDX3X; privileged scaffold; s-triazines; decoration approach; antivirals

1. Introduction

Severe acute respiratory syndrome coronavirus type 2 (SARS-CoV-2) is a positive-strand RNA virus [1], belonging to the family of Corona viridae, discovered in late 2019 [2]. It is the causative agent of the coronavirus disease 2019 (COVID-19), that led to the pandemic outbreak and the consequent global lock-down measures of virus containment in 2020. Severe diseases in animals and in humans are associated with COVID-19 at gastrointestinal and, more importantly, respiratory level, with severe pneumonia, high fever, dry cough, and difficulty in breathing as common symptoms at the onset of illness [3]. Worldwide, vaccination has been the main method to reduce the spread of infection and the severity of disease in healthy individuals. In SARS-CoV-2 infected patients at high risk of disease progression, different therapeutic agents targeting directly the viral replication cycle are currently available [4,5], including different monoclonal antibodies, antiviral drugs repurposed, such as Remdesivir **1** (FDA approved) and Molnupiravir **2** (authorized under emergency use authorization, EUA), or recently identified, such as Nirmatrelvir **3** (EUA) (Figure 1). However, the development of novel drugs remains a key priority because currently available antivirals are not highly effective, and their use is limited by a number of drug–drug interactions (Nirmatrelvir), by inconvenient administration (monoclonal antibodies and Remdesivir) or by the toxicity in fragile population (Molnupiravir) [6].

1,3,5-Triazine **5**, known as symmetric triazine (s-triazine), is an extensively studied heterocyclic nucleus in medicinal chemistry for its easy chemical manipulation and its

wide therapeutic application (Figure 1) [7]. s-Triazine is considered, in fact, a privileged structure [8] since it is the core structure of antibacterial, antiviral, anticancer, and antifungal agents [9].
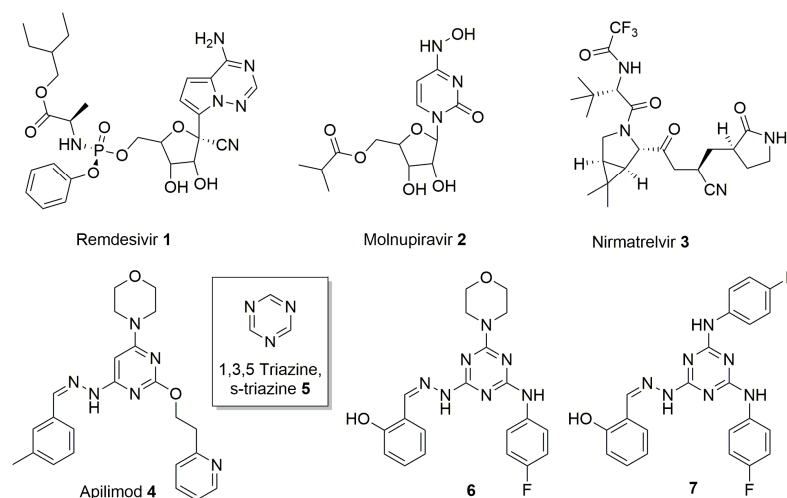

Figure 1. Chemical structures of Remdesivir **1**, Molnupiravir **2,** Nirmatrelvir **3**, Apilimod **4**, s-triazine **5,** and two highly decorated triazines previously identified **6** and **7**.

In the context of s-triazine-based compounds, in 2011, our group reported the synthesis of a series of derivatives presenting this privileged core structure, as inhibitor of the human DEAD-box RNA helicase DDX3X, endowed with anti-HIV activity [10]. DDX3X is a potential target for the development of anticancer and antiviral compounds considering its oncogenic role in promoting cancer progression and its active involvement in the replication of different viruses [11–13]. From the library of compounds synthesized, two members (compounds **6** and **7**, Figure 1) emerged for their antiretroviral effect in the low-micromolar range (EC$_{50}$ = 2.5 and 2.0 μM, respectively), even if accompanied by a moderate cytotoxicity (CC$_{50}$ = 10.0 and 8.0 μM, respectively) in peripheral blood mononuclear cells (PBMC).

Driven by our interest in the functionalization of privileged scaffolds [14] and by the possibility of developing novel antiviral agents, we decided to obtain and to test s-triazine-based compounds, starting from **6** and **7**, against the emerging SARS-CoV-2. Herein, is described the synthesis and the biological evaluation of a focused library of nine highly decorated triazines as inhibitor of the above-mentioned coronavirus. In particular, substituents with precise functions have been introduced on the azine core to investigate the chemical space around the privileged nucleus. Salicyl aldehyde, (Scheme 1, compound **11a**) and 4-fluoro aniline were chosen due to the high antiretroviral activity showed by derivatives **6** and **7**. In addition, 4-acetamidobenzaldehyde (Scheme 1, compound **11b**) was selected on the basis of the inhibitory activity on DDX3X of some 4-acetamido-phenyl-triazines presented in our previous work [10]. Morpholine was chosen on the basis of the activity of **6** and **7** and also for its capacity to improve drug-like and pharmacokinetic properties [15]. Finally, 3-tolualdehyde (Scheme 1, compound **11c**) was used to reproduce a pharmacophoric moiety present on Apilimod (Figure 1, compound **4**), a kinase inhibitor repurposed toward SARS-CoV-2 [16] and structurally similar to the hit compounds **6** and **7**, already identified. In addition, in vitro absorption, distribution, metabolism, and excretion (ADME) tests were conducted on the most active compound to further confirm its positive physical chemical properties and its potential role as optimizable hit compound.
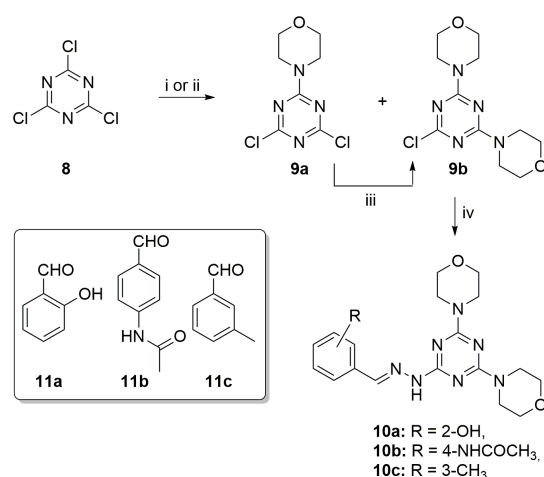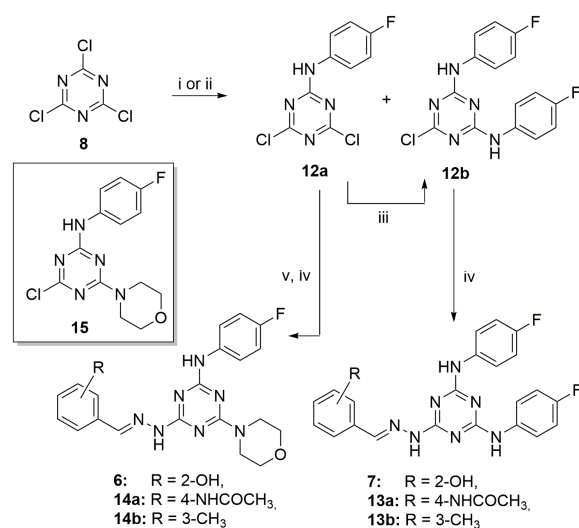
Scheme 1. Synthesis of triazine derivatives **10a–c**. Reagents and conditions: (i) DME, −60 °C, morpholine, 5 h; (ii) *N*,*N*-Diisopropylethylamine (DIPEA), morpholine, EtOH, 25 °C, 18 h; (iii) CH$_2$Cl$_2$, 25 °C, morpholine, 18 h; (iv) 1. CH$_2$Cl$_2$, NH$_2$NH$_2$, reflux 12 h, 2. toluene, **11a–c**, 3 h, reflux, Dean–Stark.

2. Results and Discussion

A series of three highly decorated triazine derivatives **10a–c**, was synthesized starting from 2,4,6-trichloro-1,3,5-triazine (cyanuric chloride) **8** following the synthetic procedure reported in Scheme 1.

Compound **8** (1.0 mmol) was reacted with morpholine (1.0 mmol) at −60 °C in dimethoxymethane as solvent, affording a mixture of the monosubstituted **9a** and disubstituted **9b** intermediates, isolated after flash column chromatography with a 55% and 15% yield, respectively. Attempts to obtain only compound **9a**, such as decreasing the temperature to −78 °C or the use of a lower amount of morpholine (0.7 mmol instead of 1.0 mmol) failed. On the other hand, it was possible to directly afford compound **9b** using a higher amount (2.2 mmol) of morpholine at 25 °C or reacting the latter (2.0 mmol) with **9a** in CH$_2$Cl$_2$ at 25 °C. Subsequently, from the disubstituted intermediate **9b,** the three final compounds **10a–c** can be synthesized by displacement of the third chlorine atom with hydrazine, and reductive amination with the desired aromatic aldehydes **11a–c** to form an imine linkage with a 50, 25, and 45% yield, respectively.

As depicted in Scheme 2, a closely related pathway was used to synthesize compounds **6** and **7** and the highly decorated triazines **13a–b** and **14a–b**. The reaction of **8** (1.0 mmol) with 4-fluoroaniline (1.0 mmol) at −60 °C or even at −78 °C furnished unselectively compounds **12a** and **12b** with a 47% and 10% yield, after chromatographic purification. The monosubstituted **12a** can be easily converted in the disubstituted **12b** by reaction with 4-fluoroaniline and *N*,*N*-Diisopropylethylamine (DIPEA) at 25 °C with a 74% yield. Then, **12b** is converted into the final derivatives **7**, **13a–b** by nucleophilic substitution in the presence of hydrated hydrazine and reaction with the opportune aldehyde.

Scheme 2. Synthesis of triazine derivatives **6**, **7**, **13a–b** and **14a–b**. Reagents and conditions: (i) DME, −60 °C, 4-fluoroaniline, 5 h; (ii) DIPEA, 4-fluoroaniline, EtOH, 25 °C, 18 h; (iii) CH_2Cl_2, 25 °C, 4-fluoroaniline, DIPEA 18 h; (iv) 1. CH_2Cl_2, NH_2NH_2, reflux 12 h, 2. MeOH, **11a–c**, acetic acid, 25 °C, 18 h; (v) CH_2Cl_2, 25 °C, morpholine, 5 h.

Finally, the monosubstituted derivative **12a** was subjected to aromatic nucleophilic substitution with morpholine to give compound **15** (Scheme 2). From intermediate **15**, the trisubstituted triazines **6**, **14a–b** were synthesized by chlorine displacement with hydrated hydrazine and the addition, in turn, of salicyl aldehyde, 4-acetamidobenzaldehyde, and 3-tolualdehyde **11a–c**, respectively. Full details of the synthetic procedures and characterization data are included in the Supplementary Materials.

The inhibitory activity of the resynthesized compounds and the novel triazines designed against SARS-CoV-2 was analyzed in vitro, using the marketed drug Remdesivir as reference (Table 1). The human colon epithelial carcinoma cell line Caco-2, permissive for SARS-CoV-2 infection [17], was used to determine the cytotoxicity and the anti-SARS-CoV-2 activity of compounds **6**, **7**, **10a–c**, **13a,b**, and **14a,b** as previously described [18] with minor modifications as indicated in the Materials and Methods section below. Briefly, the semi confluent Caco-2 cell line was infected with SARS-CoV-2 at 0.004 Multiplicity of Infection (MOI) in the presence of serial dilutions of the investigational and reference compound (Remdesivir), starting from the non-toxic dose, as previously determined in cytotoxic assay. After 72 h incubation, the antiviral activity of the compounds was measured by immunodetection of the viral N protein in the cell monolayer and expressed as half-maximal inhibitory concentration (IC_{50}). The Selectivity Index (SI) of compounds was calculated as the ratio between the half-maximal cytotoxic concentration (CC_{50}) and the IC_{50}.

Table 1. Antiviral activity, cytotoxicity, and selectivity index of the synthesized compounds in vitro in a cell-based model [1].

Entry	Compound	IC_{50} μM [2]	CC_{50} μM [3]	SI
1	**10a**	12.1	>400	>33.1
2	**10b**	NA	>200	-
3	**10c**	NA	184	-
4	**7**	NT	0.8	-
5	**13a**	NA	>200	-
6	**13b**	NA	>200	-
7	**6**	NT	3	-
8	**14a**	NT	70	-
9	**14b**	NA	22	-

| 10 | Remdesivir | 0.07 ± 0.04 | 94.9 | 1356 |

[1] All experiments were conducted in Caco-2 cells in duplicate in three independent experiments; [2] IC_{50} half-maximal compound concentration inhibiting 50% of the SARS-CoV-2 replication; [3] CC_{50}, half-maximal compound cytotoxic concentration, as determined by Cell-Titer Glo kit (Promega). SI, Selectivity Index (ratio between CC_{50} and IC_{50}); NA—not active; NT—not tested, highly cytotoxic.

Six compounds, namely **10a–c**, **13a,b**, and **14a** showed a low cytotoxicity (Table 1, entries 1–3, 5, 6, and 8, respectively), compared to the derivatives obtained in the previous study, derivatives **6** and **7** (Table 1, entries 4 and 7). These results highlighted the importance of the introduction of other pharmacophoric moieties, namely the 3-tolyl and 4-acetamidophenyl portions, compared to the salicylic one, as well as the presence of two morpholine substituents on the azine core structure. Regarding the antiviral effect, compound **10a** is the only one that highlighted micromolar (12.1 μM) activity against SARS-CoV-2. Even if the activity of **10a** was lower than that reported for Remdesivir, the low cytotoxicity showed by this compound prompted us to further evaluate its pharmacokinetic properties, in the light of possible future chemical optimizations.

In addition, all the novel compounds synthesized were also evaluated for their antiretroviral activity but, surprisingly, they seem to be unable to inhibit HIV replication compared to parent compounds **6** and **7** (Table S1 (Supplementary Materials)).

For the more promising compound, derivative **10a**, the inhibition of the ATPase activity of the human helicase DDX3X was evaluated. Different concentrations of the compound were incubated with 1 μM of purified recombinant DDX3X and ATPase activity was determined with the ADP-glo assay. This assay showed that the highly decorated triazine **10a** is able to inhibit DDX3X with a 6.6 μM ID_{50} value (Figure S1). This result further confirms the association of the antiviral activity with the inhibition of the human helicase already observed for the parent compounds **6** and **7**.

In order to perform the structure–activity relationship (SAR) studies, the in vitro ADME profile of compounds **6**, **7**, **10a–c** (Figure 2) was intensively investigated.
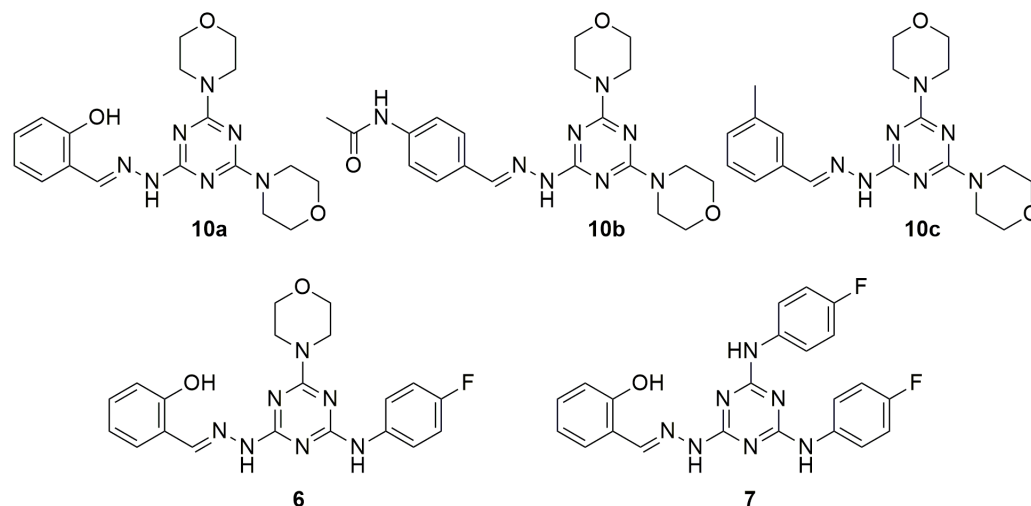

Figure 2. Structure of compounds **6**, **7**, **10a–c**.

Firstly, the water solubility of compounds was studied dissolving 1 mg of solid compound into 1.0 mL of Mill-Q H_2O. As reported in Table 2, the results obtained suggested a good water solubility for compounds **10a–c**, with LogS values around −5. The replacement of one or two morpholine moieties with para fluorophenyl groups, worsens the solubility of compounds **6** and **7**, to less than 0.1 μg/mL (limit of detection, LOD).

Table 2. Water solubility of compounds **6**, **7**, **10a–c**.

Cpd	μg/mL	LogS [1]
6	<0.1	-
7	<0.1	-
10a	3.23	−5.07
10b	3.46	−5.09
10c	4.50	−4.93

[1] Log of Solubility expressed as mol/L.

The trend appreciated in terms of solubility was confirmed by results obtained from permeability studies. In fact, parallel artificial membrane permeability assay (PAMPA) underlined how the low solubility of compounds **6** and **7** was accompanied by a major tendency of these derivatives to interact with the lipidic artificial membrane where they probably remained entrapped. Hence, compounds **6** and **7** resulted in being characterized by P_{app} of 4.74 and 4.58 cm/s × 10⁻⁶ and a general high percentage of membrane retention (MR 28.5% and 15.5%, respectively). Compounds **10a–c**, endowed with a higher water solubility, showed a lower tendency to interact with the lipidic bilayer (MR < 10%) and an improved capability to cross the membrane for passive diffusion (P_{app} from 7.89 to 9.78 cm/s × 10⁻⁶) (Table 3).

Table 3. In vitro PAMPA permeability studies of compounds **6**, **7**, **10a–c**.

Cpd	Papp [a]	MR [b] (%)
6	4.74	28.7
7	4.58	15.5
10a	7.89	4.3
10b	9.70	9.8
10c	9.78	4.9

[a] Apparent Permeability (Papp) reported in cm/s × 10⁻⁶. [b] Membrane retention %.

From a metabolic point of view, all compounds resulted in a very high stability (more than 99.9%) when incubated for 1 h in the presence of human liver microsomes (HLM). Finally, further studies were performed in order to investigate the stability in the presence of human plasma. All compounds were incubated at the fixed concentration of 100 μM in plasma for 24 h. As reported in Table 4, all compounds resulted in not being affected by the hydrolytic action of plasma esterase with percentages of plasma stability of 98–99% after 24 h of incubation.

Table 4. Plasma stability studies after 24 h of compounds **6**, **7**, **10a–c**.

	Plasma Stability % ± SD				
Time (h)	6	7	10a	10b	10c
0	100.00 ± 0.19	100.00 ± 0.28	100.00 ± 0.28	100.00 ± 0.24	100.00 ± 0.16
24	98.78 ± 4.05	99.56 ± 3.78	98.48 ± 4.02	98.41 ± 4.69	99.52 ± 3.45

The replacement of one or both the 4-fluoroaniline substituents, of compounds **6** and **7**, with morpholine increased the water solubility and positively influenced parallel artificial membrane crossing and membrane retention. Compounds **10a–c**, in fact, showed better pharmacokinetic properties compared to **6** and **7**. In addition, the presence of two morpholines lead to a decrease in the cytotoxicity. Regarding the aromatic hydrazone moiety, salicyl residue of **10a** contributed to the most pronounced decrease in the cytotoxicity and to the anti-SARS-CoV-2 activity. The 4-acetamidophenyl and 3-toluic groups of **10b** and **10c**, respectively, led to better data of membrane permeability but not to antiviral effects.

3. Materials and Methods

3.1. Chemistry-General Part

All reactions were performed in flame-dried glassware under a nitrogen atmosphere. Reagents were obtained from commercial suppliers (Merck Srl, Milan, Italy) and used without further purification. TLC chromatography was performed on precoated aluminum silica gel SIL G/UV254 plates (Macherey-Nagel GmbH & Co. Düren, Germany). The detection occurred via fluorescence quenching or development in a ninhydrin solution (0.2 g of ninhydrin in 99.5 mL ethanol and 0.5 mL acetic acid.). Merck silica gel 60 was used for chromatography (23–400 mesh). ^1H NMR and ^{13}C NMR spectra were measured on a Bruker Avance DRX400 (400 MHz/100 MHz) spectrometer. Chemical shifts for protons were reported in parts per million (ppm, δ scale) and internally referenced to the deuterated dimethyl sulfoxide (DMSO-d_6), methanol (CD$_3$OD) or chloroform (CDCl$_3$) signal at δ 2.50, 3.33 and 7.28 ppm, respectively. ^1H-NMR spectra are reported in this order: multiplicity and number of protons. Signals were characterized as: s (singlet); d (doublet); dd (doublet of doublets); t (triplet); m (multiplet); bs (broad signal). Mass spectra were recorded with an Agilent 1100 LC/MSD VL system (G1946C) (Agilent Technologies, Palo Alto, CA, USA).

3.2. Biology

3.2.1. Cells and Viruses

The SARS-CoV-2 strain belonging to lineage B.1 (EPI_ISL_2472896) was kindly provided by the Department of Biomedical and Clinical Sciences Luigi Sacco, University of Milan (Italy). Once expanded in VERO E6 (African green monkey kidney-cell line, ATCC catalog. N. CRL-1586), the SARS-CoV-2 viral stock was stored at −80 °C and titrated by plaque assay, as previously described [19]. HIV-1 wild-type reference strain NL4-3 (catalog. n. ARP2006), was obtained through the NIH AIDS Reagent Program and viral titer was calculated in TZM- bl cells through the detection of β-galactosidase expression, as previously described [20].

The Caco-2 adherent cell line (ATCC catalog. n. HTB-37), derived from a human colon carcinoma, was used to determine the cytotoxicity and the antiviral activity of candidate compounds against SARS-CoV-2. The H9 suspension cell line (repository code ARP0001; NIBSC Centre for AIDS reagents) derived from a human T cell lymphoma was used to evaluate compounds against HIV-1 in combination with the TZM-bl (repository code ARP5011, NIBSC Centre for AIDS reagents) adherent cell line as described in the antiviral assays' section.

Adherent cell lines were propagated in high glucose Dulbecco's Modified Eagle's Medium with sodium pyruvate and L-glutamine (DMEM; Euroclone), for TZM-bl, or Minimum Essential Medium Eagle (EMEM; Euroclone), for Caco-2, supplemented with 10% Fetal Bovine Serum (FBS; Euroclone) and 1% Penicillin/Streptomycin (Pen/Strep; Euroclone). The propagation medium with a lower concentration of FBS (1%) was used for viral propagation, cytotoxicity, and antiviral activity experiments in adherent cell lines. Suspension cells were propagated in RPMI 1640 medium supplemented with 10% Fetal Bovine Serum (FBS; Euroclone), 2 mM L-glutamine, and 1% Penicillin/Streptomycin (Pen/Strep; Euroclone). Cells were incubated at 37 °C in a humidified incubator supplemented with 5% CO$_2$.

3.2.2. Drugs and Cytotoxicity Assay

The cytotoxicity of investigational compounds was determined by CellTiter-Glo 2.0 Luminescent Cell Viability Assay (Promega) according to the manufacturer's protocol. Cell viability was calculated by measuring cellular ATP as a marker of metabolically active cells through a luciferase-based chemical reaction. The luminescent signal obtained from cells treated with serial dilution of the investigational compounds, or DMSO as control, was measured through the GloMax® Discover Multimode Microplate Reader

(Promega) and elaborated with the GraphPad PRISM software version 9 (La Jolla) to calculate the half-maximal cytotoxic concentration (CC_{50}). Remdesivir (MCE® cat. HY-104077) and Raltegravir (MCE® cat. HY-10353), used as reference compounds for SARS-CoV-2 and HIV-1 antiviral tests, respectively, were purchased from MedChem Express and dissolved in water (Raltegravir) or 100% DMSO (Remdesivir). Following the determination of the CC_{50}, for each compound a non-toxic dose was chosen and used as the starting drug concentration in the subsequent antiviral assays.

3.2.3. Antiviral Assays-SARS-CoV-2

To determine the antiviral activity of candidate compounds against SARS-CoV-2, a direct-yield reduction assay, based on the infection of cells in the presence of serial drug dilutions, was performed as previously described, with minor modifications. Briefly, Caco-2 cells, pre-seeded in a 96-well format, were infected with SARS-CoV-2 viral stock at 0.004 multiplicity of infection (MOI). After 1h adsorption at 37 °C, the viral inoculum was removed and serial dilutions of each tested compound, starting from the non-toxic dose, were added to the infected cells. After 72 h incubation, the antiviral activity was measured in the cell monolayer by immunodetection assay (IA), as previously described [18].

Absorbance was measured at 450 nm optical density (OD450) using the Absorbance Module of the GloMax® Discover Multimode Microplate Reader (Promega). In each plate was included the corresponding reference compound, the mock control (uninfected cells), the virus control, and the virus back titration, performed by diluting 2-fold the initial viral inoculum. Each IA run was validated when both the OD450 values of virus control and the first 2 dilutions of the virus back titration were above 1 OD450. All drug concentrations were tested in duplicate in two independent experiments and in each plate, Remdesivir was used as a reference compound. Infected and uninfected cells without drugs were used to calculate the 100% and 0% of viral replication, respectively. The half-maximal inhibitory concentration (IC_{50}) was calculated through a non-linear regression analysis of the dose–response curves generated with GraphPad PRISM software version 9. The Selectivity Index (SI) of compounds was calculated as a ratio between CC_{50} and IC_{50}.

3.3. Enzymatic Assay

The ATPase enzymatic activity of DDX3X was determined by the ADP-Glo kit (Promega, MD, USA). The reaction was performed in ATPase buffer (20 mM Tris–HCl pH 8, 2 mM DTT, 70 mM KCl, 2 mM $MgCl_2$, 5% DMSO) pre-incubating 1 μM DDX3X with different concentrations of inhibitor for 10 min at 25 °C. ATPase reaction started with the addition of 1 mM ATP. After 30 min of incubation at 25 °C, the assay was conducted following the manufacturer's instructions. The ATPase enzymatic activity was analyzed using a 384-wells plate and the GloMax Discover Microplate Reader (Promega, MD, USA) and expressed as a percentage of inhibition calculated from the light units obtained.

3.4. In Vitro ADME

3.4.1. HPLC/UV-MS Method

LC chromatographic analyses were performed by UV/LC-MS with an Agilent 1100 LC/MSD VL system (G1946C) (Agilent Technologies, Palo Alto, CA) equipped with a vacuum solvent degassing unit, a binary high-pressure gradient pump, an 1100 series UV detector, and a 1100 MSD model VL benchtop mass spectrometer. Chromatographic separations were obtained using a Phenomenex Kinetex C18-100 Å column (150 × 4.6 mm) with 5 μm particle size and gradient elution with a binary solution; (eluent A: H_2O acidified with formic acid (FA) 0.1% v/v, eluent B: ACN/MeOH 1:1 v/v) at room temperature. The analysis started with 5% of B (from t = 0 to t = 1 min), then B was increased to 95% (from t = 1 to t = 10 min), then kept at 95% (from t = 10 to t = 15 min) and finally returned

to 5% of eluent A in one minute. The instrument worked in positive mode and the UV detector operated at 254 nm.

3.4.2. Aqueous Solubility

One mg of each compound was added with 1 mL of Mill-Q H_2O. The samples were maintained under shaking at room temperature (RT) overnight. The suspensions were filtered using a 0.45 μm nylon filter (Acrodisc), and the amount of solubilized compound was determined with the HPLC-UV-MS method above reported. The quantification of the solubilized compound was created with the appropriate calibration curve realized with stock solutions in DMSO (0.1–100 μg/mL); the limit of detection (LOD) was quantified at 0.1 μg/mL.

3.4.3. Parallel Artificial Membrane Permeability Assay (PAMPA)

In order to assess the apparent permeability of selected compounds, a stock solution in DMSO of each derivative was prepared at the final concentration of 1 mM. By diluting the stocks 1:1 v/v with phosphate buffer (PBS 25 mM, pH 7.4), donor solutions were made. To mimic the gastrointestinal (GI) phospholipidic bilayer, 10 μL of a 1% w/v dodecane solution of phosphatidylcholine (PC) was used to coat filters. The acceptor solution, made of 1:1 v/v DMSO/PBS, was added to each well (300 μL), while the donor solution (150 μL) was added to each well of the filter plate. The sandwich plates were assembled and incubated for 5 h at room temperature. At the time point, the plates were separated, and the amount of compound passed through the phospholipid bilayer was measured by UV/LC-MS. Finally, apparent permeability (P_{app}) and membrane retention (MR%) were calculated as previously reported by us [21,22].

3.4.4. Metabolic Stability Assay

A DMSO stock solution of tested compounds was incubated in triplicate in the presence of phosphate buffer (25 mM, pH 7.4), human liver microsomal protein (0.2 mg/mL), and in the presence of an NADPH regenerating system in $MgCl_2$ (48 mM) at a final concentration of 50 μM. The metabolic reaction was conducted for 1 h under shaking at 37 °C and then stopped by adding 1.0 mL of cold acetonitrile (ACN). Centrifuging the reaction mixtures for 10 min at 5000 rpm, the supernatant was separated, dried under nitrogen flow, and finally resuspended in 100 μL of methanol (MeOH). The amount of parent drug and the metabolites were determined as previously described [23].

3.4.5. Plasma Stability Assay

A DMSO stock solution of each compound was incubated in triplicate in the presence of human plasma and HEPES buffer (25 mM, 140 mM NaCl, pH 7.4) at the final concentration of 100 μM at 37 °C under shaking. At the selected time point of 0 and 24 h, 50 μL of the mixture was collected, treated with 1.0 mL of cold ACN, and centrifuged at 5000 rpm for 10 min. The supernatant was collected, and the amount of unmodified compound was quantified with the HLPC-UV/MS method above reported. Calculations of modified compounds were made using time zero as 100% of the unmodified compound.

4. Conclusions

In conclusion, a series of highly decorated triazines was designed and synthesized using the s-triazine privileged scaffold as the core structure. The novel derivatives were evaluated against SARS-CoV-2 resulting in the identification of compound **10a** as the hit of the series endowed with a micromolar activity. This compound showed also a very low cytotoxicity against Caco-2 cells, making it even more suitable for further optimizations. Preliminary study regarding the mechanism of action of **10a** showed the inhibition of the human DEAD-box RNA helicase DDX3X in the micromolar range as its parent derivatives **6** and **7** obtained in a previous study. Helicase inhibition, in fact, is often correlated with

the reduction in the replication of several viruses at different steps such as the nuclear export of the newly synthesized genetic material of the pathogen [8,11,13,22].

In addition, in vitro ADME evaluations highlighted that all compounds tested (**6**, **7**, **10a–c**) were characterized by an excellent stability both in the presence of HLM and in plasma. While compound **6** and **7** showed a more lipophilic profile with a major affinity towards lipidic bilayer and lower aqueous solubility, compounds **10a–c** demonstrated a satisfactory passive permeability accompanied with low percentages of membrane retention and appreciable water solubility. These additional pharmacokinetic and enzymatic data further confirm the role of the hit compound of the series for **10a** and its potentiality as the starting point for future structure optimizations.

Supplementary Materials: The following supporting information can be downloaded at: https://www.mdpi.com/article/10.3390/molecules27248829/s1, synthetic procedures and full characterization of compounds synthesized (^{1}H-NMR, ^{13}C-NMR, MS); Table S1: Antiviral activity and cytotoxicity of the synthesized compounds in vitro in a cell-based model; Figure S1: Inhibition of the ATPase activity of the human helicase DDX3X.

Author Contributions: Conceptualization, L.B., M.Z. and E.D.; methodology, S.C., I.V. (Ilaria Vicenti), F.P. and M.S.; formal analysis, F.G., I.V. (Ilenia Varasi) and C.L.; data curation, S.C., I.V. (Ilaria Vicenti), F.P. and M.S.; writing—original draft preparation, L.B., M.Z. and E.D.; writing—review and editing, R.S.; funding acquisition, L.B., M.Z., E.D. and G.M. All authors have read and agreed to the published version of the manuscript.

Institutional Review Board Statement: Not applicable.

Informed Consent Statement: Not applicable.

Data Availability Statement: Not applicable.

Conflicts of Interest: M.Z. reports consultancy for ViiV Healthcare, Gilead Sciences, GlaxoSmithKline, Janssen-Cilag, Theratechnologies, Merck Sharp, and Dohme, and grants for his institution from ViiV Healthcare, Theratechnologies, and Gilead Sciences outside the submitted work. All other authors: no conflicts to declare.

References

1. Machhi, J.; Herskovitz, J.; Senan, A.M.; Dutta, D.; Nath, B.; Oleynikov, M.D.; Blomberg, W.R.; Meigs, D.D.; Hasan, M.; Patel, M.; et al. The Natural History, Pathobiology, and Clinical Manifestations of SARS-CoV-2 Infections. *J. Neuroimmune. Pharmacol.* **2020**, *15*, 359–386.
2. *WHO, in situation reports*; World Health Organization: Geneva, Switzerland, 2020; Volume 180.
3. Pal, M.; Berhanu, G.; Desalegn, C.; Kandi, V. Severe Acute Respiratory Syndrome Coronavirus-2 (SARS-CoV-2): An Update. *Cureus* **2020**, *12*, e7423.
4. Available online: www.covid19treatmentguidelines.nih.gov (accessed on 30 October 2022).
5. Majumdar, M.; Singh, V.; Misra, T.K.; Roy, D.N. In silico studies on structural inhibition of SARS-CoV-2 main protease M^{pro} by major secondary metabolites of Andrographis paniculata and Cinchona officinalis. *Biologia* **2022**, *77*, 1373–1389.
6. Saravolatz, L.D.; Depcinski, S.; Sharma, M. Molnupiravir and Nirmatrelvir-Ritonavir: Oral COVID Antiviral Drugs. *Clin. Infect. Dis.* **2022**, ciac180. https://doi.org/10.1093/cid/ciac180.
7. Sharma, A.; Sheyi, R.; de la Torre, B.G.; El-Faham, A.; Albericio, F. s-Triazine: A Privileged Structure for Drug Discovery and Bioconjugation. *Molecules* **2021**, *26*, 864.
8. Shah, D.R.; Modh, R.P.; Chikhalia, K.H. Privileged s-triazines: Structure and pharmacological applications. *Future Med. Chem.* **2014**, *6*, 463–477.
9. Singla, P.; Luxami, V.; Paul, K. Triazine as a promising scaffold for its versatile biological behavior. *Eur. J. Med. Chem.* **2015**, *102*, 39–57.

10. Maga, G.; Falchi, F.; Radi, M.; Botta, L.; Casaluce, G.; Bernardini, M.; Irannejad, H.; Manetti, F.; Garbelli, A.; Samuele, A.; et al. Toward the discovery of novel anti-HIV drugs. Second-generation inhibitors of the cellular ATPase DDX3 with improved anti-HIV activity: Synthesis, structure-activity relationship analysis, cytotoxicity studies, and target validation. *ChemMedChem* **2011**, *6*, 1371–1389.

11. Brai, A.; Fazi, R.; Tintori, C.; Zamperini, C.; Bugli, F.; Sanguinetti, M.; Stigliano, E.; Esté, J.; Badia, R.; Franco, S.; et al. Human DDX3 protein is a valuable target to develop broad spectrum antiviral agents. *Proc. Natl. Acad. Sci. USA* **2016**, *113*, 5388–5393.

12. Secchi, M.; Lodola, C.; Garbelli, A.; Bione, S.; Maga, G. DEAD-Box RNA Helicases DDX3X and DDX5 as Oncogenes or Oncosuppressors: A Network Perspective. *Cancers* **2022**, *14*, 3820.

13. Brai, A.; Trivisani, C.I.; Poggialini, F.; Pasqualini, C.; Vagaggini, C.; Dreassi, E. DEAD-Box Helicase DDX3X as a Host Target against Emerging Viruses: New Insights for Medicinal Chemical Approaches. *J. Med. Chem.* **2022**, *65*, 10195–10216.

14. Radi, M.; Botta, L.; Casaluce, G.; Bernardini, M.; Botta, M. Practical one-pot two-step protocol for the microwave-assisted synthesis of highly functionalized rhodanine derivatives. *J. Comb. Chem.* **2010**, *12*, 200–205.

15. Kourounakis, A.P.; Xanthopoulos, D.; Tzara, A. Morpholine as a privileged structure: A review on the medicinal chemistry and pharmacological activity of morpholine containing bioactive molecules. *Med. Res. Rev.* **2020**, *40*, 709–752.

16. Baranov, M.V.; Bianchi, F.; van den Bogaart, G. The PIKfyve Inhibitor Apilimod: A Double-Edged Sword against COVID-19. *Cells* **2020**, *10*, 30.

17. Mautner, L.; Hoyos, M.; Dangel, A.; Berger, C.; Ehrhardt, A.; Baiker, A. Replication kinetics and infectivity of SARS-CoV-2 variants of concern in common cell culture models. *Virol. J.* **2022**, *19*, 76.

18. Grazia Martina, M.; Vicenti, I.; Bauer, L.; Crespan, E.; Rango, E.; Boccuto, A.; Olivieri, N.; Incerti, M.; Zwaagstra, M.; Allodi, M.; et al. Bithiazole Inhibitors of Phosphatidylinositol 4-Kinase (PI4KIIIβ) as Broad-Spectrum Antivirals Blocking the Replication of SARS-CoV-2, Zika Virus, and Human Rhinoviruses. *ChemMedChem* **2021**, *16*, 3548–3552.

19. Vicenti, I.; Martina, M.G.; Boccuto, A.; De Angelis, M.; Giavarini, G.; Dragoni, F.; Marchi, S.; Trombetta, C.M.; Crespan, E.; Maga, G.; et al. System-oriented optimization of multi-target 2,6-diaminopurine derivatives: Easily accessible broad-spectrum antivirals active against flaviviruses, influenza virus and SARS-CoV-2. *Eur. J. Med. Chem.* **2021**, *224*, 113683.

20. Saladini, F.; Giannini, A.; Boccuto, A.; Vicenti, I.; Zazzi, M. Agreement between an in-house replication competent and a reference replication defective recombinant virus assay for measuring phenotypic resistance to HIV-1 protease, reverse transcriptase, and integrase inhibitors. *J. Clin. Lab. Anal.* **2018**, *32*, e22206.

21. Tintori, C.; Brai, A.; Dasso Lang, M.C.; Deodato, D.; Greco, A.M.; Bizzarri, B.M.; Cascone, L.; Casian, A.; Zamperini, C.; Dreassi, E.; et al. Development and in Vitro Evaluation of a Microbicide Gel Formulation for a Novel Non-Nucleoside Reverse Transcriptase Inhibitor Belonging to the N-Dihydroalkyloxybenzyloxopyrimidines (N-DABOs) Family. *J. Med. Chem.* **2016**, *59*, 2747–2759.

22. Brai, A.; Riva, V.; Saladini, F.; Zamperini, C.; Trivisani, C.I.; Garbelli, A.; Pennisi, C.; Giannini, A.; Boccuto, A.; Bugli, F.; et al. DDX3X inhibitors, an effective way to overcome HIV-1 resistance targeting host proteins. *Eur. J. Med. Chem.* **2020**, *200*, 112319.

23. Sacks, D.; Baxter, B.; Campbell, B.C.V.; Carpenter, J.S.; Cognard, C.; Dippel, D.; Eesa, M.; Fischer, U.; Hausegger, K.; Hirsch, J.A.; et al. Multisociety Consensus Quality Improvement Revised Consensus Statement for Endovascular Therapy of Acute Ischemic Stroke. *Int. J. Stroke* **2018**, *13*, 612–632.

Efficacy of Licensed Monoclonal Antibodies and Antiviral Agents against the SARS-CoV-2 Omicron Sublineages BA.1 and BA.2

Lia Fiaschi [1], **Filippo Dragoni** [1], **Elisabetta Schiaroli** [2], **Annalisa Bergna** [3], **Barbara Rossetti** [4], **Federica Giammarino** [1], **Camilla Biba** [1], **Anna Gidari** [2], **Alessia Lai** [3], **Cesira Nencioni** [4], **Daniela Francisci** [2], **Maurizio Zazzi** [1] **and Ilaria Vicenti** [1,*]

[1] Department of Medical Biotechnologies, University of Siena, 53100 Siena, Italy; lia300790@gmail.com (L.F.); dragoni16@student.unisi.it (F.D.); federica.giammari@gmail.com (F.G.); camilla.biba@student.unisi.it (C.B.); maurizio.zazzi@unisi.it (M.Z.)

[2] Department of Medicine and Surgery, Clinic of Infectious Diseases, University of Perugia, 06129 Perugia, Italy; elisabetta.schiaroli@unipg.it (E.S.); annagidari91@gmail.com (A.G.); daniela.francisci@unipg.it (D.F.)

[3] Department of Biomedical and Clinical Sciences L. Sacco, University of Milan, 20157 Milan, Italy; annalisa.bergna@unimi.it (A.B.); alessia.lai@unimi.it (A.L.);

[4] Infectious Disease Department, USL SUDEST, Toscana, Misericordia Hospital, 58100 Grosseto, Italy; brossetti1982@gmail.com (B.R.); cesira.nencioni@uslsudest.toscana.it (C.N.)

* Correspondence: vicenti@unisi.it; Tel.: +39-057-7233-855

Abstract: Newly emerging SARS-CoV-2 variants may escape monoclonal antibodies (mAbs) and antiviral drugs. By using live virus assays, we assessed the ex vivo inhibition of the B.1 wild-type (WT), delta and omicron BA.1 and BA.2 lineages by post-infusion sera from 40 individuals treated with bamlanivimab/etesevimab (BAM/ETE), casirivimab/imdevimab (CAS/IMD), and sotrovimab (SOT) as well as the activity of remdesivir, nirmatrelvir and molnupiravir. mAbs and drug activity were defined as the serum dilution (ID_{50}) and drug concentration (IC_{50}), respectively, showing 50% protection of virus-induced cytopathic effect. All pre-infusion sera were negative for SARS-CoV-2 neutralizing activity. BAM/ETE, CAS/IMD, and SOT showed activity against the WT (ID_{50} 6295 (4355–8075) for BAM/ETE; 18,214 (16,248–21,365) for CAS/IMD; and 456 (265–592) for SOT) and the delta (14,780 (ID_{50} 10,905–21,020) for BAM/ETE; 63,937 (47,211–79,971) for CAS/IMD; and 1103 (843–1334) for SOT). Notably, only SOT was active against BA.1 (ID_{50} 200 (37–233)), whereas BA.2 was neutralized by CAS/IMD (ID_{50} 174 (134–209) ID_{50}) and SOT (ID_{50} 20 (9–31) ID_{50}), but not by BAM/ETE. No significant inter-variant IC_{50} differences were observed for molnupiravir ($1.5 \pm 0.1/1.5 \pm 0.7/1.0 \pm 0.5/0.8 \pm 0.01$ μM for WT/delta/BA.1/BA.2, respectively), nirmatrelvir ($0.05 \pm 0.02/0.06 \pm 0.01/0.04 \pm 0.02/0.04 \pm 0.01$ μM) or remdesivir ($0.08 \pm 0.04/0.11 \pm 0.08/0.05 \pm 0.04/0.08 \pm 0.01$ μM). Continued evolution of SARS-CoV-2 requires updating the mAbs arsenal, although antivirals have so far remained unaffected.

Keywords: SARS-CoV-2; mAbs; nirmatrelvir; remdesivir; molnupiravir; microneutralization assay; cell-based assay; omicron sublineages

1. Introduction

While worldwide vaccination has played a key role in the global control of COVID-19, both natural and vaccine-induced immunity have been shown to wane rapidly and be subject to escape by divergent virus variants [1,2]. In addition, a proportion of individuals could not be vaccinated due to specific underlying morbidity or personal choice. Thus, development of therapeutics for treatment and prevention of COVID-19 has been set as a public health priority, delivering at fast pace a number of monoclonal antibodies (mAbs) targeting the virus spike protein as well as three small molecule antivirals interfering with

SARS-CoV-2 RNA synthesis (remdesivir, molnupiravir) or polyprotein cleavage (nirmatrelvir).

The viral enzymes have a high degree of conservation across SARS-CoV-2 lineages, thus antiviral activity is expected to be unaffected by viral variants, as preliminarily shown by limited in vitro data [3,4]. By contrast, the recent spread of the highly divergent SARS-CoV-2 omicron lineages has changed the landscape of mAbs activity with respect to previous virus variants. Namely, the BA.1 lineage lost susceptibility to the first developed bamlanivimab/etesevimab (BAM/ETE) and casirivimab/imdevimab (CAS/IMD) therapeutic mAbs combos as well as to the prophylactic cilgavimab/tixagevimab (CIL/TIX) combo while remaining partly sensitive to sotrovimab (SOT). However, SOT further decreased activity against the subsequent BA.2 variant which appears to have restored susceptibility to CIL and partly to IMD. Data about mAbs susceptibility for the minor BA.3 and the recently detected BA.4 and BA.5 lineages are scanty, with preliminary evidence for SOT activity against BA.3 [5] and partial or limited CIL activity against BA.4 and BA.5 [6,7]. According to the latest COVID-19 treatment guidelines (https://files.covid19treatmentguidelines.nih.gov/guidelines/covid19treatmentguidelines.pdf; updated 17 June 2022), the administration of BAM/ETE, CAS/IMD, and SOT mAbs is not recommended, due to the expected lack of activity against the dominating omicron lineages. Bebtelovimab, which retains activity against all SARS-CoV-2 variants, remains the only mAbs approved by the FDA and submitted for approval to the EMA for emergency use for treatment of COVID-19. In addition, CIL/TIX can be administered as pre-exposure prophylaxis.

It must be noted that due to the pressure to deliver effective treatments, mAbs activity on contemporary SARS-CoV-2 lineages is inferred exclusively from in vitro data, while pivotal clinical trials were conducted during epidemic waves dominated by virus variants which have later disappeared. In addition, in vitro data have been generated by different methods including a variety of live virus or pseudovirus neutralization assays and surrogate tests such as SARS-CoV-2 spike binding measured by enzyme immunoassay or surface plasmon resonance. This has generated some data inconsistency across studies. In this study, we expanded our previous work [8] based on an ex vivo approach to test the licensed therapeutic mAbs BAM/ETE, CAS/IMD, and SOT against the omicron BA.1 and BA.2 lineages as well as against the ancestral B.1 strain and the previously dominating delta variant. By examining mAbs activity in post-infusion sera from treated patients in an authentic in vitro neutralization assay, we provide the best surrogate data for in vivo activity. Moreover, we tested on the same SARS-CoV-2 variants the three licensed antivirals, both with and without the P-glycoprotein (P-gp) inhibitor CP-100356, to further define their resilience to virus variability and current therapeutic potential.

2. Materials and Methods

2.1. Patients and Sera

The study was approved by the local Ethics Committee and written informed consent was obtained from all the patients enrolled (Neutro-COVID observational study, protocol number 4069/21). The study was conducted in accordance with the Declaration of Helsinki. Patients undergoing mAbs treatment were enrolled consecutively and selected based on undetectable NtAb before therapy, independently from their vaccination status. A pair of patient sera was collected, one before (baseline to comply with the negative NtAb selection criterion) and another one-hour post mAbs infusion (to test mAbs activity against the different virus variants). Thirty sera from a previous study [8] were included with their original NtAb values, although a random selection of 15 sera were retested against the wild-type virus to ensure consistency across the two studies, yielding comparable results.

2.2. Cells and Viral Stocks

VERO E6 (CRL 1586TM ATCC®, Gaithersburg, USA), an adherent cell line derived from African green monkey kidney, was used to propagate and titrate the viral stocks as previously described [9]. The same cell line was used in the live virus microneutralization and drug susceptibility assays. VERO E6 cells were propagated in DMEM High Glucose (Euroclone, Pero, Italy) supplemented with 10% Fetal Bovine Serum (FBS, Euroclone, Pero, Italy) and 1% of Streptomycin/Penicillin (PS) (Euroclone, Pero, Italy) in a humified incubator at 37°C with 5% of CO_2. The same medium, containing 1% of FBS instead of 10% (infection medium), was used in all viral infection experiments. Uninfected cell cultures were handled in a Biosafety Level 2 (BSL2) laboratory, whereas all the infection experiments were performed in a BSL3 containment. The SARS-CoV-2 B.1 (D614G) wild-type, delta and omicron BA.1 and BA.2 stocks, used to challenge the mAbs sera in neutralization experiments and to determine the antiviral activity of drug compounds in drug susceptibility assays, are detailed in Supplementary Table S1. Before performing the neutralization and phenotypic experiments, six replicates of 5-fold serial dilution of each viral stock were titrated in VERO E6 cells to determine the Tissue Culture Infectious Dose per milliliter ($TCID_{50/mL}$), which is defined as the amount of virus required to infect 50% of replicate cell cultures as previously described [9]. The cytopathic effect and consequently the $TCID_{50/mL}$ was determined by luminescence as described below. In addition, each viral stock was initially quantified by plaque assay as previously published [9].

2.3. Live Virus Microneutralization Assay

Microneutralization experiments were performed as previously described [8]. Briefly, after inactivation at 56 °C for 30 min, the patient serum was prediluted 1:5 and two-fold serial dilutions were prepared in 96-well format. One hundred 50% $TCID_{50}$ of each SARS-CoV-2 viral stock were added to the sera and incubated at 37°C with 5% CO_2 for 1 h. Then, serum-virus mixtures were added to 5000 pre-seeded VERO E6 cells in 96-well plates and incubated at 37°C with 5% CO_2. After 72 h, the ability of sera to neutralize the virus was determined measuring the cell viability by the CellTiter-Glo 2.0 Luminescent Cell Viability Assay (Promega, Madison, WI, USA) with the GloMax® Discover Multimode Microplate Reader (Promega, Madison, WI, USA) and the mAbs neutralization titer was expressed as the serum dilution corresponding to half-maximal inhibition of virus-induced cell death (ID_{50}). Sera below 5 ID_{50} were scored as not neutralizing and given a 2.5 value for statistical analysis.

Each serum was tested in technical duplicates in two independent experiments. Each plate included: (i) a mock infection control (uninfected cells); (ii) a virus control (infected cells without patient serum); (iii) a known SARS-CoV-2 neutralizing serum (positive control), yielding a median titer of 69 (59.3–69.9) in five independent runs. In addition, the virus test dose was confirmed by back titration, consisting of two-fold serial dilutions of each viral stock (100, 50, 25, 12.5, and 6.25 $TCID_{50}$). The virus test dose was considered acceptable if the back-titration results were positive in at least 3 subsequent virus dilutions. For a run to be valid, the coefficient of variation for the technical duplicates and for the two independent experiments had to be both below 30%. The initial validation of the assay was performed with the First WHO International Standard [10] anti-SARS-CoV-2 immunoglobulin (Version 3.0, Dated 17 December 2020; code 20/268 NIBSC, Ridge, UK).

2.4. Drug Susceptibility Assay

The P-gp inhibitor CP-100356 hydrochloride (MCE® cat. HY-108347 distributed by DBA, Milan, Italy), Remdesivir (MCE® cat. HY-104077 distributed by DBA, Milan, Italy), Nirmatrelvir (MCE® cat. HY-138687 distributed by DBA, Milan, Italy) and EIDD-1931 (MCE® cat. HY-125033 distributed by DBA, Milan, Italy), the active form of molnupiravir, were supplied as powder and dissolved in 100% dimethyl sulfoxide (DMSO). The VERO E6 cytotoxicity of CP-100356 hydrochloride alone and of the three antiviral drugs both

with and without the addition of 0.5 μM CP-100356 was determined by the Cell Titer-Glo 2.0 Luminescent Cell Viability Assay (Promega) according to the manufacturer's protocol. The luminescence values obtained from cells treated with the antiviral compounds or DMSO were measured through the GloMax® Discover Multimode Microplate Reader (Promega), normalized with luminescence emitted by untreated cells, and elaborated with the GraphPad PRISM software version 6.01 (La Jolla, CA, USA) to calculate the half-maximal cytotoxic concentration (CC_{50}). Based on the CC_{50}, a non-toxic dose corresponding to 90–100% cell viability was used for each compound as the maximum concentration in the antiviral assays.

To determine the antiviral activity of the drugs, 4-fold decreasing concentrations of remdesivir, nirmatrelvir and EIDD-1931 were added to 5000 pre-seeded VERO E6 cells as described [11] and viral isolates were used at MOI 0.005 (corresponding to 100 $TCID_{50}$) to infect the cultures after one hour. After 72 h incubation, antiviral drug activity was determined by measuring cell viability with the Cell Titer-Glo protocol as described above and expressed as half-maximal inhibitory drug concentration (IC_{50}). Infected and uninfected cells without drugs were used to calculate the 100% and 0% of viral replication, respectively. Drugs were tested in technical duplicates in at least two independent experiments. The experiments were performed in the absence and in the presence of the P-gp inhibitor to evaluate the impact of the efflux system on the different compounds. The P-gp inhibitor concentration was set at 0.5 μM based on cytotoxicity data (Supplementary Figure S1) and previous literature [11,12].

2.5. Statistical Analysis

Data were expressed as median followed by interquartile range [IQR] as appropriate for the distribution of data based on the Shapiro–Wilk test for normality. The Kruskal–Wallis test followed by Mann–Whitney test post hoc analysis was used to compare independent groups, whereas the Friedman test followed by Wilcoxon Rank Sum test post hoc analysis was used to compare multiple paired data.

3. Results

3.1. mAb Treated Patients

Of 50 subjects screened, 40 were enrolled (19 males, 59.8 ± 17.7 years) including 6 who were previously vaccinated but lacked NtAb at baseline. Of these, 5 had haemato-oncologic disease and the remaining one was a 69-year-old male with underlying hypertension, chronic ischemic cardiomyopathy, dyslipidemia. Only one of the enrolled patients was asymptomatic whereas the others had mild symptoms of SARS-CoV-2 infection including fever (67.5%, *n*=27), cough (65.0%, *n*=26), headache (37.5%, *n*=15), arthomyalgia (30.0%, *n*=12), dysgeusia (17.5%, *n*=7), gastrointestinal disorders (12.5%, *n*=5), and dyspnea (5.0%, *n*=2). Comorbidities and detailed information about enrolled individuals are indicated in Supplementary Table S2. Patients were treated with BAM/ETE (*n*=12), CAS/IMD (*n*=14), or SOT (*n*=14) starting 3.7±1.6 days from diagnosis.

Two patients were hospitalized (one in BAM/ETE and one in the CAS/IMD group), the others resolved SARS-CoV-2 infection without clinical complications. The time from mAb infusion to SARS-CoV-2 RNA negativization was available only in 22 individuals treated with BAM/ETE (*n*=11) or CAS/IMD (*n*=11) and was not significantly different with the two cocktails (15 vs. 13 days for BAM/ETE and CAS/IMD, respectively).

3.2. Neutralizing Activity of mAbs Against Different Viral Variants

In post-infusion sera, BAM/ETE, CAS/IMD, and SOT showed activity against the wild type (6295 (4355–8075) ID_{50} for BAM/ETE; 18,214 (16,248–21,365) ID_{50} for CAS/IMD; and 456 (265–592) ID_{50} for SOT) and the delta (14,780 (10,905–21,020) ID_{50} for BAM/ETE, 63,937 (47,211–79,971) ID_{50} for CAS/IMD, and 1103 (843–1334) ID_{50} for SOT). However,

BA.1 was neutralized only by SOT (200 (37–233) ID_{50}) whereas BA.2 was neutralized by CAS/IMD (174 (134–209) ID_{50}) and SOT (20 (9–31) ID_{50}), but not by BAM/ETE (Figure 1).

When NtAb titers were analyzed as fold-change (FC) with respect to the wild-type strain, BAM/ETE, CAS/IMD and SOT neutralized the delta variant with 2.5 (1.8–3.6), 3.5 (2.4–5.1) and 2.1 (1.6–3.4) FC increase, respectively (all $p < 0.001$). With respect to wild type, SOT neutralizing activity decreased more with BA.2 (23.9 (14.2–43.5) FC) than with BA.1 (2.8 (1.1–4.1) FC) ($p < 0.001$). The partially regained activity of CAS/IMD against BA.2 was 99.3 (91.8–138.5) fold lower than that against the wild-type virus, a larger FC decrease compared with SOT ($p<0.001$), although the absolute NtAb titer of CAS/IMD remained higher than that of SOT, due to the lower dosage and/or intrinsic activity of the latter. Indeed, NtAb titers were significantly higher for CAS/IMD vs. BAM/ETE and for both CAS/IMD and BAM/ETE vs. SOT against the wild-type and delta virus, as well as for CAS/IMD vs. SOT against BA.2 ($p<0.001$ for all comparisons).
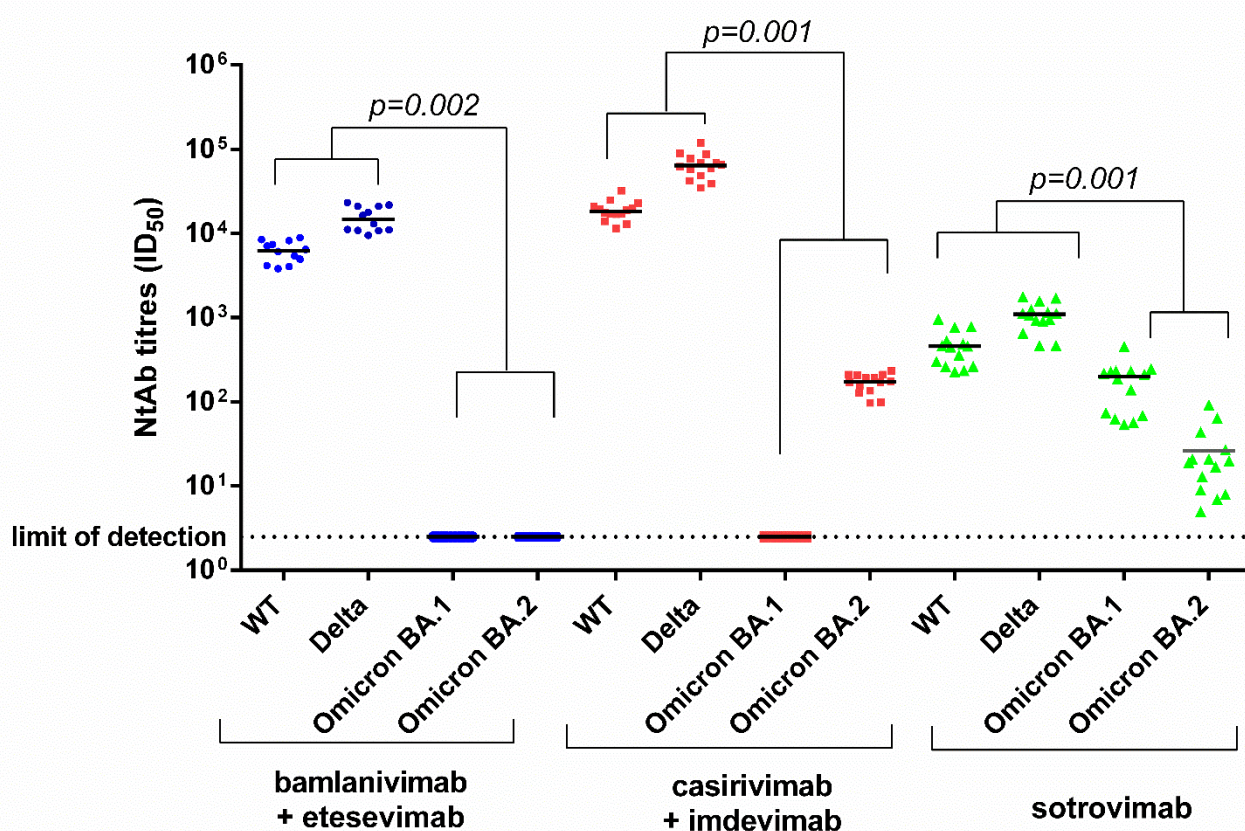
Figure 1. Ex vivo anti-SARS-CoV-2 wild type, delta, omicron (BA.1 and BA.2) neutralizing antibody titers measured in sera from 40 patients following infusion of bamlanivimab/etesevimab, casirivimab/imdevimab, or sotrovimab monoclonal antibodies. Blue dots, red squares and green triangles represents patients treated with bamlanivimab+etesevimab, casirivimab+indevimab and sotrovimab, respectively. Paired data were analyzed by the non-parametric Wilcoxon Signed Rank Sum test. NtAb titers before infusion were negative against each variant tested (not shown in figure). NtAb: neutralizing antibody; ID_{50}: the reciprocal value of the sera dilution showing the 50% protection of virus-induced cytopathic effect; WT: wild type.

3.3. Antiviral Activity of Nirmatrelvir, Molnupiravir and Remdesivir in VERO E6

Table 1 shows the cytotoxicity and the antiviral activity data for EIDD-1931, nirmatrelvir and remdesivir. No significant differences were observed for any drug IC_{50} across the viral variants considered. The impact of the P-gp inhibitor, as measured with the wild-

type virus, was negligible with EIDD-1931 but highly relevant with remdesivir and nirmatrelvir, resulting in increased antiviral activity by 88- and 126-fold, respectively (Figure 2).

Table 1. Anti-SARS-CoV-2 activity of EIDD-1931 (the active form of molnupiravir), remdesivir and nirmatrelvir in VERO E6 cells. Compounds were tested in absence of P-gp inhibitor (CP-100356 hydrochloride) against wild-type strain and in presence of 0.5 μM P-gp inhibitor against Wild Type (WT), Delta, BA.1, and BA.2 variants. . CC_{50}: half-maximal toxic drug concentration; IC_{50}: half-maximal inhibitor drug concentration; SD: Standard Deviation.

Compound	CC_{50} (μM)	IC_{50} WT (μM) mean ± SD	IC_{50} Delta (μM) mean ± SD	IC_{50} BA.1 (μM) mean ± SD	IC_{50} BA.2 (μM) mean ± SD
EIDD-1931	40.6 ± 3.7	1.10 ± 0.10			
EIDD-1931 plus P-gp inhibitor	43.3 ± 6.0	1.50 ± 0.10	1.50 ± 0.70	1.00 ± 0.50	0.80 ± 0.01
Nirmatrelvir	69.6 ± 1.0	5.80 ± 0.80			
Nirmatrelvir plus P-gp inhibitor	40.7 ± 4.4	0.05 ± 0.02	0.06 ± 0.01	0.04 ± 0.02	0.04 ± 0.01
Remdesivir	205.0 ± 35.4	6.90 ± 2.30			
Remdesivir plus P-gp inhibitor	17.2 ± 0.2	0.08 ± 0.04	0.11 ± 0.08	0.05 ± 0.04	0.08 ± 0.01
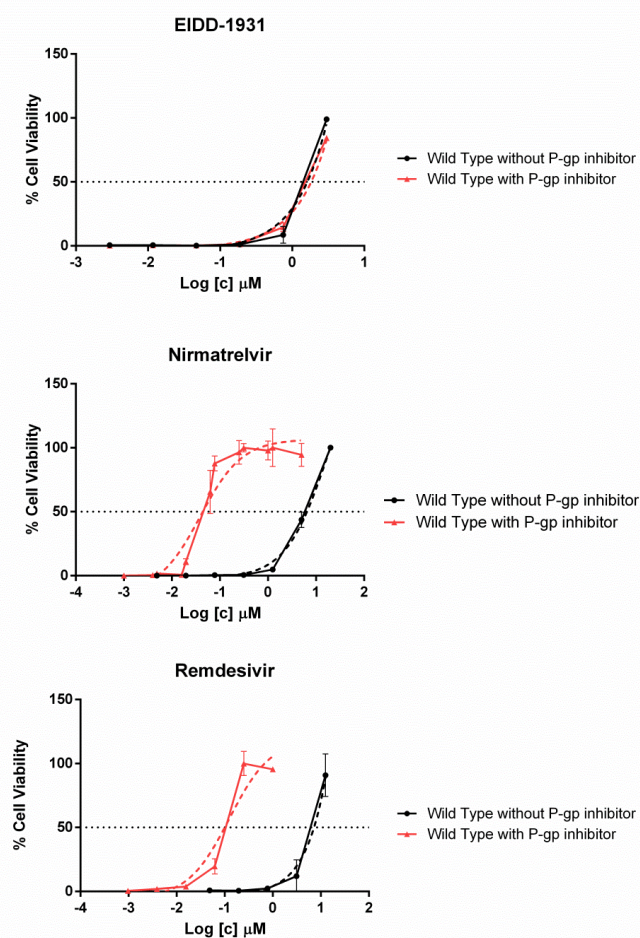
Figure 2. Comparison between antiviral activity of EIDD-1931, Nirmatrelvir and Remdesivir against wild-type SARS-CoV-2 virus with (0.5 μM) or without the addition of P-gp inhibitor. On the x-axis

is indicated the micromolar drug concentration in logarithmic scale. The horizontal dashed line indicates the drug IC_{50} corresponding to 50% cell viability whereas the dashed curves indicate the dose response fitting curve generated by GraphPad PRISM software version 6.01 (La Jolla, CA, USA).

4. Discussion

Despite a limited evolutionary rate, continuous massive worldwide replication of SARS-CoV-2 has generated an array of mutants, with new variants typically outpacing past lineages and quickly becoming dominant [13]. Not surprisingly, most mutations in evolutionarily successful variants have occurred in the spike glycoprotein resulting in improved virus entry and increased transmissibility [14]. First detected in late 2021, the omicron variant led a major shift in SARS-CoV-2 evolution [15], driven by an unprecedented number of spike mutations and further evolving into a constellation of related lineages including BA.1, BA.1.1, BA.2 and later BA.3, BA.4 and BA.5, with some sublineages spreading faster than others in specific countries such BA.2.12.1 in the US [6]. A major consequence of omicron divergence from past lineages is the markedly reduced neutralization by sera from individuals recovering from natural infection with previously dominating variants and/or immunized with vaccines derived from the ancestral virus strain [16]. Likewise, several mAbs based on virus variants dominating the first epidemic waves have lost activity against omicron lineages [17].

Unlike the other licensed mAbs, SOT was derived from the antibody repertoire of an individual recovered from SARS-CoV in 2003 and shown to be cross-reactive to SARS-CoV-2, thus targeting a highly conserved domain [18]. Indeed, when compared with BAM/ETE and CAS/IMD, SOT had the smallest-fold decrease in activity against omicron BA.1 and BA.2 with respect to the ancestral reference virus, both in previous in vitro studies [19,20] and in this ex vivo study. However, we observed higher absolute NtAb titers to BA.2 with CAS/IMD compared to SOT in our ex vivo assay. This apparently contradictory result likely derived from the combination of three factors. First, IMD may have residual activity against BA.2, despite a fold decrease with respect to the ancestral virus ranging from 20 to 500 [4,19–21]. Second, the in vivo dosage of CAS/IMD is higher than that of SOT (1200 plus 1200 mg vs. 500 mg). Third, the intrinsic in vitro neutralizing activity of SOT is one order of magnitude lower than that of CAS or IMD, as indicated by EC_{50} values with the susceptible wild-type virus [3,22,23].

At present, it is unclear how this expected activity, for both SOT and CAS/IMD, can translate into clinical benefit with BA.2 infection. It must be emphasized that in vitro neutralization assays can capture just one component of the mAbs activity. Indeed, unlike other mAbs, neither SOT nor CAS/IMD have been engineered to remove effector functions such as engagement of Fc receptors, and SOT was recently shown to trigger antibody-dependent cytotoxicity and phagocytosis [5,24]. Of note, both SOT and CAS/IMD, as well as CIL/TIX, have been recently reported to curb experimental disease progression in the BA.2 infected hamster model, as shown by decreased infectious virus titer in the lungs by a factor which was comparable with the D614G infected control animals [25].

As opposed to mAbs variant-dependent activity, it was reassuring to confirm that the three licensed antivirals retain their full potency in vitro against the BA.1 and BA.2 omicron lineages. Of note, there has been only one report documenting this activity against the currently dominating BA.2 variant in vitro [4]. While VERO cells were used both in the previous and in our study, we extended the analysis by testing drug activity both in the presence and in the absence of the CP-100356 hydrochloride P-gp inhibitor. This is important because VERO cells overexpress P-gp, a condition which should not occur in human SARS-CoV-2 cell targets in vivo. In addition, nirmatrelvir is administered in vivo together with ritonavir which inhibits the P450 cytochrome CYP3A4 isoenzyme as well as P-gp [26]. Our results without the P-gp inhibitor closely matched the activity shown in the previous in vitro work under the same experimental conditions but we also showed that under P-gp inhibitor treatment the activity is enhanced around 100-fold for

nirmatrelvir and for remdesivir. In addition, we comprehensively tested the cytotoxicity of the P-gp inhibitor in the same cell line, both alone and in combination with the different drugs, thus analyzing drug/P-gp inhibitor interactions. Indeed, the P-gp inhibitor decreased cell viability by 20% at 2 μM, a concentration which has been used in some of the previous studies evaluating the antivirals against past virus lineages [27,28]. This data helps to define how to measure antiviral activity of current and future antivirals.

Thus, our work strengthens the concept of resilience to SARS-CoV-2 variability with antivirals as opposed to the continuous challenge with mAbs. However, both antivirals and mAbs should be retested with any new virus variant. We believe our work contributes to the need to set technical aspects and procedures to comprehensively define the potential of the antiviral armamentarium, including mAbs and small molecules, and keep pace with virus variability during the ongoing pandemic.

References

1. Markov, P.v.; Katzourakis, A.; Stilianakis, N.I. Antigenic Evolution Will Lead to New SARS-CoV-2 Variants with Unpredictable Severity. *Nat. Rev. Microbiol.* **2022**, *20*, 251–252. https://doi.org/10.1038/S41579-022-00722-Z.
2. Tao, K.; Tzou, P.L.; Nouhin, J.; Gupta, R.K.; de Oliveira, T.; Kosakovsky Pond, S.L.; Fera, D.; Shafer, R.W. The Biological and Clinical Significance of Emerging SARS-CoV-2 Variants. *Nat. Rev. Genet.* **2021**, *22*, 757–773. https://doi.org/10.1038/S41576-021-00408-X.
3. Takashita, E.; Kinoshita, N.; Yamayoshi, S.; Sakai-Tagawa, Y.; Fujisaki, S.; Ito, M.; Iwatsuki-Horimoto, K.; Chiba, S.; Halfmann, P.; Nagai, H.; et al. Efficacy of Antibodies and Antiviral Drugs against Covid-19 Omicron Variant. *N. Engl. J. Med.* **2022**, *386*, 995–998. https://doi.org/10.1056/NEJMC2119407.
4. Takashita, E.; Kinoshita, N.; Yamayoshi, S.; Sakai-Tagawa, Y.; Fujisaki, S.; Ito, M.; Iwatsuki-Horimoto, K.; Halfmann, P.; Watanabe, S.; Maeda, K.; et al. Efficacy of Antiviral Agents against the SARS-CoV-2 Omicron Subvariant BA.2. *N. Engl. J. Med.* **2022**, *386*, 1475–1477. https://doi.org/10.1056/NEJMC2201933.

5. Cathcart, A.L.; Havenar-Daughton, C.; Lempp, F.A.; Ma, D.; Schmid, M.A.; Agostini, M.L.; Guarino, B.; di iulio, J.; Rosen, L.E.; Tucker, H.; et al. The Dual Function Monoclonal Antibodies VIR-7831 and VIR-7832 Demonstrate Potent in Vitro and in Vivo Activity against SARS-CoV-2. *bioRxiv* **2022**, 2021.03.09.434607. https://doi.org/10.1101/2021.03.09.434607.

6. Cao, Y.; Yisimayi, A.; Jian, F.; Song, W.; Xiao, T.; Wang, L.; Du, S.; Wang, J.; Li, Q.; Chen, X.; et al. BA.2.12.1, BA.4 and BA.5 Escape Antibodies Elicited by Omicron Infection. *bioRxiv* **2022**, 2022.04.30.489997. https://doi.org/10.1101/2022.04.30.489997.

7. Yamasoba, D.; Kosugi, Y.; Kimura, I.; Fujita, S.; Uriu, K.; Ito, J.; Sato, K.; Consortium, T.G. to P.J. (G2P-J. Sensitivity of Novel SARS-CoV-2 Omicron Subvariants, BA.2.11, BA.2.12.1, BA.4 and BA.5 to Therapeutic Monoclonal Antibodies. *bioRxiv* **2022**, 2022.05.03.490409. https://doi.org/10.1101/2022.05.03.490409.

8. Dragoni, F.; Schiaroli, E.; Micheli, V.; Fiaschi, L.; Lai, A.; Zehender, G.; Rossetti, B.; Gismondo, M.R.; Francisci, D.; Zazzi, M.; et al. Impact of SARS-CoV-2 Omicron BA.1 and Delta AY.4.2 Variants on the Neutralization by Sera of Patients Treated with Different Authorized Monoclonal Antibodies. *Clin. Microbiol Infect.* **2022**, *28*, 1037–1039. https://doi.org/10.1016/J.CMI.2022.03.005.

9. Vicenti, I.; Martina, M.G.; Boccuto, A.; de Angelis, M.; Giavarini, G.; Dragoni, F.; Marchi, S.; Trombetta, C.M.; Crespan, E.; Maga, G.; et al. System-Oriented Optimization of Multi-Target 2,6-Diaminopurine Derivatives: Easily Accessible Broad-Spectrum Antivirals Active against Flaviviruses, Influenza Virus and SARS-CoV-2. *Eur J. Med. Chem* **2021**, *224*, 113683. https://doi.org/10.1016/J.EJMECH.2021.113683.

10. Kristiansen, P.A.; Page, M.; Bernasconi, V.; Mattiuzzo, G.; Dull, P.; Makar, K.; Plotkin, S.; Knezevic, I. WHO International Standard for Anti-SARS-CoV-2 Immunoglobulin. *Lancet* **2021**, *397*, 1347–1348. https://doi.org/10.1016/S0140-6736(21)00527-4.

11. Vangeel, L.; Chiu, W.; de Jonghe, S.; Maes, P.; Slechten, B.; Raymenants, J.; André, E.; Leyssen, P.; Neyts, J.; Jochmans, D. Remdesivir, Molnupiravir and Nirmatrelvir Remain Active against SARS-CoV-2 Omicron and Other Variants of Concern. *Antiviral Res.* **2022**, *198*, 105252. https://doi.org/10.1016/J.ANTIVIRAL.2022.105252.

12. Hoffman, R.L.; Kania, R.S.; Brothers, M.A.; Davies, J.F.; Ferre, R.A.; Gajiwala, K.S.; He, M.; Hogan, R.J.; Kozminski, K.; Li, L.Y.; et al. Discovery of Ketone-Based Covalent Inhibitors of Coronavirus 3CL Proteases for the Potential Therapeutic Treatment of COVID-19. *J. Med. Chem.* **2020**, *63*, 12725–12747. https://doi.org/10.1021/ACS.JMEDCHEM.0C01063.

13. Flores-Vega, V.R.; Monroy-Molina, J.V.; Jiménez-Hernández, L.E.; Torres, A.G.; Santos-Preciado, J.I.; Rosales-Reyes, R. SARS-CoV-2: Evolution and Emergence of New Viral Variants. *Viruses* **2022**, *14*, 653. https://doi.org/10.3390/V14040653.

14. de Souza, A.S.; de Freitas Amorim, V.M.; Guardia, G.D.A.; dos Santos, F.F.; Ulrich, H.; Galante, P.A.F.; de Souza, R.F.; Guzzo, C.R. Severe Acute Respiratory Syndrome Coronavirus 2 Variants of Concern: A Perspective for Emerging More Transmissible and Vaccine-Resistant Strains. *Viruses* **2022**, *14*, 827. https://doi.org/10.3390/V14040827.

15. Guo, Y.; Han, J.; Zhang, Y.; He, J.; Yu, W.; Zhang, X.; Wu, J.; Zhang, S.; Kong, Y.; Guo, Y.; et al. SARS-CoV-2 Omicron Variant: Epidemiological Features, Biological Characteristics, and Clinical Significance. *Front. Immunol.* **2022**, *13*, 877101. https://doi.org/10.3389/FIMMU.2022.877101.

16. Evans, J.P.; Zeng, C.; Qu, P.; Faraone, J.; Zheng, Y.-M.; Carlin, C.; Bednash, J.S.; Zhou, T.; Lozanski, G.; Mallampalli, R.; et al. Neutralization of SARS-CoV-2 Omicron Sub-Lineages BA.1, BA.1.1, and BA.2. *Cell Host Microbe.* **2022**, S1931-3128(22)00220-7. https://doi.org/10.1016/J.CHOM.2022.04.014.

17. Ai, J.; Wang, X.; He, X.; Zhao, X.; Zhang, Y.; Jiang, Y.; Li, M.; Cui, Y.; Chen, Y.; Qiao, R.; et al. Antibody Evasion of SARS-CoV-2 Omicron BA.1, BA.1.1, BA.2, and BA.3 Sub-Lineages. *Cell Host Microbe.* **2022**, S1931-3128(22)00243-8. https://doi.org/10.1016/J.CHOM.2022.05.001.

18. Pinto, D.; Park, Y.J.; Beltramello, M.; Walls, A.C.; Tortorici, M.A.; Bianchi, S.; Jaconi, S.; Culap, K.; Zatta, F.; de Marco, A.; et al. Cross-Neutralization of SARS-CoV-2 by a Human Monoclonal SARS-CoV Antibody. *Nature* **2020**, *583*, 290–295. https://doi.org/10.1038/S41586-020-2349-Y.

19. Bruel, T.; Hadjadj, J.; Maes, P.; Planas, D.; Seve, A.; Staropoli, I.; Guivel-Benhassine, F.; Porrot, F.; Bolland, W.-H.; Nguyen, Y.; et al. Serum Neutralization of SARS-CoV-2 Omicron Sublineages BA.1 and BA.2 in Patients Receiving Monoclonal Antibodies. *Nat. Med.* **2022**, *6*, 1297-1302. https://doi.org/10.1038/S41591-022-01792-5.

20. Arora, P.; Zhang, L.; Krüger, N.; Rocha, C.; Sidarovich, A.; Schulz, S.; Kempf, A.; Graichen, L.; Moldenhauer, A.-S.; Cossmann, A.; et al. SARS-CoV-2 Omicron Sublineages Show Comparable Cell Entry but Differential Neutralization by Therapeutic Antibodies. *Cell Host Microbe.* **2022**, S1931-3128(22)00223-2. https://doi.org/10.1016/J.CHOM.2022.04.017.

21. Iketani, S.; Liu, L.; Guo, Y.; Liu, L.; Chan, J.F.-W.; Huang, Y.; Wang, M.; Luo, Y.; Yu, J.; Chu, H.; et al. Antibody Evasion Properties of SARS-CoV-2 Omicron Sublineages. *Nature* **2022**, *604*, 553–556. https://doi.org/10.1038/S41586-022-04594-4.

22. Touret, F.; Baronti, C.; Bouzidi, H.S.; de Lamballerie, X. In Vitro Evaluation of Therapeutic Antibodies against a SARS-CoV-2 Omicron B.1.1.529 Isolate. *Sci. Rep.* **2022**, *12*, 4683. https://doi.org/10.1038/S41598-022-08559-5.

23. VanBlargan, L.A.; Errico, J.M.; Halfmann, P.J.; Zost, S.J.; Crowe, J.E.; Purcell, L.A.; Kawaoka, Y.; Corti, D.; Fremont, D.H.; Diamond, M.S. An Infectious SARS-CoV-2 B.1.1.529 Omicron Virus Escapes Neutralization by Therapeutic Monoclonal Antibodies. *Nature Medicine* **2022**, *28*, 490–495. https://doi.org/10.1038/s41591-021-01678-y.

24. Case, J.B.; Mackin, S.; Errico, J.; Chong, Z.; Madden, E.A.; Guarino, B.; Schmid, M.A.; Rosenthal, K.; Ren, K.; Jung, A.; et al. Resilience of S309 and AZD7442 Monoclonal Antibody Treatments against Infection by SARS-CoV-2 Omicron Lineage Strains. *bioRxiv* **2022**, 2022.03.17.484787. https://doi.org/10.1101/2022.03.17.484787

25. Uraki, R.; Kiso, M.; Iida, S.; Imai, M.; Takashita, E.; Kuroda, M.; Halfmann, P.J.; Loeber, S.; Maemura, T.; Yamayoshi, S.; et al. Characterization and Antiviral Susceptibility of SARS-CoV-2 Omicron/BA.2. *Nature* **2022**. https://doi.org/10.1038/S41586-022-04856-1.

26. Marzolini, C.; Kuritzkes, D.R.; Marra, F.; Boyle, A.; Gibbons, S.; Flexner, C.; Pozniak, A.; Boffito, M.; Waters, L.; Burger, D.; et al. Prescribing Nirmatrelvir-Ritonavir: How to Recognize and Manage Drug-Drug Interactions. *Ann. Intern. Med.* **2022**, *175*, 744–746. https://doi.org/10.7326/M22-0281.

27. Owen, D.R.; Allerton, C.M.N.; Anderson, A.S.; Aschenbrenner, L.; Avery, M.; Berritt, S.; Boras, B.; Cardin, R.D.; Carlo, A.; Coffman, K.J.; et al. An Oral SARS-CoV-2 M pro Inhibitor Clinical Candidate for the Treatment of COVID-19. *Science* **2021**, *374*, 1586–1593. https://doi.org/10.1126/SCIENCE.ABL4784.

28. Rosales, R.; McGovern, B.L.; Rodriguez, M.L.; Rai, D.K.; Cardin, R.D.; Anderson, A.S.; group, P.S.P. study; Sordillo, E.M.; van Bakel, H.; Simon, V.; et al. Nirmatrelvir, Molnupiravir, and Remdesivir Maintain Potent <Em>in Vitro</Em> Activity against the SARS-CoV-2 Omicron Variant. *bioRxiv* **2022**, 2022.01.17.476685. https://doi.org/10.1101/2022.01.17.476685